
TARGETING PEPTIDES CONTAINING SUPRAMOLECULAR AGGREGATES TOWARD CANCER CELLS

Anna Morisco

Dottorato in Scienze Biotecnologiche – XXII ciclo
Indirizzo Biotecnologie Molecolari
Università di Napoli Federico II



Dottorato in Scienze Biotechologiche – XXII ciclo
Indirizzo Biotecnologie Molecolari
Università di Napoli Federico II



TARGETING PEPTIDES CONTAINING SUPRAMOLECULAR AGGREGATES TOWARD CANCER CELLS

Anna Morisco

Dottoranda: Anna Morisco

Relatore: Prof. Ettore Benedetti

Coordinatore: Prof. Ettore Benedetti

INDEX

SUMMARY	1
RIASSUNTO	3
1. INTRODUCTION	6
1.1. SUPRAMOLECULAR SYSTEMS	7
1.1.1 <i>Micelles</i>	8
1.1.2 <i>Liposomes</i>	9
1.2. SUPRAMOLECULAR AGGREGATES AS THERAPEUTIC TOOLS	11
1.3 SUPRAMOLECULAR AGGREGATES AS DIAGNOSTIC TOOLS	12
1.4 TARGET SELECTIVE SUPRAMOLECULAR AGGREGATES	14
1.5 TARGET SELECTIVE AGGREGATES FOR DRUG DELIVERY	15
1.6 TARGET SELECTIVE AGGREGATES FOR MRI	17
1.7 SPECIFIC-TARGETING PEPTIDE	19
2. AIM OF THESIS	20
3. OCTREOTIDE LABELED SUPRAMOLECULAR AGGREGATES	21
3.1 INTRODUCTION	21
3.2 RESULTS & DISCUSSION	23
3.2.1 <i>Monomers Design and Synthesis</i>	23
3.2.2 <i>Aggregates Preparation and Characterization</i>	26
3.2.3 <i>Physicochemical Studies on the Octreotide Moiety</i>	28
3.2.4 <i>Relaxivity Measurements</i>	31
3.2.5 <i>Structural characterization</i>	32
3.3. EXPERIMENTAL SECTION: OCTREOTIDE	35
3.3.1 <i>Materials</i>	35
3.3.2 <i>Peptide Conjugate Synthesis</i>	35
3.3.3 <i>Preparation of Gadolinium complexes:</i>	38
3.3.4 <i>Aggregates Preparation</i>	38
3.3.5 <i>Fluorescence Measurements</i>	39
3.3.6 <i>Small-Angle Neutron Scattering (SANS)</i>	39
3.3.7 <i>Dynamic Light Scattering (DLS)</i>	40
3.3.8 <i>Water proton relaxation measurements:</i>	40
3.3.9 <i>¹⁷O-NMR water relaxation rate measurements:</i>	40
3.3.10 <i>Circular Dichroism (CD) Experiments</i>	41
4. BOMBESIN LABELED SUPRAMOLECULAR AGGREGATES	42
4.1 INTRODUCTION	42
4.2 RESULTS & DISCUSSION	43
4.2.1 <i>Monomers Synthesis and Aggregates Preparation</i>	43
4.2.2 <i>Fluorescence studies</i>	44
4.2.5 <i>In Vivo studies</i>	50
4.3 EXPERIMENTAL SECTION: BOMBESIN	52
4.3.1 <i>Materials</i>	52

4.3.2 Peptide Conjugate Synthesis	52
4.3.3 Aggregates Preparation	53
4.3.4 Preparation of the Radiotracers	53
4.3.5 In vitro studies	54
4.3.6 In vivo studies.....	54
5. SUPRAMOLECULAR AGGREGATES LABELED WITH CHOLECYSTOKININ	55
5.1 INTRODUCTION	55
5.2 RESULTS & DISCUSSION	56
5.2.1 Monomer Synthesis and Aggregate Preparation	56
5.2.2 Doxorubicin loading and release from liposomes	56
5.2.3 Cellular uptake and in vitro cytotoxicity of liposomal DOX.....	57
5.3 EXPERIMENTAL SECTION: CCK8.....	61
5.3.1 Materials	61
5.3.2 Peptide conjugate synthesis	61
5.3.3 Aggregate formulation and DLS characterization.....	62
5.3.4 Doxorubicin Loading	62
5.3.5 Doxorubicin release	62
5.3.6 Cell culture.....	63
5.3.7 Flow cytometric analysis.....	63
5.3.8 Cytotoxicity assay.....	63
6. CONCLUSIONS	64
7. Techniques.....	66
7.1 SOLID PHASE PEPTIDE SYNTHESIS (SPPS).....	66
7.2 FLUORESCENCE.....	69
7.2.1 Fluorescence Quenching.....	72
7.3 DYNAMIC LIGHT SCATTERING (DLS).....	74
7.4 SMALL ANGLE NEUTRON SCATTERING (SANS).....	76
7.4 FLOW CYTOMETRY	78
7.4.1 Light Scatter	78
7.4.2 Fluorescence	79
7.4.3 Display and Interpretation of Flow Cytometry Data.....	80
ACKNOWLEDGEMENTS.....	82
REFERENCES.....	83
ABBREVIATIONS	89
PUBLICATION LIST	91
SYMPOSIUM COMUNICATIONS	91

Summary

Multimodal supramolecular compounds that combine imaging and therapeutic capabilities are the focus of intensive research for applications in the growing field of nanomedicine. These compounds offer the prospect to increase diagnostic accuracy and therapeutic effectiveness, while minimizing side effects from treatment. Nanoparticles with a micellar or liposomal structure obtained by assembling amphiphilic compounds are promising candidates for such multifunctional therapeutic platforms.

Selective target of these nanoparticles for cancer cells can be obtained by labeling supramolecular aggregates with peptides able to recognize transmembrane receptors overexpressed in many human tumors. Examples of peptide that can be used to drive selectively the nanoparticle on the cancer cells are the octreotide (analog of the somatostatin), [7-14] bombesin and CCK8 peptides. To reach this result, new amphiphilic monomers were designed, synthesized and structurally characterized. Amphiphilic monomers are functionalized with polydentate chelating agent (such as DOTA, DTPA and DTPAGlu) able to coordinate radioactive or paramagnetic metals for diagnostic applications, or with bioactive molecules able to recognize the cellular target. These molecules are able to auto assemble or to aggregate in mixed micelles or liposomes in aqueous solution.

All monomers were synthesized in solid-phase following an Fmoc strategy. The aggregates formulated are investigated by physical chemical methods like Small Angle Neutron Scattering (SANS) and Dynamic Light Scattering (DLS), relaxivity measurement and spectroscopy techniques (fluorescence and UV-Vis). These studies have allowed selecting the best systems for shape and size with relation to relaxivity parameters and aggregation stability. To validate the specificity and the cytotoxicity of the delivery systems *in vitro* and *in vivo* studies were also performed.

The monomers containing the chelating agent, (C18)₂DOTA, (C18)₂DTPA and (C18)₂DTPAGlu are able to auto assemble. Moreover in mixed aggregates they showed to drive the aggregation process. Aggregates functionalized with octreotide were investigated as promising target-selective contrast agent for MRI (Magnetic Resonance Imaging). The high relaxivity values, associated with the supramolecular aggregates, confirm the obtainment of a more rigid contrast agent able to carry numerous gadolinium ions on target cells.

In vitro binding assays on bombesin labeled liposomes allowed to select (C18)₂DOTA/(C18)₂-L5-bombesin as the lead compound. In these supramolecular aggregate, the peptidic monomer contains the more appropriate spacer of the length between the peptide and the hydrophobic moiety. *In vivo* studies confirmed the specificity towards to the receptor of the bombesin labeled liposome with respect to the liposome exposing a scrambled peptide sequence. Aggregates functionalized with CCK8 peptide were investigated as target-selective drug delivery systems.

The drug delivery of chemioterapeutics (i.e. doxorubicin) was studied on A431 cells overexpressing CCK receptors. The loading and release of the drug were carried out in (C18)₂DOTA/(C18)₂-L5-CCK8 liposome. The results obtained show the specificity and the efficacy of the system on cellular target, compared with control aggregate.

In conclusion this research has permitted the achievement of new supramolecular systems containing a bioactive molecule and a chelating agent able to target tumor cells, as possible of diagnostic and therapeutic.

Riassunto

La diagnosi e il trattamento di tumori a livello cellulare sono attualmente affrontati con metodologie convenzionali quali la radioterapia e la chemioterapia, strategie che nella maggior parte dei casi, permettono di individuare l'insorgenza del tumore solo quando quest'ultimo è in stadi avanzati. Ed è proprio per superare i limiti di queste tecniche, che negli ultimi anni si stanno sviluppando e intensificando metodi basati sulle nanotecnologie e sul bersaglio molecolare per un'efficace veicolazione di farmaci. Attualmente, nel campo della nanomedicina viene promossa la realizzazione di nanosistemi per mezzi di contrasto più sensibili e specifici, e sistemi per la veicolazione di farmaci con problemi di biodisponibilità, solubilità, tossicità. I nanosistemi, con maggiore successo per la diagnosi o la terapia sono i Quantum dots (Qdots), le nanoparticelle di silice, i dendrimeri e i sistemi supramolecolari come le micelle e i liposomi.

Un sistema supramolecolare si ottiene per interazioni intermolecolari fra molecole anfifiliche, e può svolgere un ruolo multifunzionale in quanto ha le potenzialità per poter veicolare un elevato numero di agenti di contrasto basati su complessi di metalli radioattivi o paramagnetici, e farmaci incapsulati nel core idrofobico o idrofilico. Infatti l'elevato accumulo di complessi di uno ione paramagnetico come il Gd(III), in grado di indurre variazioni sul tempo di rilassamento dei protoni dell'acqua, parametro sul quale è basata la tecnica della risonanza magnetica MRI (Magnetic Resonance Imaging), sul bersaglio cellulare è una condizione necessaria. Infatti per ottenere immagini ad alta risoluzione la tecnica richiede una concentrazione almeno 10^{-2} M di mezzo di contrasto. Per la veicolazione specifica, il sistema supramolecolare può essere funzionalizzato con molecole bioattive come peptidi, anticorpi o altre macromolecole di natura organica, come gli zuccheri. In letteratura sono riportati diversi aggregati supramolecolari veicolati sulle cellule tumorali mediante l'impiego di anticorpi, ed altre molecole bioattive come ad esempio l'acido folico in grado di riconoscere selettivamente un antigene o il recettore transmembrana del folato.

Obiettivo di questa tesi di dottorato è stato lo sviluppo di nuovi aggregati supramolecolari capaci di veicolare sulle cellule tumorali agenti di contrasto per tecniche di medicina nucleare e MRI, e in grado di incapsulare e rilasciare nel tempo farmaci chemioterapici. La selettività degli aggregati è indotta da un peptide bioattivo, esposto all'esterno del sistema, in grado di riconoscere un recettore cellulare sovraespresso in cellule tumorali. I peptidi presi in esame sono l'octreotide (uno degli analoghi della somatostatina), la bombesina 7-14, e il CCK8 (colecistochinina) in quanto questi peptidi possono legare con elevata affinità rispettivamente il recettore della somatostatina SSTR2, il recettore GRPR (Gastrin-Releasing Peptide Receptor) e i CCKR1 e CCKR2, sovraespressi in un'ampia classe di tumori di varia origine. Di seguito sono riportate le sequenze dei peptidi prima citati:

- a. Octreotide: H-D•Phe¹-Cys²-Phe³-D•Trp⁴-Lys⁵-Thr⁶-Cys⁷-Thr⁸(ol)
- b. Bombesina 7-14: H -Gln⁷-Trp⁸-Ala⁹-Val¹⁰-Gly¹¹-His¹²-Leu¹³-Met¹⁴- NH₂
- c. CCK8: H-Asp²⁶-Tyr²⁷-Met²⁸-Gly²⁹-Trp³⁰-Met³¹-Asp³²-Phe³³- NH₂

Sulla base di queste informazioni, sono stati progettati e sintetizzati monomeri anfifilici contenenti agenti chelanti in grado di coordinare ioni metallici radioattivi o paramagnetici che espletano funzione di mezzi di contrasto e molecole peptidiche

bioattive. Un primo set di molecole anfifiliche è costituito, quindi, da una porzione peptidica, da uno spaziatore di natura etossilica in grado di conferire alla molecola caratteristiche idrofiliche e da due code idrofobiche a 18 atomi di carbonio. In un secondo set di monomeri, la porzione peptidica è sostituita da un agente chelante. Un terzo set è costituito da molecole che legano covalentemente nella molecola la porzione bioattiva e l'agente chelante. I prodotti sono stati ottenuti in buone rese e con alto grado di purezza e l'identificazione è stata eseguita mediante tecniche di analisi cromatografica RP-HPLC e di spettrometria di massa Maldi-Tof e ESI. Gli aggregati sono stati ottenuti formulando i monomeri in diversi rapporti oppure per auto assemblaggio. Questi sistemi sono stati caratterizzati dal punto di vista strutturale e indagati sia *in vitro* che *in vivo*.

Gli studi strutturali hanno permesso di selezionare i migliori sistemi in termini di dimensioni e di forma in relazione ai parametri di rilassività e di stabilità; le indagini *in vitro* e poi *in vivo*, invece, hanno contribuito ad individuare i migliori sistemi, in termini di selettività, specificità ed attività verso il target cellulare d'interesse. Quindi tutti gli aggregati sono stati caratterizzati strutturalmente con tecniche chimico-fisiche (SANS, DLS), di spettroscopia fluorescenza e dicroismo circolare (CD) e misure di rilassività. Gli studi di SANS (Small-Angle Neutron Scattering) di indagare la forma degli aggregati e la loro natura, mentre la tecnica del DLS (Dynamic Light Scattering) è stata usata per determinare, laddove necessario, le dimensioni e il numero di aggregazione. La tecnica della fluorescenza ha permesso di determinare nel caso delle micelle la concentrazione micellare critica (cmc) e l'esposizione del peptide in ambiente idrofilico rispetto alla superficie dell'aggregato sfruttando la presenza in tutti i peptidi del residuo amminoacidico triptofano. La struttura secondaria del peptide è stata studiata mediante la tecnica del dicroismo circolare. L'insieme delle caratterizzazioni chimico fisiche hanno permesso quindi di selezionare gli aggregati che maggiormente avessero la possibilità di essere attivi *in vitro* ed *in vivo*.

Gli aggregati derivatizzati con l'octreotide indagati mediante la tecnica della fluorescenza per definire la posizione della porzione bioattiva rispetto alla superficie dell'aggregato, hanno dimostrato aver una fluorescenza del triptofano di circa 350 nm, valore indicativo di una buona esposizione del peptide rispetto all'aggregato. Per dimostrare che l'octeotide effettivamente mantenesse la sua conformazione attiva con un *beta turn* fra i residui 3-6, sono state eseguite sui composti OCA-DOTA e OCA-DTPAGlu (Figura n) misure di CD. Inoltre questi sistemi sono stati caratterizzati anche con studi di rilassività, in quanto questi aggregati sono da impiegare come potenziali mezzi di contrasto indirizzati verso specifici target da utilizzare nella tecnica dell'MRI. Le misure forniscono elevati valori rilassometrici, intorno a $15-18 \text{ mM}^{-1}\text{s}^{-1}$, questo risultato è attribuibile alla maggiore rigidità dei sistemi rispetto ai singoli complessi dei chelanti con gadolinio. Pertanto la validità della scelta operata a favore di mezzi di contrasto di tipo supramolecolare permette non solo di veicolare una quantità maggiore di ioni gadolinio contemporaneamente sulle cellule tumorali, ma anche di migliorare l'efficienza del mezzo di contrasto.

Per veicolare specificamente il sistema supramolecolare sulle cellule PC3 sovraesprimenti i recettori della bombesina sono stati progettati e sintetizzati monomeri sia per ottenere aggregati misti che autoassemblanti. I monomeri sono stati derivatizzati con la bombesina 7-14 e con il peptide *scramble* per paragonare la specificità e selettività degli aggregati. Anche in questo caso il chelante anionico ne guida l'aggregazione determinandone, cmc, forma e dimensione come dimostrato da studi di fluorescenza, DLS e SANS. Fra tutti i sistemi caratterizzati sono stati presi in

esame per le prove *in vitro* gli aggregati misti in rapporto molare 90/10 DOTA / monomero funzionalizzato con la bombesina. In particolare la porzione bioattiva è stata distanziata dalla parte idrofobica con spaziatori di natura etossilica di diversa lunghezza, cinque linker (L5=AdOO₅, Fmoc-21-amino-4,7,10,13,16,19-hexaoxa heneicosanoic acid) e un linker di 45 unità etossiliche (Peg3000).

Dai risultati ottenuti si evince che il sistema (C18)₂DOTA/bombesina-L5-(C18)₂, rispetto al sistema (C18)₂DOTA/bombesina-Peg3000-(C18)₂, mostra maggiore affinità e specificità per il recettore preso in esame. Questo risultato è imputabile al Peg, presente nel sistema (C18)₂DOTA/bombesina-Peg3000-(C18)₂, che provoca un mascheramento e ripiegamento della molecola bioattiva diminuendo la specificità nei confronti del recettore. Per indagare il sistema come mezzo per il drug delivery selettivo è stato formulato l'aggregato (C18)₂DOTA/CCK8-L5-(C18)₂, in rapporto molare 90:10, come per i sistemi precedenti. Gli aggregati di tipo liposomiale funzionalizzati con il CCK8 sono stati studiati *in vitro* per saggiare la loro tossicità e specificità sulle cellule A431, linea cellulare che esprime i recettori delle colecistochinina. Gli stessi aggregati sono stati caricati con un chemioterapico, doxorubicina, e quindi è stata valutata, la veicolazione del farmaco e il suo rilascio controllato nel tempo. I risultati ottenuti mostrano la specificità e l'efficacia del sistema verso il target cellulare scelto, in quanto parallelamente sono stati saggiati dei sistemi controllo, come il sistema con il solo agente chelante (C18)₂DOTA, e la sola doxorubicina.

Concludendo tutti gli aggregati preparati, indipendentemente dalla porzione bioattiva hanno valori delle cmc dell'ordine di 10⁻⁵ M-10⁻⁶ M, in accordo con i dati di letteratura per sistemi in cui sono presenti due code idrofobiche. Questi valori sono molto promettenti per un uso anche di aggregati micellari *in vivo*. Infatti la diluizione delle soluzioni iniettabili non comporta una concentrazione inferiore alla CMC riscontrata. Dalle indagini strutturali si evidenzia che le proprietà degli aggregati sono fortemente, come era prevedibile, influenzate dalla carica del gruppo idrofilico dei tre chelanti, per cui sono state ottenute micelle cilindriche, doppi strati ed vescicole. Gli studi di rilassività riscontrando elevati valori rilassometrici, mostrano la validità di questi sistemi da impiegare come mezzi di contrasto in grado di veicolare una quantità maggiore di ioni gadolinio contemporaneamente sulle cellule tumorali in modo da avere un'immagine ad elevata risoluzione.

Gli studi *in vitro* per valutare la selettività e la specificità degli aggregati verso la cellula bersaglio sono stati effettuati per la maggior parte dei sistemi supramolecolari, e buona parte di questi sistemi hanno dimostrato di essere altamente specifici verso il target cellulare. I risultati ottenuti con gli studi *in vitro* sono stati fondamentali e significativi per poi poter selezionare, tra tutti gli aggregati sviluppati, il sistema-guida da saggiare e valutare *in vivo*. Inoltre, questi sistemi supramolecolari in ambito terapeutico possono essere impiegati come veicoli di chemioterapici e controllare il loro rilascio nel tempo.

1. Introduction

The diagnosis and treatment of tumor pathologies at the cellular level will be greatly improved with the development of techniques that enable the delivery of analyte probes and therapeutic agents into cells and cellular compartments.

Today's diagnosis is not efficient to detect tumors to the early stage because of the contrast agents employed actually are not sensitive and specific enough to target tissues or organ; also the actual therapies sometimes have significant toxicities and side effects. There are two general, synergistic goals that should be striven for to increase the efficacy per dose of any therapeutic or imaging contrast formulation: to increase its targeting selectivity¹ and to endow the agent(s) comprising the therapeutic formulation with the means to overcome the biological barriers that prevent it from reaching its target.²

An ideal therapeutic system would be selectively directed against cell clusters that are in the early stages of the transformation towards the malignant phenotype.³ The realization of such a system faces formidable challenges, including the identification of suitable early markers of neoplastic disease, and understanding their evolution over time; the deployment of these markers in screening and early detection protocols; and the development of technology for the biomarker-targeted delivery of multiple therapeutic agents, and for the simultaneous capability of avoiding biological and biophysical barriers.

Several types of non-specific nanoparticles or supramolecular aggregates for the enhancement of diagnostic and therapeutic efficiency have been developed by basic research and used in clinical protocols. These include multiple-mode imaging contrast nano-agents and drugs that combine magnetic resonance, drug delivery with biological targeting. This is particularly important in cancer management: in fact, the selective accumulation of high-efficient contrast agents on cancer cells allows the obtainment of well-defined images, thus helping in biological characterization of tumours and accurate diagnosis. At the same time it's important also improve the potency of therapeutics agents (drug delivery). In the last years methodologies based on nanotechnology and on the molecular targeting founded several employments in the pharmaceutical field for the delivery of drug with poor bioavailability and solubility, high toxicity, or for the obtainment of therapeutic and diagnostic systems able to reach the specific target and/ or to give controlled release.

Nanosystems, which can be designed to have different compositions, have unique physical and biological properties that might be used to overcome the limitations of molecular imaging and drug delivery in recent years.⁴⁻⁷

Some of these systems, such as quantum dots (Qdots), silica nanoparticles, dendrimers, micelles, liposomes, and ultrasound microbubbles, have been extensively investigated for imaging and drug delivery applications.^{5, 8-11}

The selective delivery of diagnostic agents and anticancer drug on the target cells can be achieved by using bioactive peptides as carrier molecules. Bioactive peptides containing supramolecular aggregates will allow the reduction of undesired effects on non target organs and increase the efficacy on the desired tissues. The peptide as targeting tool has been validated in a number of applications.¹²⁻¹⁴ The bioactive peptide exposed on the external surface of the macroaggregates will be chosen in the class of bioactive peptides known for their binding ability to membrane receptors overexpressed by tumour cells. Three classes of peptides has been explored: somatostatin analogs for binding of somatostatin receptors, CCK/gastrin analogs for

binding of cholecystinin receptors and bombesin peptide for binding of the gastrin-releasing peptide receptor (GRPR). In the last ten years five somatostatin receptor sub-classes^{15, 16} receptors, and the gastrin-releasing peptide receptor, all belonging to the family of G-protein coupled receptors, have been found overexpressed in many different cancers.

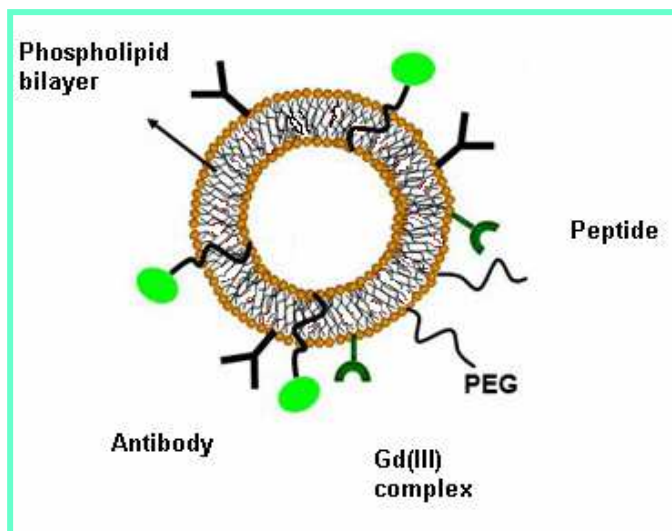


Figure 1.1: Multifunctional nanoparticle. the ability to carry one or more therapeutic agents; biomolecular targeting through one or more conjugated antibodies or peptides; imaging signal amplification, by way of co-encapsulated contrast agents; and biobarrier avoidance, exemplified by an endothelial tight-junction opening permeation enhancer, and by polyethylene glycol (PEG) for the avoidance of macrophage uptake by macrophages.

1.1. Supramolecular Systems

A supramolecular system is an excellent and functional candidate to use as diagnostic and therapeutic tool.

A supramolecular system is formed by molecules which interact by intermolecular forces like hydrogen bridges or Van der Waals interactions. Micelles and liposomes are supramolecular aggregates (Figure 1.2) obtained by spontaneous assembling in aqueous solution of amphiphilic molecules consisting of a hydrophobic and a hydrophilic moiety. The major forces that direct the self-assembly of amphiphilic molecules into well-defined structures in water derive from the hydrophobic associative interactions of the tails and the repulsive interactions between the hydrophilic head-groups.¹⁷

There is a wide variability in both the hydrophobic and hydrophilic moieties of amphiphilic molecules. The hydrophobic part can vary in length and can consist of multiple chains, creating different ratios between the size of the hydrophobic and hydrophilic parts. Moreover, the size and charge of the polar head-group can vary, dividing these molecules into ionic (anionic or cationic) or non-ionic amphiphiles. Other parameters such as pH, ionic strength, temperature and concentration, determine the geometry of the aggregate that is formed in aqueous solution and whether a micelle-like structure (spherical, cylindrical, or ellipsoidal micelles) or a bilayer-like structure (open bilayers, vesicles, or liposomes) will be formed.

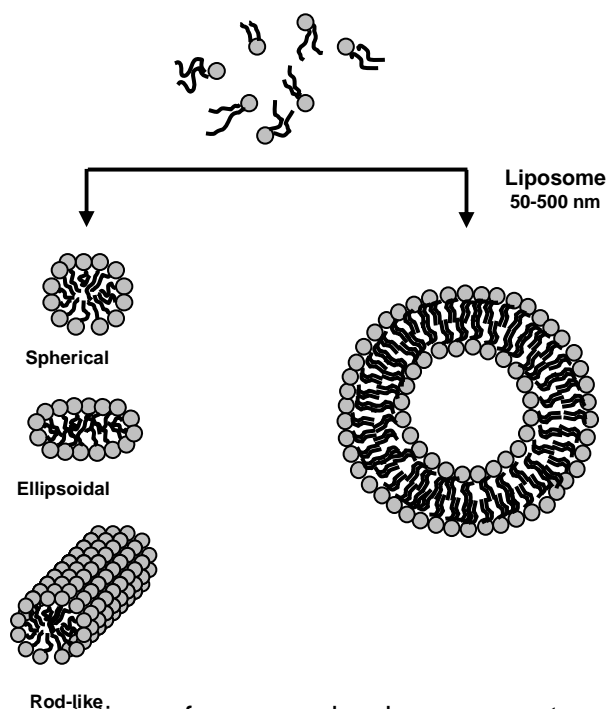


Figure 1.2: Schematic representation of supramolecular aggregates (micelles and liposomes) obtained by assembling in aqueous solution amphiphilic molecules consisting of a hydrophobic and a hydrophilic moiety. More common size and shape of these aggregates are also reported.

1.1.1 Micelles

Micelles are amphiphilic compound-formed colloidal particles with hydrophobic core and hydrophilic corona that have recently drawn much attention owing to their easily controlled properties and good pharmacological characteristics. In recent years, micelles have largely been employed as drug carriers and for controlled diagnostic agent delivery to specific target sites thanks their capability to solubilize poorly soluble drugs and to stay in the blood (tissues) rather long without recognized by certain protein or phagocyte cells. In the pursuit of different *in vivo* delivery purposes, one can easily change the size, charge and surface properties of these carriers imply by adding new ingredients to the mixture of amphiphilic substances before micelle preparation and/ or by variation of preparation methods.

The micelle aggregates have particle size within 5 to 50-100 nm range. These values allow micelles to fill the gap between such drug carriers as individual

macromolecules (antibodies, albumin, and dextran) with the size below 5 nm and nanoparticulates (liposomes, microcapsules) with the size above 100 nm. The smaller micelle size is important for selected drug administration routes since the particulate's size might control its penetration across physiological barriers. Micelles in this size range are also large enough to escape the renal filtration, which increase their blood circulation time.¹⁸⁻²⁰

The concentration of a monomeric amphiphile at which micelles appear is called critical micelle concentration (CMC), while the number of individual monomeric molecules forming a micelle is called the aggregation number of the micelle.

The CMC of these surfactants are usually in millimolar range. In *vivo*, in term of drug delivery carrier development, it's necessary to form stable micelles with lower CMC values. This is especially important from the pharmacological point of view, since upon dilution with a large volume of the blood only micelles with low CMC value still exist, while micelles with high CMC value can dissociate into monomers and their content may precipitate in the blood.

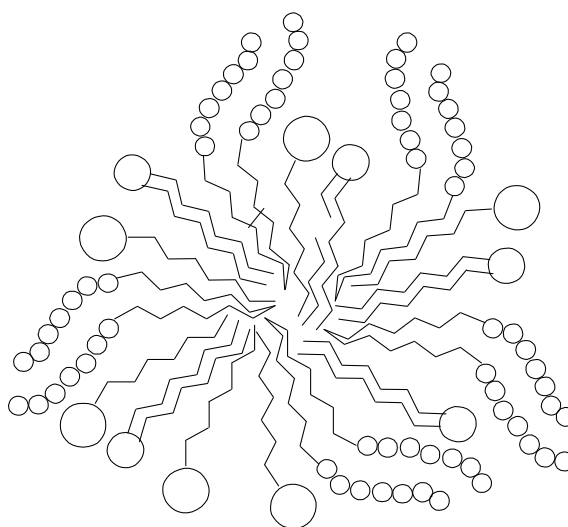


Figure 1.3: Schematic representation of the mixed micelle.

1.1.2 Liposomes

Liposomes are formed when thin lipid films are hydrated and stacks of liquid crystalline bilayers become fluid and swell. Once these particles have formed, reducing the size of the particle requires energy input in the form of sonic energy (sonication) or mechanical energy (extrusion). Liposomes have applications both as physical models of biological membranes and as prototypical drug delivery systems. Properties of lipid formulations can vary depending on the composition (cationic, anionic, neutral lipid species). The general elements of the procedure involve preparation of the lipid for hydration, hydration with agitation, and sizing to a homogeneous distribution of liposomes.²¹

The product of hydration is a large, multilamellar vesicle (LMV), with each lipid bilayer separated by a water layer. The spacing between lipid layers is dictated by

composition with poly hydrating layers being closer together than highly charged layers which separate based on electrostatic repulsion.

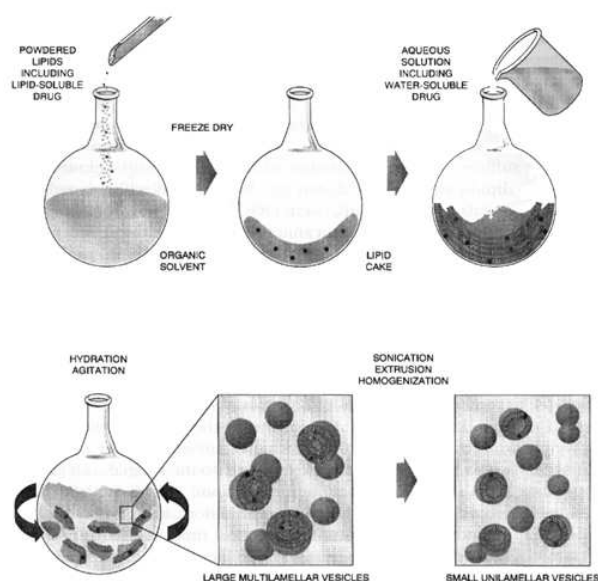


Figure 1.4: Liposome preparation: lipids are dissolved and mixed in organic solvent to assure a homogeneous mixture of lipids. Then, the solvent is removed to yield a lipid film, which is hydrated with a water solution by vortex. Finally, the solution can be sonicated for homogenization process.

Once a stable, hydrated LMV suspension has been produced, the particles can be downsized by a variety of techniques, including sonication or extrusion.

(a) Sonication: Disruption of LMV suspensions using sonic energy (sonication) typically produces small, unilamellar vesicles (SUV) with diameters in the range of 15-50nm. The most common instrumentation for preparation of sonicated particles is bath and probe tip sonicators. Also, due to the high degree of curvature of these membranes, SUV are inherently unstable and will spontaneously fuse to form larger vesicles when stored below their phase transition temperature.

(b) Extrusion: Lipid extrusion is a technique in which a lipid suspension is forced through a polycarbonate filter with a defined pore size to yield particles having a diameter near the pore size of the filter used. Prior to extrusion through the final pore size, LMV suspensions are disrupted either by several freeze-thaw cycles or by prefiltering the suspension through a larger pore size (typically 0.2 μ m-1.0 μ m). This method helps prevent the membranes from fouling and improves the homogeneity of the size distribution of the final suspension. As with all procedures for downsizing LMV dispersions, the extrusion should be done at a temperature above the T_c of the lipid. Attempts to extrude below the T_c will be unsuccessful as the membrane has a tendency to foul with rigid membranes which cannot pass through the pores. Extrusion through filters with 100nm pores typically yields large, unilamellar vesicles (LUV) with a mean diameter of 120-140nm. Mean particle size also depends on lipid composition and is quite reproducible from batch to batch.

1.2. Supramolecular aggregates as therapeutic tools

Multimodal supramolecular compounds that combine imaging and therapeutic capabilities are the focus of intensive research for applications in the growing field of nanomedicine.²²⁻²⁸

Nanoparticles with a micellar or liposomal structure obtained by assembling amphiphilic compounds²⁹⁻³¹ are promising candidates for such multifunctional therapeutic platforms, since these materials are conveniently synthesized, variably functionalized, and can be assembled to a range of sizes and compositions. Many varieties of nanoparticles are available,³² such as different polymeric and metal nanoparticles, liposomes, niosomes, solid lipid particles, micelles, quantum dots, dendrimers, microcapsules, cells, cell ghosts, lipoproteins, and different nanoassemblies. Among the most popular and well-investigated drug carriers are liposomes (mainly, for the delivery of water-soluble drugs) (Figure 1.5). For more than 2 decades they have been considered to be promising drug carriers.^{33, 34}

They are biologically inert and completely biocompatible, and they cause practically no toxic or antigenic reactions; drugs included in liposomes are protected from the destructive action of external media.

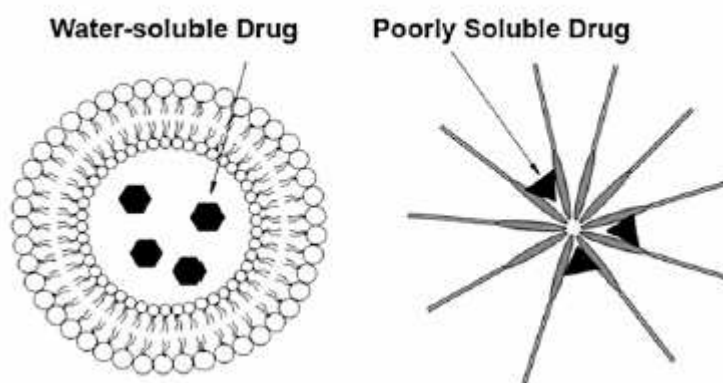


Figure 1.5: Schematic pictures of the liposome (left) and micelle (right) and their load with various drugs.

Moreover, the development of drug nanocarriers for poorly soluble pharmaceuticals is an important task, particularly because large proportions of new drug candidates emerging from high-throughput drug screening initiatives are water-insoluble, but there are some unresolved issues. The therapeutic application of hydrophobic, poorly water-soluble agents is associated with some serious problems, since low water-solubility results in poor absorption and low bioavailability.³⁵ In addition, drug aggregation upon intravenous administration of poorly soluble drugs might lead to such complications as embolism³⁶ and local toxicity.³⁷ On the other hand, the hydrophobicity and low solubility in water appear to be intrinsic properties of many drugs,³⁸ since it helps a drug molecule to penetrate a cell membrane and reach important intracellular targets.^{39, 40} Diffusion and accumulation parameters for drug carriers in tumors have recently been shown to be strongly dependent on the cutoff size of the tumor blood vessel wall, and the cutoff size varies for different tumors.⁴¹

In recent years we have been facing a progressive development of new drugs involved in cancer treatment. This new anticancer therapy can also result in cardiac and vascular adverse side effects. Cardiotoxicity can result in the alteration of cardiac rhythm, changes in blood pressure and ischaemia, and can also alter the ability of the heart to contract and/or relax. Knowledge of these toxicities can aid clinicians to choose the optimal and least toxic regimen suitable for an individual patient.

Anthracyclines, in particular doxorubicin, has been and still is among the most commonly used cytotoxic drugs given their potent anticancer activity. Its use in clinical practice is, however, limited due to the risk of congestive heart failure (CHF), which is peculiar to this class of agents. Cardiotoxicity is thought to be related to free radical damage, and is cumulative across all anthracyclines.

Acute cardiotoxicity is not dose-related and it may occur during or immediately after a single dose of anthracycline treatment.

The efforts to overcome this limit of anthracyclines have led in recent years to the development of modified formulations of liposomal doxorubicin (Myocet® and Doxil®/Caelix®) In the first product the drug is loaded in non-pegylated nanoparticles, while long PEG chains are present on the liposome surface of the latter product (PDL).⁴³ Doxil®/Caelix® is now in use for treatment of recurrent and platinum resistant ovarian cancers.⁴⁴

Preclinical studies showed that liposomal packaging of doxorubicin results in prolongation of plasma half-life and alteration in tissue distribution, with reduced cardiotoxicity demonstrated in three clinical trials in patients with metastatic breast cancer (BC), though survival rates were of concern in one of these studies. The encapsulation of doxorubicin in polyethylene glycol (PEG)-coated liposomes alters the pharmacokinetics of the drug, providing protection of the liposomes from detection by the mononuclear phagocyte system and a stabilization effect that reduces adhesion to cells, blood vessel walls and other surfaces. During circulation, at least 90% of PLD remains encapsulated within the liposomes, resulting in an extended half-life compared to conventional doxorubicin.

All the liposomal drugs on the market, as well the others now in development, are based on non-specific nanovectors. To increase therapeutic efficacy of the encapsulated drug and reduce potential toxic side effects on non-target organs, the development of nanovectors able to deliver a constant dose of the chemo-therapeutic agent directly and selectively to cancer cells over an extended period of time, may result in alternative or complementary therapeutic options for patients in early-stage cancer. The challenge lies in the design and preparation of functionalized nanoparticles that are specifically taken up by the targeted cells and release their payload over an extended period to achieve a clinical response.

1.3 Supramolecular aggregates as diagnostic tools

Currently the more promising medical diagnostic imaging procedures in use are γ -Scintigraphy (PET, SPECT, NM) and Magnetic Resonance Imaging (MRI). γ -Scintigraphy is based on the application of γ -emitting radioactive atoms, such as ^{99m}Tc, ¹¹¹In, ¹²⁵I, ¹³¹I, ⁶⁷Ga, and some other isotopes with variable decay time; Magnetic Resonance Imaging concerns with the phenomenon involving the transition between different energy levels of atomic nuclei under the action of radiofrequency. The critical point for these techniques is that both modalities require a different amount of reporter compounds (CAs) to be accumulated in the area of interest.^{44, 45}

In fact, contrast agents, able to absorb or to emit radioactive or electromagnetic signals stronger than surrounding tissues help to discriminate between normal and pathological regions. The quantity of reporter compound to be accumulated in the area of interest strongly varies between the two imaging techniques. The very sensible γ -scintigraphy requires very low tissue concentration (10^{-10} M) of radionuclides such as ^{111}In and $^{99\text{m}}\text{Tc}$ to give diagnostically significant, low resolved images. In contrast, MRI gives very resolved images but, due to its very low sensitivity, needs high concentration (10^{-2} M) of contrast agent such as paramagnetic Gd^{3+} complexes. To reach the required local concentration of the contrast agent many carriers have been developed such as liposomes⁴⁶ and other microparticulates,⁴⁷ micelles,⁴⁸ dendrimers,⁴⁹ linear polymers,^{50, 51} proteins,⁵² or peptides,⁵³ all of these derivatized with the metal complex of interest. Among those carriers, micelle and vesicles have recently drawn much attention owing to their easy controlled properties and good pharmacological characteristics.⁵⁴ For example, the self-assembling micelle organization of Gd^{3+} (DOTA) complex derivatized with a lipophilic tail allows the obtaining of a high relaxivity MRI contrast agent.⁵⁵

There is an increasing interest in developing new contrast agents with enhanced properties. First, the new contrast agents should have high contrast activity of the metal complex. This is critical for MRI applications: high relaxivity of the paramagnetic Gd complexes allows reducing of the reporter compound the very high concentration to be realized in the area of interest. Second, the new contrast agents should be selective for a specific target, such as membrane receptors overexpressed by cancer cells. Therefore the total amount of the contrast agent to be injected for diagnostic analysis could be reduced.

In the last years, micelles and liposomes have been also investigated as possible carriers of Gd(III)-chelates to enhance the contrast efficacy and to change the pharmacokinetic properties of MRI contrast agents. The biodistribution of micelles and liposomes is highly dependent on their physicochemical properties such as size, surface charge or membrane composition.⁵⁶⁻⁵⁹

In the pursuit of different *in vivo* delivery purposes, one can easily change the size, charge and surface properties of these carriers simply by adding new ingredient to the mixture of amphiphilic substances used in their preparation and/or by changing the preparation methods. However, conventional micelles and liposomes are to a large extent taken-up by the reticuloendothelial system (RES). These properties make supramolecular aggregates excellent candidates to carry contrast agents for MRI, and in the 1980s the first studies about the use of liposomes as carriers of MRI contrast agents appeared in the literature. It is possible to distinguish between two different classes of liposomal contrast agents: in the first one, contrast agents are entrapped within the internal aqueous space of liposomes⁶⁰; in the second class, lipophilic contrast agents are incorporated in the lipid bilayer of the liposome.^{61, 62} Classical gadolinium complexes such as Gd-DTPA, Gd-DTPA-BMA and Gd-HPDO3A are entrapped within the internal aqueous space of lipid vesicles: the main target for these supramolecular aggregates is the liver (Kupffer cells), and the clearance of gadolinium complexes is slow.⁶³ While investigating blood vessels and the possibility of using these liposomes for MRA application, it was observed that the relaxivity enhancement is limited and the relaxivity of liposomes entrapping gadolinium chelates is about two to five times lower than that of the isolated gadolinium complexes in solution. The relaxivity of the entrapped paramagnetic species is lowered because of the limited exchange of bulk water with the contrast agents.^{60, 64} This exchange is dependent on the permeability of the liposomal

membrane to water.⁶⁵ In the second class of liposomal contrast agents a hydrophilic chelating agent is covalently linked to a hydrophobic chain. The lipid part of the molecule is anchored either in the liposome bilayer while the more hydrophilic gadolinium complex is localized on the liposome surface.^{66, 67} Chelating probes of this type can be divided into at least three categories: in the first one, aggregates are obtained directly by the self-assembly of an amphiphilic chelating agent; in the second one, aggregates are obtained by mixing a synthetic amphiphilic chelating agent with one or more commercial phospholipids; in the third example, the formulations based on the self-assembly of polymeric amphiphiles functionalized with the contrast agent.

1.4 Target selective supramolecular aggregates

Selective delivery of drugs and/or contrast agents to the target organs can be achieved by functionalizing the supramolecular aggregates with a bioactive targeting molecule. The use of targeted supramolecular aggregates offers the prospect to increase diagnostic accuracy and therapeutic effectiveness, while minimizing side effects from treatment. Nowadays, different synthetic procedures have been developed to introduce the bioactive molecule on the external surface of the supramolecular aggregate.⁶⁸

The choice of synthetic strategy depends on whether coupling is performed before or after assembly of the supramolecular aggregate. The obvious goal of each approach is to achieve high coupling efficiency, but with the ligand retaining full binding affinity for its target receptor. The coupling of a ligand after the aggregate has been assembled involves the introduction of suitable activated functional groups onto the terminus of one of the aggregate components. Activated functional groups must be compatible with the aggregation process and should remain available on the aggregate surface for efficient chemical ligation of the bioactive ligand. Another example with this approach is based on the obtainment of biotinylated aggregates using a biotinylated lipophilic monomer in the surfactant mixture; in a two-steps process the biotinylated supramolecular aggregates react with avidin and then with the biotinylated peptide or antibody giving a non-covalently labelled compound (Figure. 1.6b). This strategy has proven to be particularly successful for the coupling of large ligands such as monoclonal antibodies. The coupling of a bioactive ligand to an aggregate component before aggregation is, in principle, chemically less complicated, but has the disadvantage that, at least in the case of liposomes, following final assembly of the aggregate a fraction of the conjugated bioactive ligand remains entrapped in the interior region and is not more available for receptor binding. This labelling procedure, based on the use of amphiphilic peptides that assemble together with amphiphilic gadolinium complexes in the peptide labeled supramolecular aggregates, is schematized in Figure. 1.6 c.

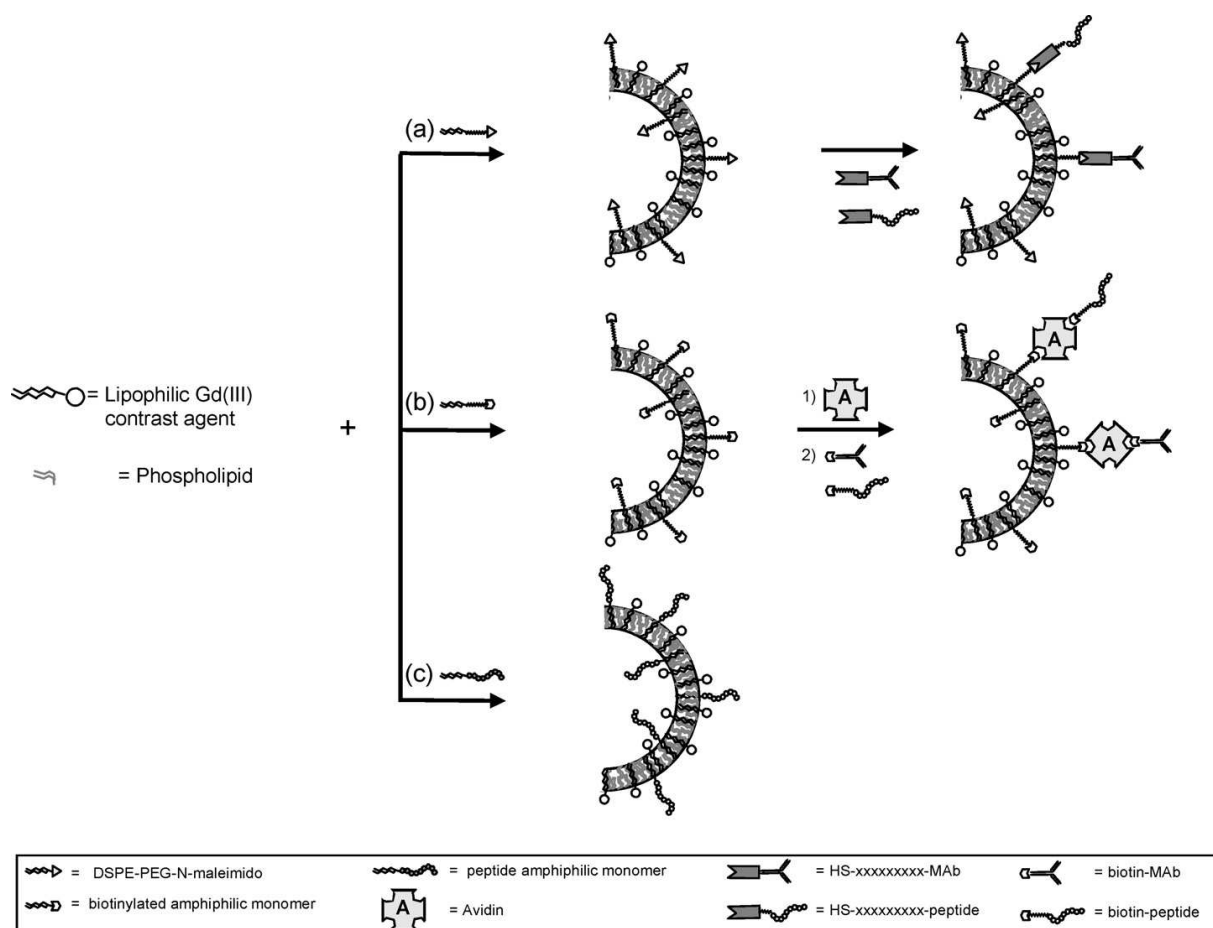


Figure 1.6: Examples of labelling procedures to introduce the bioactive molecule on the external surface of supramolecular aggregates.

1.5 Target selective aggregates for drug delivery

Liposomes and polymeric micelles are excellent drug carriers. These drug carriers as well as any other pharmaceutical nanocarriers when they are surface modified by a variety of different moieties to impart them with certain properties and functionalities. These functionalities are expected to provide nanocarriers: (1) prolonged circulation in the blood^{69, 70} and ability to accumulate in various pathological areas (eg, solid tumors) via the EPR effect (protective polymeric coating with polyethylene glycol [PEG] is frequently used for this purpose),^{71, 72} (2) the ability to specifically recognize and bind target tissues or cells via the surface-attached specific ligand (monoclonal antibodies as well as their Fab fragments and some other moieties, eg, folate or transferrin, are used for this purpose),⁷³ (3) the ability to respond to local stimuli characteristic of the pathological site by, for example, releasing an entrapped drug or specifically acting on cellular membranes under the abnormal pH or temperature in disease sites (this property could be provided by surface-attached pH- or temperature-sensitive components); and (4) the ability to penetrate inside cells bypassing lysosomal degradation for efficient targeting of intracellular drug targets (for this purpose, the surface of nanocarriers is additionally modified by cell-penetrating peptides).

The targeting molecule can be a macromolecule such as antibodies, peptides, peptidomimetics, or smaller organic molecules such as folic acid.

The antibody-mediated liposome targeting, although various monoclonal antibodies have been shown to deliver liposomes to many targets, the optimization of properties of immunoliposomes is an ongoing concern. The majority of research in this area relates to cancer targeting, which utilizes a variety of antibodies. Internalizing antibodies are required to achieve a much-improved therapeutic efficacy with antibody-targeted liposomal drugs, as shown with B-lymphoma cells and internalizable epitopes (CD19), for example.⁷⁴

In 2001 Papahadjopoulos et al. developed an interesting liposomal system (anti-HER2 liposomes) able to target HER2-overexpressing tumours.⁷⁵

NUCLEOSOME-specific antibodies capable of recognizing various tumour cells through tumour-cell-surface-bound nucleosomes improved Doxil (Alza) targeting to tumour cells and increased its cytotoxicity.⁷⁶

Immunoliposomes containing the novel antitumoral drug fenretinide, and targeting the GANGLIOSIDE GD2, induced apoptosis in neuroblastoma and melanoma cell lines, and demonstrated strong antineuroblastoma activity both *in vitro* and *in vivo* in mice.⁷⁷

A combination of immunoliposome and endosome-disruptive peptide improves the cytosolic delivery of the liposomal drug, increases cytotoxicity and opens up new avenues for constructing targeted liposomal systems; this was shown with the diphtheria toxin A chain, which was combined with pH-dependent fusogenic peptide diINF-7 into integrated liposomes specifically targeted to ovarian carcinoma.⁷⁸

Targeting tumours with folate-modified liposomes represents a popular approach, because folate receptors (FR) are frequently overexpressed in a range of tumour cells. Liposomal daunorubicin⁷⁹ as well as doxorubicin⁸⁰ have been delivered into various tumour cells through FR and demonstrated increased cytotoxicity. Transferrin (Tf) receptors (TfR) are overexpressed on the surface of many tumour cells, and so antibodies against TfR, as well as Tf itself, are popular ligands for liposome targeting to tumours and inside tumour cells.⁸¹

Recent studies involve the coupling of Tf to PEG on PEGylated liposomes to combine longevity and targetability for drug delivery into solid tumours.⁸²

The search for new ligands for liposome targeting is focused on specific receptors that are overexpressed on target cells (particularly cancer cells) and certain specific components of pathological cells. For example, liposome targeting to tumours has been achieved by using vitamin and growth factor receptors.⁸³

Several examples of drug delivery supramolecular systems derivatized with peptidic moiety are also reported in literature. As first, vasoactive intestinal peptide (VIP) has been used to target PEG liposomes with radionuclides to VIP receptors on the surface of tumour cells, and resulted in enhanced breast cancer inhibition in rats.⁸⁴

In addition, PEG liposomes loaded with doxorubicin have been targeted by RGD peptides to the integrins of tumour vasculature and demonstrated increased efficiency against C26 colon carcinoma in murine model.⁸⁵ RGD peptides were also used for targeting liposomes to integrins on activated platelets, and could therefore be used to specifically target the cardiovascular system.⁸⁶

Another new approach to liposome targeting involves the functionalization of liposomes with peptide as CCK, bombesin, somatostatin (analogs octreotide, vapreotide, lanreotide) and VIP targeted on overexpressing tumor cells receptors.

1.6 Target selective Aggregates for MRI

Mulder et al.⁸⁷ developed pegylated paramagnetic liposomes, immuno-liposomes, derivatized with antibody molecules coupled to the distal end of the PEG chains. The chosen antibody is able to detect E-selectin expression on human umbilical vein endothelial cells. The T₁-weighted image of pellets containing 10⁶ TNF α treated human umbilical vein endothelial cells, incubated with the E-selectinAB-liposomes had a much higher signal intensity than that of control systems, due to a large shortening of T₁ in this system. The same authors described, very recently, the use of pegylated, fluorescent and paramagnetic micelles (immuno-micelles) for imaging of macrophages in atherosclerotic plaques.²⁸ A different approach in preparing immuno-micelles was used by the same authors:^{88,90-92} they obtained mixed micelles containing a little amount of DPPE-biotin. Immuno-micelles are obtained by adding, first, a specific amount of avidin to the biotinylated micelles and, then, the biotinylated antibodies. They were used for ex-vivo images⁸⁹ and *in vivo* experiments⁹⁰ to detect atherosclerosis, targeting macrophage scavenger receptors. Both studies confirmed that this kind of immuno-micelles provides excellent validated *in vivo* enhancement of atherosclerotic plaques. The same approach based on biotin-avidin affinity interaction has been used by Li and co-workers in their pioneeristic work on immuno-liposomes. They prepared polymerized vesicles of 300-350 nm in diameter by UV irradiation^{88, 91,92}, then derivatized the liposomes with a LM609 monoclonal antibody. Very interesting results have been obtained for *in vivo* detection of tumour angiogenesis targeting the integrin $\alpha_v\beta_3$.⁹² This approach provides enhanced and detailed imaging of rabbit carcinomas by directly targeting the gadolinium based contrast agent to the angiogenic vasculature. In addition, angiogenic “hot spots” not seen by standard MRI were detected. Similar antibody conjugated paramagnetic polymerized liposomes were used to target the intercellular adhesion molecule-1, an endothelial leukocyte receptor on cerebral microvasculature in experimental autoimmune encephalitis.⁹³ High resolution MRI of mouse brains *ex vivo* demonstrated that antibody conjugated gadolinium based liposomes binding conferred significant enhancement of signal intensity as compared to control images. Gadolinium based paramagnetic supramolecular aggregates derivatized with bioactive peptides have been essentially developed in order to have selective contrast agents capable of visualizing neovascularization and angiogenic processes targeting $\alpha_v\beta_3$ integrins or tumour proliferation and metastasis targeting cellular receptors that are overexpressed by cancer cells. Some interesting supramolecular constructs, containing the RGD peptide sequences, were initially developed by Stupp and co-workers.^{94, 95} Moreover, van Tilborg recently developed lipid-based bimodal contrast agents that enable the detection of apoptotic cells, by functionalizing liposomes with the apoptosis target protein Annexin-5.⁹⁶ Schimeder et al.⁹⁷ prepared nanoparticles assembling together perfluorooctylbromide (PFOB), a surfactant mixture, the lipophilic gadolinium complex Gd-DTPA-bisoleate, and a little amount of MPB-PEG2000-DSPE; the nanoparticles were derivatized by conjugating a thiolated peptidomimetic vitronectin antagonist to the maleimidophenyl function of MPB-PEG2000-DSPE. These nanoparticles were used to detect and characterize angiogenesis of developing melanoma xenografts in nude mice. Similar liposomes, conjugated with the $\alpha_v\beta_3$ -specific RGD peptide attached to PEG moieties, have been developed by Mulder et co-workers.^{98, 99} These liposomes were used as MRI contrast agents in *in vitro* and *in vivo* studies for detection of $\alpha_v\beta_3$ -integrin and visualization of proliferating human activated endothelium tumour.

Moreover these nanoparticles can be used, by MRI techniques, to non-invasively measure the efficacy of angiogenesis inhibitors during the course of a therapy.⁹⁹

Griffioen et co-workers used Anginex, a synthetic 33-mer angiostatic peptide that is capable of homing to activated endothelium, as targeting ligand.¹⁰⁰ Paramagnetic liposomes obtained by co-aggregation of Gd-DTPA-BC18, maleimide-PEG2000-DSPE, DSPC and cholesterol, were derivatized with Anginex by covalently attaching the synthetic peptide by sulphhydryl-maleimide coupling to maleimide-PEG-DSPE and studied *in vitro* on cell cultures and by MRI of cell pellets. The results indicate that the angiostatic peptide Anginex is a potent ligand for the targeting of paramagnetic liposomes to activated endothelial cells; in addition the *in vitro* results showed a high specificity of the anginex-conjugated paramagnetic liposomes for endothelial cells that was confirmed by MRI.

A different approach was used by Mulder¹⁰¹ that developed MRI detectable and targeted quantum dots. Quantum dots were coated with paramagnetic and pegylated lipids, which resulted in a relaxivity, r_1 , of nearly 2000 mM⁻¹s⁻¹ per quantum dot. The quantum dots were functionalized by covalently linking $\alpha_v\beta_3$ -specific RGD peptides, and the specificity was assessed and confirmed on cultured endothelial cells. For their high relaxivity and target specificity these constructs seem excellent contrast agents for molecular imaging of tumour angiogenesis. Polymeric constructs have been developed by Ke et al.¹⁰² They prepared cyclic RGDdFK target poly(L-glutamic acid)-(Gd-DO3A) conjugate with a biodegradable cystamine spacer, and evaluated these construct for *in vivo* detection the angiogenic biomarker $\alpha_v\beta_3$ -integrin in neoplastic tissues with T₁ mapping by MRI. The targeted conjugate showed high specific binding to human prostate carcinoma cells with a significant decrease of T₁ values.

Gadolinium-based paramagnetic supramolecular aggregates derivatized with bioactive peptides have been essentially developed in order to have selective contrast agents capable of visualizing tumour proliferation and metastasis targeting cellular receptors that are overexpressed by cancer cells. Several supramolecular aggregates derivatized with the CCK8 bioactive peptide on their surface have been developed by Morelli and Paduano.^{88, 103-106}

Most of these systems have been obtained by co-assembling two amphiphilic monomers, one containing the gadolinium complex and the other the bioactive peptide CCK8. The presence in the aggregates of two separated monomers allows the tuning of the ratio between the active components in order to find the right compromise between the number of peptide targeting molecules on the aggregate surface, and of the gadolinium-chelate complexes. The peptide sequence (Asp-Tyr-Met-Gly-Trp-Met-Asp-Phe-amide, CCK26-33 or CCK8) corresponds to the C-terminal fragment of the cholecystokinin hormone and provides the binding sequence for the cholecystokinin receptor subtypes A and B (CCKA-R and CCKB-R).¹⁰⁷

Overexpression of both of these receptor subtypes has been demonstrated in certain human tumours: CCKA-R is overexpressed in pancreatic cancer, and CCKB-R has been found in small cell lung cancer, colon and gastric cancers, medullary thyroid carcinomas, astrocytomas and stromal ovarian tumours.¹⁰⁸

The design of the molecules has been developed with the main aim to realize supramolecular aggregates (micelles or liposomes) suitable for *in vivo* use as target selective contrast agents. The possibility of using micellar or liposomal compounds for imaging purpose depends on the degree of stability of the imaging agent in the body. Liposomes show high stability in biological fluid, while micellar stability depends by its critical micellar concentration. Physiologically stable micelles (cmc value in a

micromolar or low millimolar region) can be performed by using either monomers with two or more alkyl chains, or by polymerizable amphiphilic Gd(III) complexes. High contrast efficacy can be achieved by designing supramolecular paramagnetic MR-contrast agents characterized by high rigidity and good access of bulk water to the paramagnetic center. High rigidity can be obtained combining together a restricted motion of the contrast agent of the amphiphilic gadolinium complexes in the aggregate and a high molecular weight of the particle.

1.7 Specific-targeting Peptide

The field of peptide targeting of tumors is moving fast at the moment. Cancer research on peptides is presently dominated by two active fields: one is the search for new peptide receptors overexpressed in specific tumors, i. e., suitable peptide targets. The second field consists of the search and the discovery of new radiopeptides and cytotoxic peptides, their development for potential clinical use in the previously defined targets, and the resulting clinical efforts to optimize peptide receptor targeting.

Then in the last twenty years, the targeting of overexpressed peptide receptors in tumors by small peptides has become a very strong focus of interest for nuclear medicine as diagnostic and therapeutic tools. For a better understanding of these clinical applications is fundamental/opportune a knowledge about peptides and peptide receptors, in particular their tissue expression, their role, or potential applications, in cancer pathogenesis, diagnosis, and treatment.

Peptides are molecules consisting of several amino acids linked together with peptide bonds. The size of peptides can vary from molecules with only two amino acids to as many as 50. In contrast to proteins, they generally do not possess a well-defined three-dimensional (tertiary) structure. Moreover, peptides do not only exist in natural form but also can be designed synthetically as novel molecules. Thus, their actual number is presently very large. There is a large group of peptides so-called regulatory peptides that includes the neuropeptides present in the brain, the gut peptide hormones, as well as peptides present in the vasculature (vasoactive peptides) and peptides of the endocrine system. Recently particular attention has been devoted to somatostatin, vasoactive intestinal peptide (VIP), cholecystokinin (CCK), gastrin-releasing peptide (GRP), and neurotensin. In general terms, these regulatory peptides represent a group of different families of molecules known to act on multiple targets in the human body at extremely low concentrations.¹⁰⁹ Targets of these peptides are not only the brain and the gastrointestinal tract, but also the endocrine system, the kidneys, the lungs, and the immune, vascular, and peripheral nervous systems. Therefore, regulatory peptides control and modulate the function of almost all key organs and metabolic processes. Their action is mediated through specific membrane-bound receptors; almost all belong to the group of G protein-coupled receptors. They can influence many intracellular effector systems; for instance, the emerging role of peptides in MAPK pathways, known to play an important role in cell proliferation, or in apoptosis, may contribute to the current interest for peptides in cancer research.^{110, 111} Receptor subtypes with their own ligand specificity and second messenger systems exist for almost all regulatory peptides, thus increasing the diversity of their mode of action. These peptides may play prominent roles in not only normal conditions but also pathological processes. They may be factors involved in inflammation, but may also play a receptor-mediated role in cancer and cancer progression.

2. Aim of thesis

The aim of the doctorate thesis is that developing supramolecular aggregates able to vehicle contrast agents on cancer cells for nuclear medicine techniques and MRI, and to prepare new chemiotherapeutic drugs. The selectivity of the aggregates is caused by bioactive peptides able to recognize receptor cells.

The bioactive peptides are selected in order to prepare aggregates able to join a wide number of cancer cells class. As reported in the previous section octreotide, bombesin and CCK8 can bind with high affinity somatostatin, GPR and cholecystokinin receptors respectively. On the basis of this results, new amphiphilic monomers containing the peptide moiety, a hydrophilic spacer and the lipophilic tails are designed and synthesized. In the same molecules in some case a chelating agent able to coordinate radioactive or paramagnetic metals is also inserted. To increase the chelating agent units versus the bioactive peptide, new amphiphilic monomers bearing the lipophilic tails are designed. These monomers can act as anionic surfactant agent pushing the co-aggregation with the peptide monomers. The aggregates formulated are investigated by physical chemical methods like DLS (Dynamic Light Scattering), SANS (Small Angle Neutron Scattering), relaxivity measurements and spectroscopy techniques. These studies allow to select the best systems for shape and size in relation with the relaxivity parameters and the aggregation stability. To validate the specificity and the toxicity of the delivery systems, studies *in vitro* are conducted. The results allow to evaluate the lead system to test *in vivo* the effective ability to target tumor in mice.

3. Octreotide labeled supramolecular aggregates

3.1 Introduction

Somatostatin consists of a family of a 14-amino-acid (somatostatin-14) and a 28-amino-acid (somatostatin-28) peptide (Figure.3.1). It appears in several organ systems, such as the central nervous system, the hypothalamopituitary system, the gastrointestinal tract, the exocrine and endocrine pancreas, and the immune system. In these different organ systems, somatostatin can be considered to be a neurotransmitter, a neurohormone, or a local hormone acting via autocrine or paracrine mechanism.¹¹² There are five human somatostatin receptor subtypes (SSTR1-SSTR5), belonging to a superfamily of G protein-coupled receptors that can functionally couple to various intracellular effector systems. All five Somatostatin-receptors (SSTRs) have been found in numerous kinds of human tumors (e.g., breast tumors, small-cell lung cancer), first of all the SSTR2 subtype.

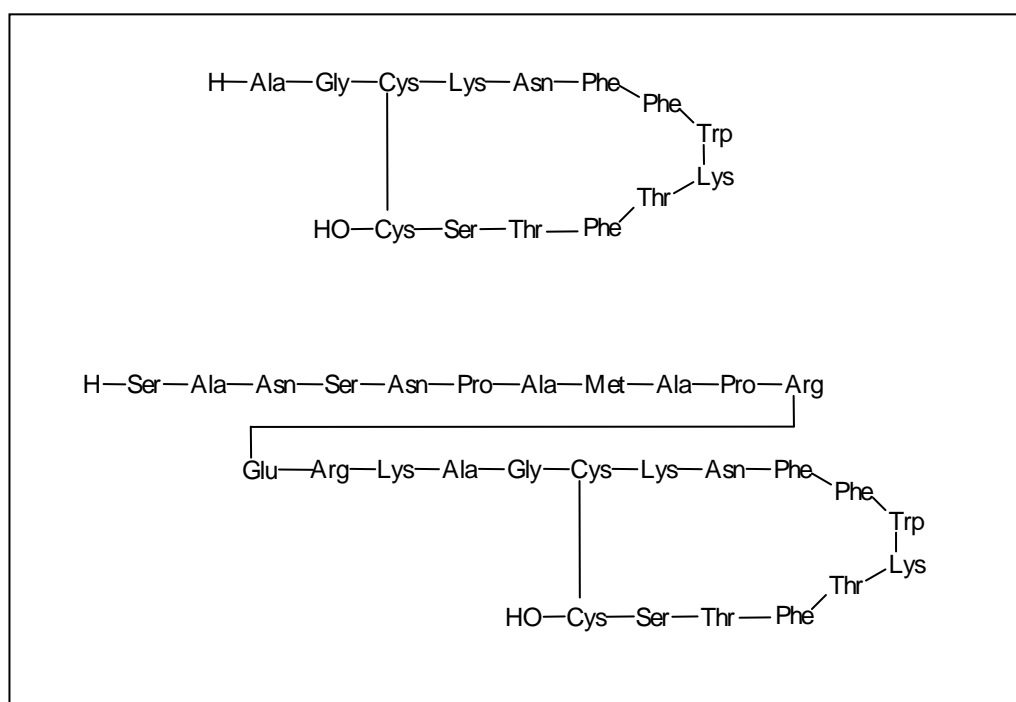


Figure 3.1: Schematic representation of somatostatin-14 and somatostatin-28 peptides

The native peptide somatostatin is rapidly degraded in vivo and has a very rapid blood clearance time ($T_{1/2}$, 2-4 minutes). This issue push to develop analogs able to improve the circulating time and enhance the stability to enzymatic cleavage. The most successful derivative is octreotide, a cyclic octapeptide (Figure 3.2), that adopts in solution two conformational families, differing mainly by the conformation of the C-terminal moiety. The molecule adopts an overall antiparallel β sheet conformation, with a type II' β turn in the D-Trp⁴-Lys⁵ residues. In one conformational family, the residues after this β turn continue the β sheet structure, and in the second family, the

residues after the β turn adopt a 3_{10} helical conformation.^{113, 114} These conformation have to be hold in octreotide conjugate. These requirements allow to modify only the N-terminal moiety introducing a spacer, chelating agents or fluorophore groups.

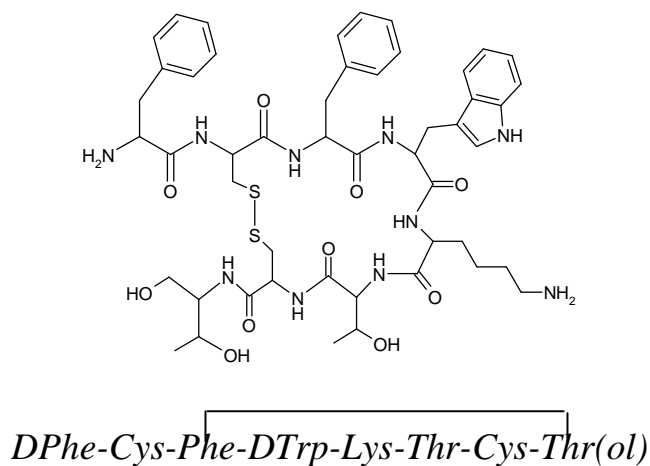


Figure 3.2: Schematic representation of octreotide peptide

Moving from these assessments, the monomers design provides a hydrophilic and a hydrophobic moiety to push the self-aggregation or the insertion in ionic surfactants to achieve mixed aggregates. The hydrophilic moiety has to contain the peptide which has to be well-exposed on the aggregate surface and/or a chelating agent which can improve the hydrophilic characteristic of the molecules. Instead, the hydrophobic moiety is formed by a fat chain. The major forces that direct the self-assembly of amphiphilic molecules in water towards well-defined structures derive from the hydrophobic associative interactions of the tails and the repulsive interactions between the hydrophilic head-groups.¹⁷ The hydrophobic tail can vary in length and can consist of multiple chains of the alkyl nature, creating different ratios between the size of the hydrophobic and hydrophilic parts. Moreover, the size and charge of the polar head-group can induce the shape and the size of the aggregate. The achievement of this monomers has to fulfill two requirements: (i) chemical modifications on octreotide should preserve the peptide receptor binding capability; (ii) after the aggregation process, the peptide molecules and the gadolinium complexes have to lie in hydrophilic shell of the supramolecular aggregates to preserve the peptide bioactivity and to allow water exchange in the gadolinium coordination sphere. The first requirement was fulfilled by introducing modifications at *N*-terminal end of the peptide sequence. In fact, recent studies show that a hydrophilic or hydrophobic chain covalently bound on the *N*-terminus of *D*•Phe residue results in low effect on binding constants of octreotide to the receptors.¹¹⁵ The second need could be satisfied by introducing linkers of variable length, chosen to increase the hydrophilicity of the head without change the charge of the monomers.

3.2 Results & Discussion

3.2.1 Monomers Design and Synthesis

The requirements discussed in the previous section set up the selection of chelating agents and the hydrophilic spacer able to increase the octreotide exposition towards the outer sphere. The chelating agents chosen as head group of the monomers are DOTA, DTPA, or DTPAGlu. The first one belongs to the macrocycle class of chelating agents, while DTPA and DTPAGlu to the branched chelating agent. They were selected to study the influence of the steric hindrance and of the residual charge presents in the hydrophilic shell on the aggregation behavior. In fact, the difference between the three chelating agents is the number of charges (carboxylic groups). They have 3,4 and 5 negative charges as free bases and 0, 1 and 2 as gadolinium complex, respectively

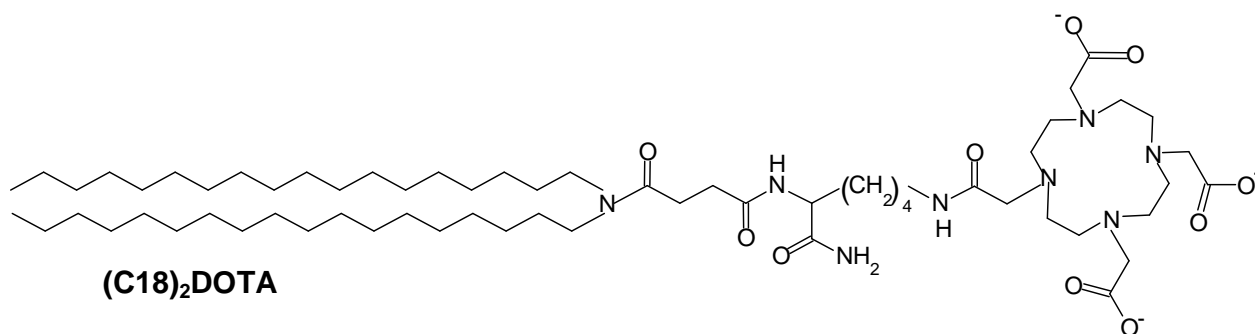
The five ethoxylic spacers were bound on N terminal moiety of the octreotide to compromise between the hydrophilic length and the exposition of the peptide. The oxoethylene moieties are not toxic and reduce aggregate clearance through the reticulo-endothelial system (RES).¹¹⁶

Two alkyl chains at eighteen carbon atoms were chosen as hydrophobic moiety in order to obtain a structure similar to the phospholipidic bilayer of the membrane and to avoid the haemolytic effect on the cells. Moreover, the eighteen carbon chains allow a sufficient number of Van der Waals interactions to obtain stable aggregates.

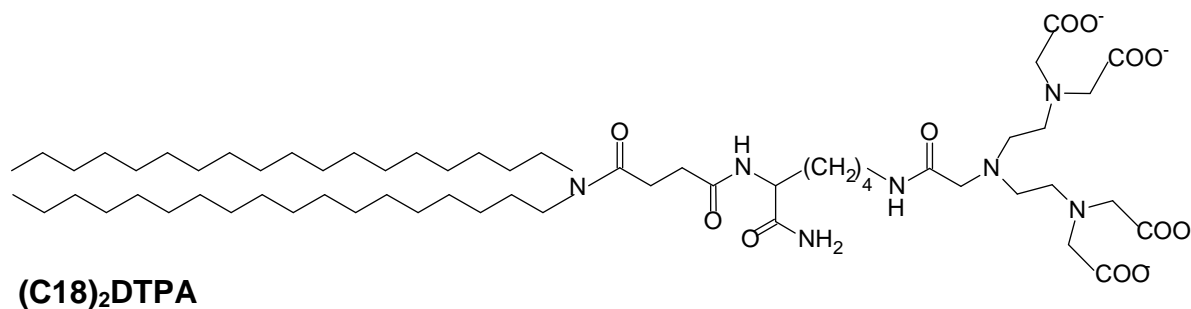
In Figure 3.3 are reported the schematic representation of the synthetic monomers containing the chelating agents or the peptide moiety. Moreover, we have been synthesized amphiphilic monomers (OCA-DTPAGlu and OCA-DOTA) containing (Figure. 3.4), in the same molecule, three different functions: (i) the chelating agent (ii) the octreotide (iii) a hydrophobic moiety. To preserve the peptide bioactivity and to allow water exchange in the gadolinium coordination sphere can be introduced two units of 21-amino-4,7,10,13,16,19-hexaoxa heneicosanoic acid (AhOH) between the lysine and the octreotide *N*-terminal residue. The branching of the monomers head group was achieved using a lysine residue. On its α amine function, another unit of the linker was bound to space the hydrophilic head from the lipophilic tails; while on lysine side chain, the selected DOTA or DTPAGlu chelating agent was condensed to distance them far away from the octreotide moiety.

The chelating agents containing monomers were synthesized by solid-phase methods according to standard SPPS protocols. The Rink Amide MBHA polymeric resin was used to obtain the amide function on the *C*-terminal carboxyl group.

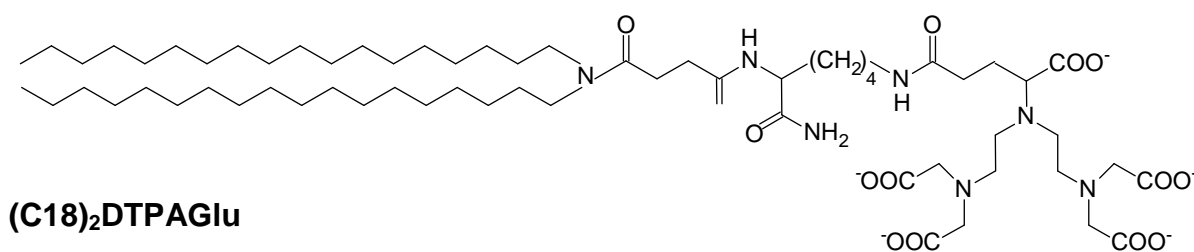
(a)



(b)



(c)



(d)

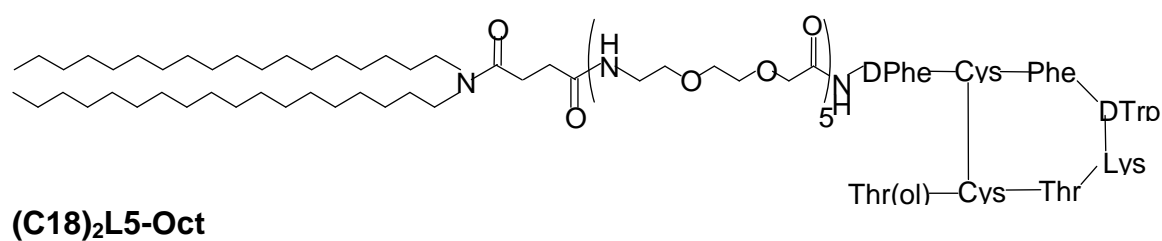


Figure 3.3: Schematic representation of (C18)₂DTPAGlu, (C18)₂DTPA, (C18)₂DOTA and (C18)₂L5-Oct amphiphilic monomers.

already reported for other DTPAGlu or DOTA gadolinium complexes. The Gd(III) titration is conveniently followed by measuring ^1H -relaxation rates.

3.2.2 Aggregates Preparation and Characterization

Supramolecular aggregates have been prepared by self-assembling of $(\text{C18})_2\text{DOTA}$, $(\text{C18})_2\text{DTPA}$, $(\text{C18})_2\text{DTPAGlu}$ and the OCA-DOTA and OCA-DTPAGlu as free base or their corresponding gadolinium complexes. All supramolecular aggregates were formulated dissolving monomers in phosphate buffer at pH 7.4 following well-assessed procedures. All mixed aggregates as reported in the Table 2 were prepared at 90:10 molar ratios mixing the chelating agents containing monomer and the Octreotide containing monomer. Critical micellar concentration (*cmc*) value were determined by the fluorescence based method using 8-anilinonaphthalene-1-sulfonate (ANS) and Pyrene (Pyr) as probes. ANS and Pyr are two fluorescent probes poorly soluble in aqueous media that change their emission spectrum in function of solvent polarity (hydrophobic or hydrophilic). ANS fluorophore gives fluorescence emission at 480 nm only in hydrophobic environment such as the inner micellar compartment;¹¹⁸ whereas the fluorescence emission spectrum of pyrene shows vibrational bands which are affected by the polarity of the surrounding environment of the probe molecules. Specifically, changes in the relative intensity of the first (I_1 at 373 nm) and the third (I_3 at 385 nm) vibrational bands in the pyrene emission spectrum have been proven to be reliable tools in examining the polarity of the microenvironment.¹¹⁹ In the ANS method, the fluorescence intensity at 480 nm corresponding to the maximum of spectrum, is reported on function of the amphiphile concentration. The break-point in Figure 3.5 indicates a *cmc* value of $2.3 \cdot 10^{-6} \text{ mol kg}^{-1}$ and $2.0 \cdot 10^{-5} \text{ mol kg}^{-1}$ for OCA-DTPAGlu monomer as metal free base and as gadolinium complex, respectively. Cmc values were also evaluated by steady-state fluorescence spectroscopy of pyrene. In this approach, the ratio between the intensities of the first (I_1) and third (I_3) vibrational bands of the pyrene emission spectrum decreases with the polarity of the medium in which pyrene is dissolved. I_1/I_3 remains constant (1.4–1.5) at monomer concentrations $10^{-6} \text{ mol kg}^{-1}$, below which pyrene is in an aqueous environment, which indicates the absence of micelles. As soon as micelles are formed, pyrene migrates into the hydrophobic core (or into the core/corona interface) and I_1/I_3 decreases. Cmc values measured by the Pyr method both for micellar systems in which chelating agent monomers are present as free bases and as gadolinium complexes are in good agreement with values obtained by the ANS method.

Critical micelle concentration values of the self-assembling aggregates are in the $3.2 \cdot 10^{-5} \text{ mol Kg}^{-1}$ and $6 \cdot 10^{-7} \text{ mol Kg}^{-1}$ range. Analyzing the trend is possible to highlight two assessments: i) the influence of the negative charge ii) the influence of steric hindrance. The *cmc* increases in relation with the number charges. In fact the aggregates containing gadolinium complex show the lower values with respect to aggregates containing the chelating agents as free base. Moreover, the steric hindrance increases the *cmc* of $(\text{C18})_2\text{DOTA}$ related to the $(\text{C18})_2\text{DTPA}$ (Table 3.1). The same trend is show with both methods (ANS and Pyrene). The mixed systems show the same *cmc* trend that the self-assembling aggregates (Table 3.2). On the basis of structural characterizations performed on self-assembling aggregates of a similar branched amphiphilic compound containing the CCK8 peptide and the DTPAGlu chelating agent, small micelles are expected for OCA-DOTA, OCA-DTPAGlu and their gadolinium complexes, in water solution (Table 3.3).¹²⁰

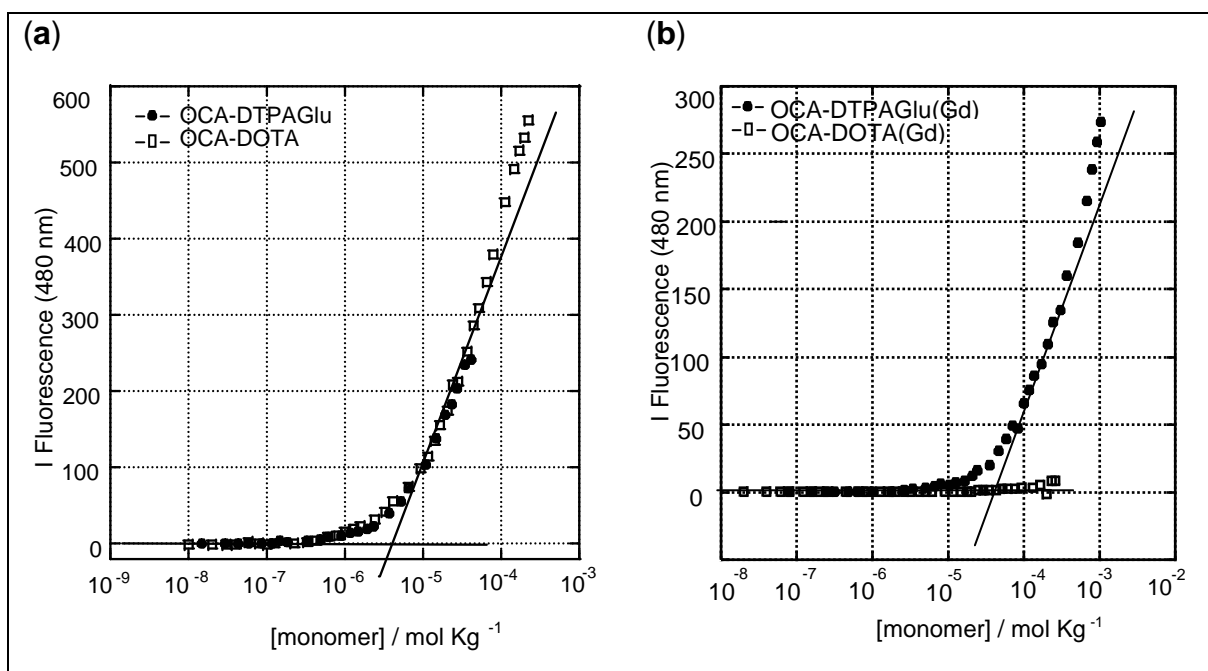


Figure 3.5: Fluorescence intensity of ANS fluorophore at 480 nm versus: (a) OCA-DTPAGlu and OCA-DOTA concentration; (b) OCA-DTPAGlu(Gd) and OCA-DOTA(Gd) concentration. The cmc values are established from graphical break-points.

Table 3.1: Critical micellar Concentration (cmc) values of binary systems obtained by using ANS and Pyr fluorescent probe.

Systems	CMC ANS (mol Kg ⁻¹)	CMC Pyr (mol Kg ⁻¹)	CMC mean
(C18) ₂ DOTA	8.90E-06	2.40E-06	5.65E-06
(C18) ₂ DOTA(Gd)	4.35E-06	-	
(C18) ₂ DTPA	1.20E-06	1.13E-06	1.16E-06
(C18) ₂ DTPA(Gd)	6.00E-07	-	
(C18) ₂ DTPAGlu	3.20E-05	2.37E-06	1.72E-05
(C18) ₂ DTPAGlu(Gd)	2.24E-06	3.14E-06	2.69E-06

Table 3.2: Cmc values of ternary systems obtained by using ANS fluorescent probe.

Systems	CMC ANS (mol Kg ⁻¹)
(C18) ₂ DOTA/(C18) ₂ L5-OCT	-
(C18) ₂ DOTA(Gd)/(C18) ₂ L5-OCT	-
(C18) ₂ DTPA/(C18) ₂ L5-OCT	5.84E-07
(C18) ₂ DTPA(Gd)/(C18) ₂ L5-OCT	2.22E-07
(C18) ₂ DTPAGlu/(C18) ₂ L5-OCT	1.84E-06
(C18) ₂ DTPAGlu(Gd)/(C18) ₂ L5-OCT	2.80E-07

The break points for OCA-DTPAGlu and OCA-DOTA, respectively indicate cmc values of $2.3 \cdot 10^{-6} \text{ mol kg}^{-1}$ and $2.5 \cdot 10^{-6} \text{ mol kg}^{-1}$, thus confirming the expected high stability of the resulting supramolecular aggregates. The same experiments were performed for the corresponding gadolinium complexes OCA-DTPAGlu(Gd) and OCA-DOTA(Gd). The first monomer aggregates at concentrations higher than $2.0 \cdot 10^{-5} \text{ mol kg}^{-1}$, while the second one does not give supramolecular structures at concentrations lower than $2.6 \cdot 10^{-4} \text{ mol kg}^{-1}$, as clearly indicated by the fluorescence experiment. In fact, ANS probe remains not fluorescent during the titration with the amphiphilic molecule, thus indicating that an aggregation process occurs.

The different behavior between the two monomers could be explained as a function of the different number of negative charges preserved on the head group after the gadolinium complexation: OCA-DTPAGlu(Gd) monomer retains two negative charges, while OCA-DOTA has no charges. The complete loss of charges on the Gd-DOTA gadolinium complex produces a remarkable reduction of the anionic character of the amphiphilic monomer which is unable to aggregate.¹²¹

Table 3.3: Cmc values of OCA-DTPAGlu and OCA-DOTA binary systems as free base or as gadolinium complexes.

Systems	CMC ANS (mol Kg ⁻¹)
OCA-DTPAGlu	2.30E-06
OCA-DOTA	2.50E-06
OCA-DTPAGlu(Gd)	2.00E-05
OCA-DOTA(Gd)	2.60E-04

3.2.3 Physicochemical Studies on the Octreotide Moiety

Biological data concerning SST analogs obtained by introducing covalent conformational constraints, suggested that -Phe-D-Trp-Lys-Thr- aminoacidic sequence contains all the elements necessary for the expression of the SST biological activities *versus* SSTR2.¹²² All octreotide conjugates should preserve this conformation and chemical alterations should not affect the D-Trp residue. Fluorescence experiments and CD studies were carried out to prove that the peptide moiety in the amphiphilic molecules keeps the conformational requirements unaltered also after micelles formation and that it remains well exposed on the micelle surface. The experiments were carried out on self-assembling OCA-DOTA(Gd) and OCA-DTPAGlu(Gd). In these aggregates the octreotide conformation could be more affected for steric hindrance of the chelating agent. The exposure of the bioactive portion of the monomers on aggregates surface was assessed by monitoring the fluorescence emission due to the indole moiety of the tryptophan residue. Usually, this fluorophore shows an emission peak centered at 350 nm in polar solvents while in hydrophobic solvents the maximum shifts occurs at 330 nm.¹²³ The fluorescence emission spectra of the three aggregates (Figure 3.6) were recorded at 25 °C and at

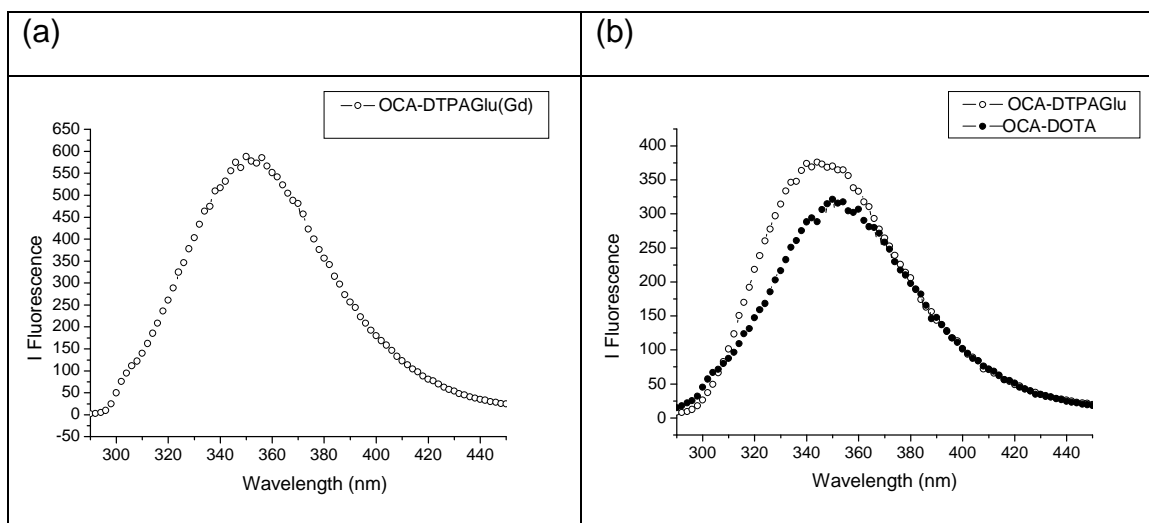
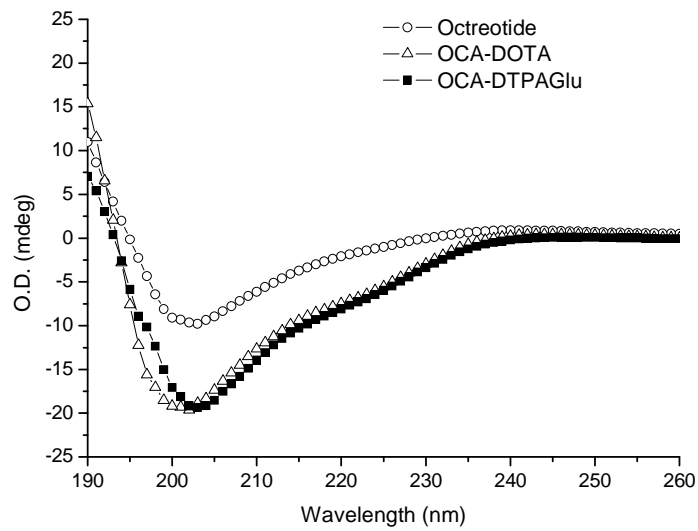


Figure 3.6: Fluorescence spectrum of tryptophan residue of: (a) OCA-DTPAGlu and OCA-DOTA aggregates; (b) OCA-DTPAGlu(Gd) aggregate. Fluorescence spectra were excited at 280 nm.

monomer concentration (1.0×10^{-5} M for OCA-DOTA and OCA-DTPAGlu; 1.0×10^{-4} M for OCA-DTPAGlu(Gd)), higher than cmc to be sure of the presence of aggregates in solution. The fluorescence maximum at 350 nm suggests for OCA-DOTA, a complete exposure of D-Trp residue in the hydrophilic external space. In the case of OCA-DTPAGlu and OCA-DTPAGlu(Gd), the maximum is centered at 346 nm, this value, slightly shifted with respect to 350 nm, indicates that most of the indole groups on tryptophan side-chain lies in the hydrophilic environment.

All spectra indicate predominant presence of an antiparallel β -sheet conformation characterized by a β -like turn, clearly suggesting that the disulphide bridge is conserved on the aggregates surface. OCA-DTPAGlu and octreotide spectra are nearly super imposable in the 190–260 nm range. Instead, the OCA-DOTA spectrum in 190–210 nm range shows a blue shift of the minimum, which may indicate some conformational modifications, but widely confirms the β -sheet conformation. Moreover, OCA-DTPAGlu spectra at three different concentrations are also reported in Figure 3.7(b). The presence of oxoethylene linkers and lipophilic tails on peptide *N*-terminus could induce some changes in peptide conformation. By decreasing concentration below the cmc, even if some spectral modifications are observed, the β -sheet rearrangement is preserved. This variation disappears when the monomer self-aggregates in solution above cmc. The steric hindrance on micelles surface might reduce the degree of freedom and restore the minimum octreotide conformation.

a)



b)

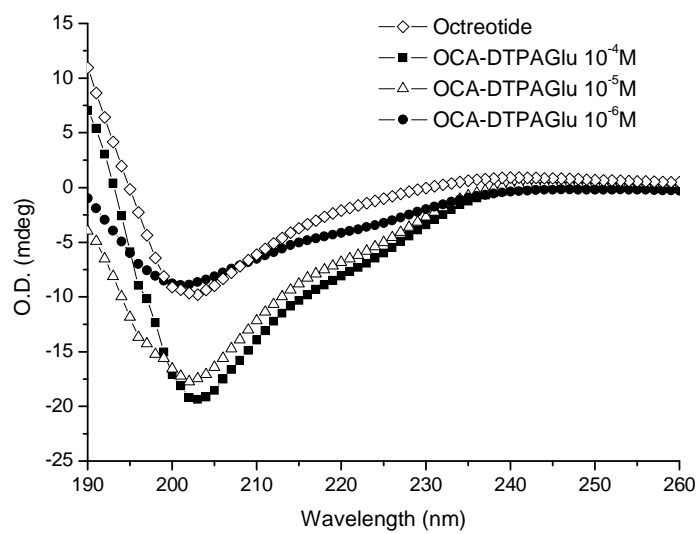


Figure 3.7: Circular dichroism profiles of: (a) octreotide, OCA-DTPAGlu and OCA-DOTA (b) of octreotide and OCA-DTPAGlu at 1.0×10^{-4} M, 1.0×10^{-5} M, 1.0×10^{-6} M concentrations.

3.2.4 Relaxivity Measurements

The parameter for an evaluation of an MRI contrast agent is its relaxivity, i.e. the potency to shorten the relaxation times of the solvent water protons. The measured relaxivity value (r_{1p}) is defined as the paramagnetic contribution to the measured proton longitudinal relaxation rate (R_{1obs}) of a solution containing 1.0 mM concentration of gadolinium according to Eqn (1) ¹²⁴

$$R_{1obs} = [Gd] \cdot r_{1p} + R_{1W} \quad (1)$$

where R_{1W} is the diamagnetic contribution of pure water (0.38 s^{-1}).

The relaxivity of all aggregates, was measured at monomer concentration higher than the calculated cmc to be sure that the molecules are aggregated in the micellar form.

The values are reported in the table and they has been determined at 20 MHz and 25 °C. The relaxivity are reported in figures in function of Proton Lamor frequency. The values were then confirmed mineralizing, with HCl 37% at 120 °C overnight, a given quantity of sample solution to determine the exact concentration of Gd(III) present in the solution: from the measure of the observed relaxation rate (R_{1obs}) of the acidic solution, knowing the relaxivity (r_{1p}) of Gd(III) aquoion in acidic conditions ($13.5 \text{ mM}^{-1} \text{ s}^{-1}$), it was possible to calculate the exact Gd(III) concentration (Eqn (1)) (This method was calibrated using standard inductively coupled plasma (ICP) solutions, and the accuracy was determined to be 1%). At this point, knowing $[GdL]$ and measuring R_{1obs} of the micellar mother solution, the same Eqn (1) was used to calculate the micellar relaxivity.

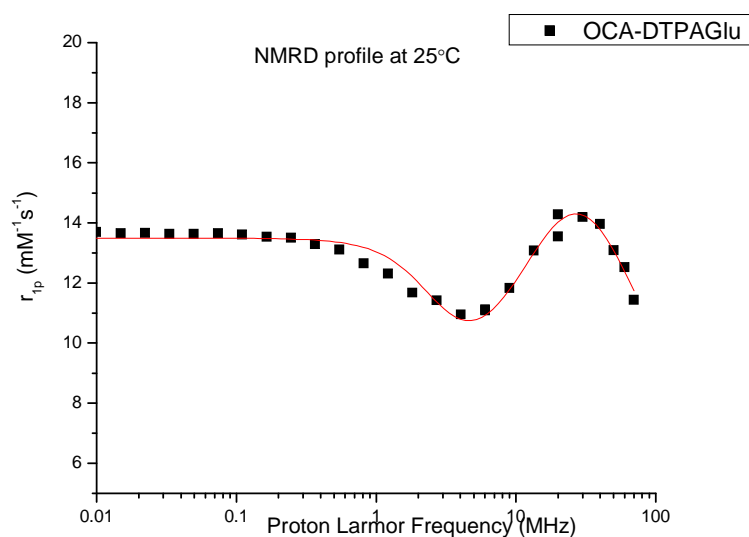


Figure 3.8: $1/T_1$ NMRD profile of OCA-DTPAGlu(Gd) at pH 7.4 and 25°C, normalized to 1 mM Gd (III) ion.

The self-assembling aggregates show quite different relaxivity values. The measurements of the (C18)₂DTPAGlu(Gd) and (C18)₂DTPA(Gd) are in accordance with other similar gadolinium containing micellar systems. In fact the values is almost five/four times higher than the gadolinium complexes. To reach high relaxivity values is a very important parameter to account for is the exchange life time coordinated water molecules (τ_M) of a Gd(III) complex. The (C18)₂DOTA(Gd) show a low value (Table 3.4). This result could be attributed at a lower ratio of water exchange in the inner sphere of coordination. The ternary systems show the same trend of the relaxivity parameter. Relaxivity value of OCA-DTPAGlu(Gd) micelles ($13.9 \text{ mM}^{-1} \text{ s}^{-1}$) is in the same range of the value previously reported ($15.0 \text{ mM}^{-1} \text{ s}^{-1}$) for aggregates obtained by self assembling of a similar monomer containing the CCK8 peptide (*MonY*-Gd).¹²⁰

The slight difference could be probably ascribed to different aggregation number or size. The analysis of nuclear magnetic relaxation dispersion (NMRD) profile of the lipophilic aggregated system has been made according to the Solomon–Bloembergen–Morgan model, modified according to the Lipari-Szabo approach^{125, 126, 127} to obtain an accurate determination of the reorientational correlation time (τ_R), that is strictly related to the molecular size of the investigated system. This model is generally applied to the systems with a faster local motion (governed by τ_l) and a slower global motion (governed by τ_g); the extent of local to global contribution to the overall motion is determined by an order parameter (S) that can vary from 0 to 1.

The experimental data τ_l , τ_g and S were fitted by considering one water molecule in the inner coordination sphere for each Gd(III) complex ($n_w = 1$) and fixing the exchange lifetime of the coordinated water molecule (τ_M) to the previously determined direct ¹⁷O-NMR R_{2p} versus T measurement.¹²⁰

Table 3.4: Relaxometric parameters measured at pH 7.4, T = 298 K, normalized to 1.0 mM concentration of Gd(III) ion.

Systems	r_{1p} (20MHz, 25°C)	τ_l (ps)	τ_g (ps)	S	τ_M (ns)
(C18) ₂ DTPAGlu(Gd)	23.9	432	2940	0.44	81
(C18) ₂ DTPA(Gd)	17.3	114	2112	0.53	205
(C18) ₂ DOTA(Gd)	4.2	-	-	-	-
OCA-DTPAGlu(Gd)	13.9	250	2900	0.3	60
(C18) ₂ DTPAGlu(Gd)/(C18) ₂ L5-Oct	17.6	302	2546	0.41	81
(C18) ₂ DTPA(Gd)/ (C18) ₂ L5-Oct	15.2	63.5	2111	0.49	205
(C18) ₂ DOTA(Gd)/(C18) ₂ L5-Oct	1.97	-	-	-	-

3.2.5 Structural characterization

Sans measurements were performed on the (C18)₂DOTA-D₂O, (C18)₂DTPA-D₂O and (C18)₂DTPAGlu-D₂O binary systems and (C18)₂DOTA/(C18)₂L5-Oct-D₂O, (C18)₂DTPA/(C18)₂L5-Oct-D₂O and (C18)₂DTPAGlu/(C18)₂L5-Oct-D₂O ternary systems at several concentration above the observed value of cmc. The same kind of experiments were carried out on the systems where the binary systems were

replaced by the corresponding monomers in which chelating agents complex Gd(III) ion.

In Figure 3.9 and 3.10 are reported the scattering intensity distribution, $I(Q)$ vs Q , of the binary systems and ternary systems, respectively.

Inspection of figures reveals that $(C18)_2DOTA-D_2O$ and $(C18)_2DOTA(Gd)-D_2O$ binary systems, and the respective ternary system have scattering cross sections $d\Sigma/d\Omega$, at high q , showing a power low (q^{-2}) typical of vesicles and liposomes. Instead, the binary systems $(C18)_2DTPAGlu(Gd)-D_2O$ and $(C18)_2DTPAGlu-D_2O$, and the respective ternary system have power high (q^{-1}) typical of micellar aggregates.

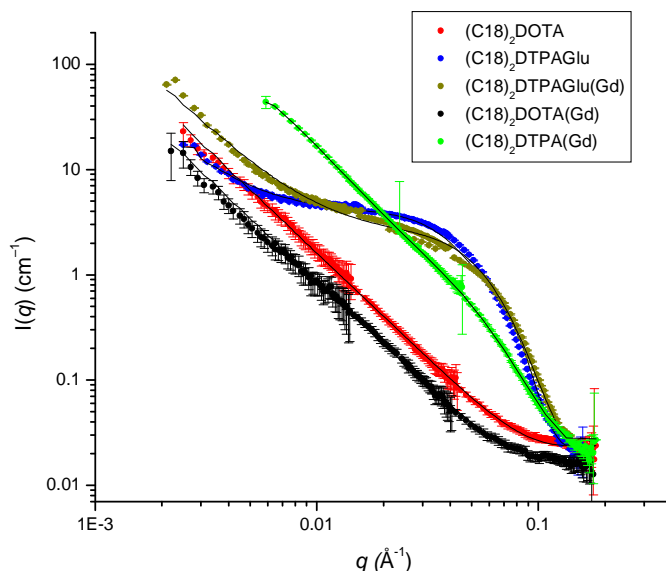


Figure 3.9

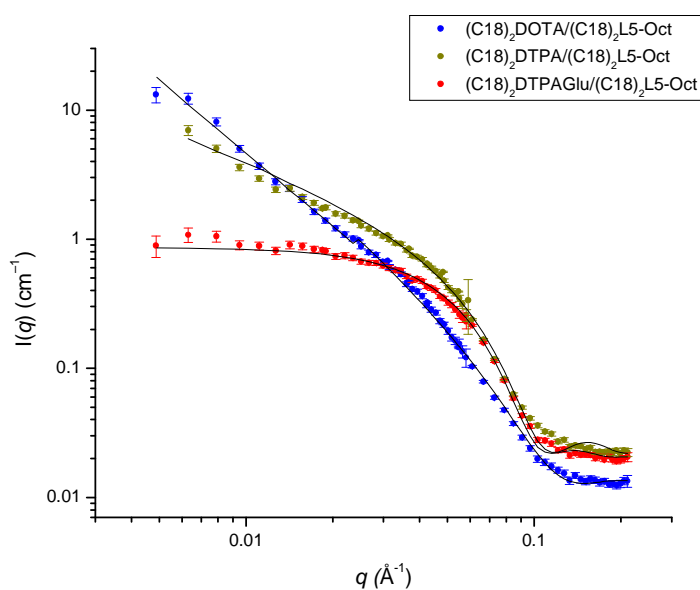


Figure 3.10

Finally, the binary systems (C18)₂DTPA(Gd)-D₂O show the coexistence of the both values of q ; therefore micelles and vesicles are present at same time. The shape of the respective ternary system is represented by cylindrical micelle. The data of the aggregates presented in our systems have been fitted by the equation (1),

$$\frac{d\Sigma}{d\Omega} = 2\pi \Delta^2 \rho S d^2 \frac{1}{q^2} \frac{\sin^2\left(\frac{qd}{2}\right)}{\left(\frac{qd}{2}\right)^2} + \left(\frac{d\Sigma}{d\Omega}\right)_{\text{incoh}} \quad (1)$$

where Δ_p is the scattering length density difference between the scattering aggregates and the solvent, d is the plane thickness, S is the total surface per unit volume and $(d\Sigma/d\Omega)_{\text{incoh}}$ represents the incoherent contribution to the scattering cross section, mainly due to the presence of hydrogen nuclei. From a fitting of equation (1) to the experimental data it is possible to evaluate the thickness d of the liposome double layer of the system analyzed. These values are collected in Table 3.5 join to the values obtained from DLS experiments.

Table 3.5: Liposomal bilayer thickness (d) and hydrodynamical radius (R_h) obtained for the systems investigated by means of SANS and DLS.

Aqueous System	d(Å)	R_h(nm)
(C18) ₂ DOTA(Gd)-D ₂ O	45 ± 4	-
(C18) ₂ DOTA-D ₂ O	41 ± 2	190 ± 11
(C18) ₂ DTPA(Gd)-D ₂ O	50 ± 5	-
(C18) ₂ DTPAGlu(Gd)-D ₂ O	72 ± 9	6.6 ± 1
(C18) ₂ DTPAGlu-D ₂ O	53 ± 8	7.6 ± 1

3.3. Experimental Section: Octreotide

3.3.1 Materials

Protected N^α-Fmoc-amino acid derivatives, coupling reagents, H-Thr(*t*Bu)-ol-(2-chloro-trityl)-resin and Rink amide MBHA resin were purchased from Calbiochem-Novabiochem (Laufelfingen, Switzerland). The Fmoc-8-amino-3,6-dioxaoctanoic acid (Fmoc-AdOO-OH) and the Fmoc-21-amino-4,7,10,13,16,19-hexaoxaheneicosanoic acid (Fmoc-AhOH-OH) were purchased from Neosystem (Strasbourg, France). The DTPAGlu pentaester, N,N-Bis[2-[bis[2-(1,1-dimethyletoxy)-2-oxoethyl]-amino]ethyl]-L-glutamic acid 1-(1,1-Dimethylethyl)ester and N,N-dioctadecylsuccinamic acid, were prepared according to the experimental procedure reported in literature.^{128, 129} [(DOTA(*t*Bu)₃] (1,4,7,10-tetraazacyclododecane-1,4,7,10-tetraacetate *tert*butyl ester) and [(DTPA(*t*Bu)₄] (1,4,7,10-Tetraazacyclododecane-1,4,7,10-tetracetic acid, diethylenetriaminepentaacetic acid) were purchased from Macrocycles (Dallas TX USA). All other chemicals were commercially available by Sigma-Aldrich or Fluka (Bucks, Switzerland) or LabScan (Stillorgan, Dublin, Ireland) and were used as received unless otherwise stated. All solutions were prepared by weight with doubly distilled water. Solid phase peptide synthesis was performed on a by using 433A Applied Biosystems automatic synthesizer. Analytical RP-HPLC runs were carried out on a HP Agilent Series 1100 apparatus (Santa Clara, CA, USA) using a Phenomenex (Torrance, CA) C18 column, 4.6mm×250mm with a flow rate of 1.0 mLmin⁻¹. For all the RP-HPLC procedures, the system solvent used was H₂O 0.1% TFA (A) and CH₃CN 0.1% TFA (B). The column was eluted with two gradients at 1.0 mL/min flow rate. The first was a linear gradient from 5 to 70% B in 30 min followed by 70 to 95%B in 10 min, the second from 60% to 80% B over 10 min and from 80% to 95% B over 15 min. Preparative RP-HPLC were carried out on a Shimadzu 8A (Kyoto, Japan) apparatus equipped with an UV Shimadzu detector using a Phenomenex (Torrance, CA) C4 column, 22 mm×250mm with a flow rate of 20 mLmin⁻¹, eluted with the H₂O/0.1% TFA (A) and CH₃CN/0.1% TFA (B) mixture previously described and a linear gradient at 20 mL/min flow rate. Mass spectral analysis were carried out on MALDI-TOF Voyager-DE mass spectrometer Perseptive Biosystems (Framingham, MA, USA), and LC-MS analyses were performed by using Finnigan Surveyor MSQ single quadrupole electrospray ionization (Finnigan/Thermo Electron Corporation San Jose, CA USA). ¹H and ¹³C NMR spectra were recorded by using 400 spectrometer Varian (Palo Alto, CA USA). The fluorescence emission spectra were recorded using a Jasco Model FP-750 spectrofluorimeter equipped with a Peltier temperature controller in 1.0 cm path length quartz cell at 25 °C. Equal excitation and emission bandwidths were used throughout experiments, with a recording speed of 125 nm min⁻¹ and automatic selection of the time constant. UV measurements were performed on a UV-vis Jasco V-5505 spectrophotometer equipped with a Jasco ETC-505T Peltier temperature controller with a 1cm quartz cuvette (Hellma).

3.3.2 Peptide Conjugate Synthesis

Peptide synthesis was carried out in solid-phase under standard conditions using Fmoc strategy,¹¹⁷ on H-Thr(*t*Bu)-ol-(2-chlorotrityl)-resin (0.70 mmol/g, 0.15 mmol scale, 0.214 g). The peptide chain was elongated by sequential coupling and Fmoc deprotection of the Fmoc-amino acid derivatives: Fmoc-Cys(Acm)-OH, Fmoc-

Thr(O t Bu)-OH, Fmoc-Lys(Boc)-OH, Fmoc-DTrp(Boc)-OH, Fmoc-Phe-OH, Fmoc-Cys(Acm)-OH, Fmoc-DPhe-OH. All couplings were performed twice for 1 hour, by using an excess of 4 equivalents for the single amino acid derivative. The α -amino acids were activated *in situ* by the standard HOBt/PyBop/DIPEA procedure. DMF was used as a solvent. Fmoc deprotection was carried out by 30% solution of piperidine in DMF after the coupling of each amino acidic residue. The coupling steps were monitored by the qualitative Kaiser test. When the synthesis was complete, for the synthesis of the monomer (C₁₈H₃₇)₂-CONH(AdOO)₅-Octreotide, (C₁₈)₂L5-Octreotide, the Fmoc N-terminal protecting group was removed and five residues of Fmoc-AdOO-OH were added. They were condensed to the α -NH₂ of the phenylalanine residue in successive single couplings. An excess of 2 equivalents of Fmoc-AdOO-OH, PyBop and HOBt and 4 equivalents of DIPEA were dissolved in DMF and added to the manual vessel. When all five linkers were coupled on the peptide chain, the N,N-dioctadecylsuccinamic acid, was bonded. The coupling was carried out by an excess of 4 equivalents (2.48 g, 4.0 mmol) of the lipophilic compound dissolved in 10 ml of DMF/DCM (50/50) mixture. 2.080 g (4.0 mmol) of PyBop, 0.612 g (4.0 mmol) of HOBt and 1.34 mL (8.0 mmol) of DIPEA, dissolved in DMF were introduced in the vessel like activating agents. The coupling time was 1 h under N₂ flow at room temperature. Yield for aliphatic acid coupling, monitored by the Kaiser test, was in the range 95-98%. Instead, for the synthesis of the monomers OCA-DOTA and OCA-DTPAGlu, when the peptide synthesis was complete, the Fmoc N-terminal protecting group was removed and two residues of Fmoc-AhOH-OH were condensed by using, for each residue, an excess of two equivalents activating the carboxylic function similarly in a single coupling for 60 min under N₂ flow at room temperature. After Fmoc removal from the N-terminal end of the peptide derivative, 0,320 g (0.60 mmol) of Dde-Lys(Fmoc)-OH, activated by a stoichiometric amount of PyBop and HOBt and two equivalents of DIPEA in DMF, were coupled by stirring the slurry suspension of the resin for 60 min. The solution was filtered and the resin was washed with three portions of DMF. After removal of the Fmoc group on side chain of lysine residue, the chelating agent (DTPAGlu pentaester or DOTA trisester) was linked, through its free carboxyl function, to the ϵ -NH₂ of the lysine residue. This coupling step was performed using two equivalents of the chelating agent, HATU and four equivalents of DIPEA in DMF as a solvent. The coupling time, compared with the classical solid-phase peptide synthesis protocol, was increased up to 120 min. The resin was washed three times with DMF, then, the 1-(4,4-dimethyl-2,6-dioxo-cyclohexylidene)3-methylbutyl group (Dde) was removed by treatment with DMF/Hydrazine mixture (98 : 2). The peptide-resin was stirred with 3.0 ml of this solution for 10 min. The treatment was repeated twice, and the reaction was monitored by the qualitative Kaiser test. On N-terminal moiety, the Fmoc-AhOH-OH linker was coupled following the same procedure above described. After the removal of N-terminal Fmoc protecting group, N,N-dioctadecylsuccinamic acid were condensed as previously described. The deprotection (Acm removal) and the oxidation reaction of cysteine residues were carried out at same time adding 1.2 eq Ti(CF₃CO₂)₃ to a suspension of the peptidyl resin in DMF/anisole (19 : 1) stirring the mixture for 18 h at 0°C monitoring at times by the colorimetric Ellmann test.¹³⁰ The peptide derivatives were cleaved from the solid support by suspending the resin in 10 ml of TFA/TIS/H₂O (95.5/2/2.5) mixture for 120 min. During this step all the amino acid side chains and the carboxylic groups of the chelating moiety were simultaneously freed from their protecting groups. Free peptide derivatives were precipitated in cold water and lyophilized from a 50% H₂O/CH₃CN solution. The

crude compounds were purified by preparative RP-HPLC. The single peaks were analyzed by HPLC and mass spectrometry. Mass spectral analysis were carried out on MALDI-TOF. The desired compounds (~180 mg) were obtained at HPLC purity higher than 95% with a final yield of around 10%.

(C₁₈H₃₇)₂-CONH(AdOO)₅-Octreotide, (C₁₈)₂L5-Octreotide, *Rt* = 38.0 min; *MW* = 2328 amu

(C₁₈)₂-(AhOH)-Lys(DTPAGlu)-(AhOH)₂-octreotide, OCA-DTPAGlu, *Rt* = 41.0 min; *MW* = 3204 amu.

(C₁₈)₂-(AhOH)-Lys(DOTA)-(AhOH)₂-octreotide, OCA-DOTA, *Rt* = 41.3 min; *MW* = 3144 amu.

Synthesis of (C₁₈H₃₇)₂CONHLys-(DOTA)CONH₂ (C₁₈)₂DOTA, (C₁₈H₃₇)₂CONHLys-(DTPA)CONH₂ (C₁₈)₂DTPA, (C₁₈H₃₇)₂CONHLys-(DTPAGlu)CONH₂ (C₁₈)₂DTPAGlu

The monomers were synthesized on solid phase using Rink-amide (MBHA) resin (0.85 mmol/g; 0.2 mmol, 0.235 g) as polymeric support. The activation of the carboxylic group of Fmoc-Lys(Mtt)-OH, the coupling of the DTPA(OtBu)₄-OH (2 equiv., 0.252 g) and DTPAGlu(OtBu)₅-OH (2 equiv., 0.185 g) and the condensation of the *N,N*-dioctadecylsuccinamic acid were as described in the paragraph 3.3.2 The cleavage from the resin and deprotection of the tBu protecting groups were performed in 10 mL of TFA/TIS/H₂O (95.5/2/2.5) mixture for 120 min. The crude product was washed several times with small portions of cold water and lyophilized. The white solid was recrystallized from MeOH/H₂O and recovered in high yield (> 85%). The product was identified by mass spectra (electrospray ionization ESI) and NMR spectroscopy.

(C₁₈)₂DOTA: MS (ESI⁺): *m/z* (%): 1134 (100) [M-H⁺]

(C₁₈)₂DTPA: MS (ESI⁺): *m/z* (%): 1123 (100) [M-H⁺]

(C₁₈)₂DTPAGlu: MS (ESI⁺): *m/z* (%): 1195 (100) [M-H⁺]

(C₁₈)₂DOTA:

¹H-NMR (CDCl₃/CD₃OD 50/50) (chemical shifts in δ, CHCl₃ as internal standard 7.26) = 4.1 (m, 1H, CH Lys α), 3.6 (m, 2H, R₂NCH₂CONH), 3.1 (m, 6H, R₂N-CH₂COOH), 3.0 2H, CH₂ Lys ε), 3.1 (m, 16 R₂N-CH₂CH₂NR₂) 2.4-2.1 (m, 4H, COCH₂CH₂CO), 1.7 (m, 2H, CH₂ Lys β), 1.4 (m, 2H, CH₂ Lys δ), 1.3 (m, 2H, CH₂ Lys γ), 1.1 (m, 4H, RCH₂CH₂N), 1.0 (m, 60 CH₂ aliphatic), 0.70 (t, 6H, CH₃).

¹³C-NMR (CDCl₃/CD₃OD 50/50) (chemical shifts in δ, CDCl₃ as internal standard 77.00) = 174.0 (3, COOH), 172.8, 172.6, 172.1, 163.0 (4 CONH), 54.5 (CH-Lys α), 53.2 (CH₂COOH), 51.50 (NCH₂CH₂N), 49.7 (CH₃(CH₂)₁₆CH₂N), 46.4 (CH₃(CH₂)₁₅CH₂CH₂N), 38.0 (CH₂-Lys ε), 36.0 (CH₂-Lys β), 32.0

(NCOCH₂CH₂CONH), 31.8 (CH₂-Lys γ), 29.60-27.0 (CH₃CH₂CH₂(CH₂)₁₃CH₂CH₂N), 22.57 (CH₃CH₂CH₂(CH₂)₁₅), 22.2 (CH₂-Lys δ), 13.73 (CH₃CH₂(CH₂)₁₆).

(C18)₂DTPA:

¹H-NMR (CDCl₃/CD₃OD 50/50) (chemical shifts in δ , CHCl₃ as internal standard 7.26) = 4.3 (m, 1H, CH Lys α , m, 2H, R₂NCH₂CONHR), 3.6 (s, 8H, R₂NCH₂COOH), 3.44 (m, 4H, R₂N-CH₂CH₂N R₂), 3.30-3.27 (m, 4H, N-CH₂), 3.19 (m, 4H, R₂N-CH₂CH₂NR₂), 3.1 (m 2H, CH₂ Lys ϵ), 2.6-2.3 (m, 4H, NHCOCH₂CH₂CO), 1.90 (m, 2H, CH₂ Lys β), 1.6 (m, 2H, CH₂ Lys δ), 1.45 (m, 2H, CH₂ Lys γ), 1.4 (m, 4H, RCH₂CH₂N), 1.27 (m, 60 CH₂ aliphatic), 0.89 (t, 6H, CH₃).

¹³C-NMR (CDCl₃/CD₃OD 50/50) (chemical shifts in δ , CDCl₃ as internal standard 77.00) = 173.31 (4, CO), 172.1 (2, CONH), 163.4 (2, CONH), 55.04 (CH₂COOH), 54.51 (NH(CH₂)₄CH), 52.91 (NCH₂CH₂N), 49.7 (CH₃(CH₂)₁₆CH₂N), 46.4 (CH₃(CH₂)₁₅CH₂CH₂N), 38.0 (NHCH₂(CH₂)₂CH₂CH), 36.0 (NH(CH₂)₃CH₂CH), 32.0 (NCOCH₂CH₂CONH), 31.8 (NHCH₂CH₂(CH₂)₂CH), 29.6-27.0 (CH₃CH₂CH₂(CH₂)₁₃CH₂CH₂N), 22.57 (CH₃CH₂CH₂(CH₂)₁₅), 22.18 (NH(CH₂)₂CH₂CH₂CH), 13.73 (CH₃CH₂(CH₂)₁₆).

(C18)₂DTPAGlu:

¹H-NMR (CDCl₃/CD₃OD 50/50) (chemical shifts in δ , CHCl₃ as internal standard 7.26) = 4.1 (m, 1H, α CH Lys), 3.5 (overlapped, 1H, α CH Glu), 3.3 (s, 8H, NCH₂COOH), 2.7-2.8 (m, 8H, RNCH₂CH₂NR), 2.14 (m 2H, C(O)CH₂CH₂R), 1.87 (m, γ CH₂ Lys), 1.76 (m, 2H, δ CH₂ Lys), 1.65 (m, 2H, β CH₂ Lys), 1.5 (overlapped, 2H, RCH₂CH₃), 1.1-1.3 (m, 30 H, 15 CH₂), δ 0.8 (t, 3H, 1 CH₃).

3.3.3 Preparation of Gadolinium complexes:

Gadolinium complexes have been obtained by adding light excess of the GdCl₃ to aqueous solution of OCA-DTPAGlu and OCA-DOTA ligands at neutral pH and room temperature. The formation of the gadolinium complexes was followed by measuring the solvent proton relaxation rate (1/T₁). The excess of uncomplexed Gd(III) ions, which yields a variation of the observed relaxation rate, was removed by centrifugation of the solution brought to pH 10; further relaxation rate measurements were made to check the complete Gd(III) ions removal. On the contrary, in the presence of free Gd(III) ion basic relaxation rate would have been lower as a consequence of the precipitation of insoluble Gd(OH)₃. Furthermore, xylenol orange test ¹³¹ has been performed and it gave no free Gd(III) positive answer.

The coordination of the gadolinium to (C18)₂DOTA, (C18)₂DTPA and (C18)₂DTPAGlu was carried out as previously described.

3.3.4 Aggregates Preparation

Stock solutions of OCA-DTPAGlu and OCA-DOTA monomers and of their gadolinium complexes were prepared by stirring the monomers until complete dissolution in 0.1 M phosphate buffer at pH 7.4 NaCl 0.9 wt % and filtering through a 0.45 μ m filter. pH was controlled by using pHmeter MeterLab PHM 220. Concentrations of all solutions

($1.0 \cdot 10^{-3}$ M for OCA-DTPAGlu, OCA-DOTA and OCA-DTPAGlu(Gd); and $1.0 \cdot 10^{-4}$ M for OCA-DOTA(Gd) were determined by absorbance on a UV-vis using a molar absorptivity (ϵ_{280}) of $5630 \text{ M}^{-1} \text{ cm}^{-1}$ for octreotide, due to the contribution of tryptophan residue present in the primary octreotide structure.^{132, 133}

Self-assembling aggregates of (C18)₂DOTA, (C18)₂DTPA and (C18)₂DTPAGlu and mixed aggregates of (C18)₂DTPAGlu/(C18)₂L5-Oct, (C18)₂DTPA / (C18)₂L5-Oct and (C18)₂DOTA/(C18)₂L5-Oct (or their corresponding gadolinium complexes) were prepared by dissolving the amphiphiles, in a small amount of a methanol/chloroform (50/50) mixture, and subsequently evaporating the solvent by slowly rotating the tube containing the solution under a stream of nitrogen. In this way a thin film of amphiphile was obtained. Then the film was hydrated by addition of 0.1 M phosphate buffer pH = 7.4 NaCl 0.9 wt % solution in the vial and sonicated for 30 min. All mixed aggregates were prepared at 90:10 molar ratios mixing the chelating agent containing monomer and the Octreotide containing monomer.

Concentrations of solutions were determined by absorbance measurement as previously described. In all solutions used for SANS investigations, H₂O has been replaced by D₂O in order to minimize the incoherent contribution to the total scattering cross section. The total concentration in the samples used in structural measurements (DLS and SANS) are in the 2×10^{-3} M range.

3.3.5 Fluorescence Measurements

Critical micellar concentration (cmc) values of micelle samples of (C18)₂DOTA, (C18)₂DTPA and (C18)₂DTPAGlu as free bases or as gadolinium complexes (C18)₂DOTA(Gd), (C18)₂DTPA(Gd) and (C18)₂DTPAGlu(Gd), and of the mixed aggregates with octreotide were obtained by fluorescence spectroscopy. The cmc were measured by using 8-anilino-naphthalene-1-sulfonate (ANS) and Pyrene (Pyr) as fluorescent probes. Small aliquots of 1×10^{-4} M aggregate solution, were added to a fixed volume of fluorophore in cell (1×10^{-5} M ANS or 2×10^{-6} M Pyr) dissolved in the same buffer. In the ANS method, the cmc values were determined by linear least-squares fitting of the fluorescence emission at 480 nm, upon excitation at 350 nm versus the amphiphile concentration as previously reported.^{134, 135} In the Pyr method the cmc values were determined by the break-point of the fitting of I_1/I_3 upon excitation at 335 nm versus the amphiphile concentration. For the aggregates solution of the OCA-DTPAGlu and OCA-DOTA, and the respective molecules complexed with gadolinium, the cmc values were obtained only by using 8-anilino-naphthalene-1-sulfonate (ANS) as fluorescent probe, as reported for the other systems. Tryptophan emission spectra in 290–450 nm range were obtained exciting at 280 nm micelle solutions at peptide concentration of 1.0×10^{-5} M.

3.3.6 Small-Angle Neutron Scattering (SANS)

Small Angle Neutron Scattering measurements were performed at 25°C with the KWS2 instrument located at the Heinz Meier Leibnitz Source, Garching Forschungszentrum (Germany). Neutrons with a wavelength spread $\Delta\lambda/\lambda \leq 0.2$ were used. A two-dimensional array detector at three different wavelengths (W)/collimation (C)/sample-to-detector (D) distance combinations ($W_{7\text{\AA}}C_{8\text{m}}D_{2\text{m}}$, $W_{7\text{\AA}}C_{8\text{m}}D_{8\text{m}}$ and $W_{19\text{\AA}}C_{8\text{m}}D_{8\text{m}}$), measured neutrons scattered from the samples. These configurations allowed collecting data in a range of the scattering vector modulus $q = 4\pi/\lambda \cdot \sin(\theta/2)$ between 0.0019 \AA^{-1} and 0.179 \AA^{-1} , with θ scattering angle.

The investigated systems were contained in a closed quartz cell, in order to prevent the solvent evaporation and kept under measurements for a period such to have ~ 2 million counts. The obtained raw data were then corrected for background and empty cell scattering. Detector efficiency corrections, radial average and transformation to absolute scattering cross sections $d\Sigma/d\Omega$ were made with a secondary plexiglass standard.^{136, 137}

3.3.7 Dynamic Light Scattering (DLS)

The light scattering setup was composed by a Photocor compact goniometer, a SMD 6000 Laser Quantum 50 mW light source operating at 5325 Å and a PMT and correlator acquired from Correlator.com. In DLS, the intensity autocorrelation function $g^{(2)}(t)$ is measured and related to the electric field autocorrelation $g^{(1)}(t)$ by the Siegert relation. The parameter $g^{(1)}(t)$ can be written as the Laplace transform of the distribution of the relaxation rate Γ . Such Laplace transformations were performed using algorithm incorporated in Precision Deconvolve software. From the relaxation rates, the translational diffusion coefficient D may be obtained as¹³⁸

$$D = \lim_{q \rightarrow 0} \frac{\Gamma}{q^2}$$

where $q = 4\pi/\lambda \sin(\theta/2)$ is the modulus of the scattering vector, n_0 is the refractive index of the solution, λ is the incident wavelength and θ represents the scattering angle. Thus D is obtained from the limit slope of Γ as a function of q^2 , where Γ is measured at different scattering angles. All the measurements were performed at $(25.00 \pm 0.05)^\circ\text{C}$ by using a thermostat bath.

3.3.8 Water proton relaxation measurements:

The proton $1/T_1$ NMRD profiles were measured over a continuum of magnetic field strength from 0.00024 to 0.47 T (corresponding to 0.01-20 MHz proton Larmor Frequency) on a Stellar Fast Field-Cycling relaxometer. This relaxometer works under complete computer control with an absolute uncertainty in $1/T_1$ of $\pm 1\%$. Data points at from 0.47 T (20 MHz) to 1.7 T (70 MHz) were added to the experimental NMRD profiles and were recorded on the Stellar Spinmaster spectrometer with switchable field from 20 to 70 MHz, by means of the standard inversion-recovery technique (16 experiments, 2 scans). A typical 90° pulse width was 4 μs and the reproducibility of the T_1 data was $\pm 0.5\%$. The temperature was kept at 25 $^\circ\text{C}$ with a Stellar VTC-91 airflow heater equipped with a copper-constantan thermocouple (uncertainty $\pm 0.1^\circ\text{C}$), respectively. Relaxivity data at 20MHz were measured on both instruments.

3.3.9 ^{17}O -NMR water relaxation rate measurements:

The exchange lifetime of a metal bound water molecule in a paramagnetic chelate may be accurately assessed by measuring the temperature dependence of the paramagnetic contribution to the water ^{17}O transverse relaxation rate (R_{2p}^0). Variable temperature ^{17}O NMR measurements were recorded on the JEOL EX-90 spectrometer, equipped with a 5 mm probe, by using a D_2O external lock. Experimental settings were spectral width 10 000 Hz, 90° pulse (7 μs), acquisition time 10 ms, 1000 scans and no sample spinning. Solutions containing 2.6% of ^{17}O

isotope (Yeda, Israel) were used. The paramagnetic contribution to the transverse relaxation rates (R_{2p}^o) were calculated from the signal width at half-height ($\Delta\nu_{1/2}$ corrected for the diamagnetic contribution ($\Delta\nu_{1/2}^{dia}$): $R_{2p}^o = \pi(\Delta\nu_{1/2} - \Delta\nu_{1/2}^{dia})$. The temperature dependences of the diamagnetic contribution to the observed transverse relaxation rates were measured by using ^{17}O isotope enriched pure water.

3.3.10 Circular Dichroism (CD) Experiments

Far-UV CD spectra were collected at room temperature on a Jasco J-810 spectropolarimeter equipped with a NesLab RTE111 thermal controller unit using a 1-mm quartz cell. Other experimental settings were: scan speed, 10 nm/min; sensitivity, 50 mdeg; time constant, 16 s; bandwidth, 3 nm. CD measurements were conducted on solutions containing peptide amphiphilic surfactant at concentrations of 1×10^{-4} M, 1×10^{-5} M and 1×10^{-6} M in 2.5 mM phosphate buffer at pH 7.4. The CD spectra were collected from 260 to 190 nm, corrected for blank and adjusted for dilution.

4. Bombesin labeled supramolecular aggregates

4.1 Introduction

The members of the Bombesin receptor family consist of four receptor subtypes including the neuromedin B receptor (BB1), the gastrin-releasing peptide receptor (GRPR, BB2), the orphan receptor subtype (BB3), and the amphibian receptor (BB4).^{88, 139-141} The Bombesin receptor subtype 2 (GRPR) has been found overexpressed by tumor cell lines of several human tumors (ovarian cancers, breast cancers and prostate cancer)¹⁴²⁻¹⁴⁴ and thus it is indicated as potential target for tumor diagnosis and selective therapy. The fourteen-residues Bombesin peptide (BN) (Figure 4.1); its eight-residues C-terminal peptide sequence ([7-14]BN), or some Bombesin analogues acting as antagonists, could be used to target these receptors.

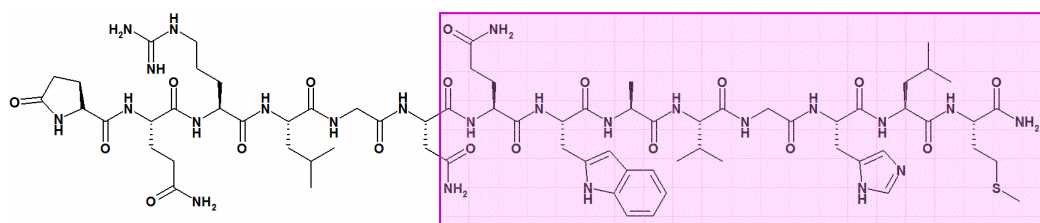


Figure 4.1: Schematic representation of [1-14]bombesin peptide.

In literature many studies demonstrated the activity of the C terminal moiety. For this reason some modifications on this peptide have to be performed on the N-terminal moiety by adding hydrophilic or hydrophobic spacers.¹⁴⁵ On these bases the amphiphilic molecules were design in the same way than the octreotide conjugate reported in the previous chapter.

4.2 Results & Discussion

4.2.1 Monomers Synthesis and Aggregates Preparation

The DOTA-βAla-[7-14]BN peptide conjugate and the corresponding scrambled peptide compound retaining the bombesin [7-14] amino acid residue composition, but with a reordered sequence, were synthesized in order to confirm the effective binding capability of [7-14]BN on cells assays and to evaluate if the peptide sequence chosen as scrambled peptide (*scr*BN) is a good candidate to have a negative control for the aggregate systems. Both conjugates were prepared using the well assessed procedures for peptide synthesis.

DOTA chelating agent bounded on the bombesin peptide was chosen for its capability to coordinate Indium radioisotope ions used currently as tracer in *in vitro* experiments. On the bases of the results achieved and reported in the below section, novel amphiphilic monomers bearing the [7-14]BN and the scramble sequence have been synthesized (Figure 4.2).

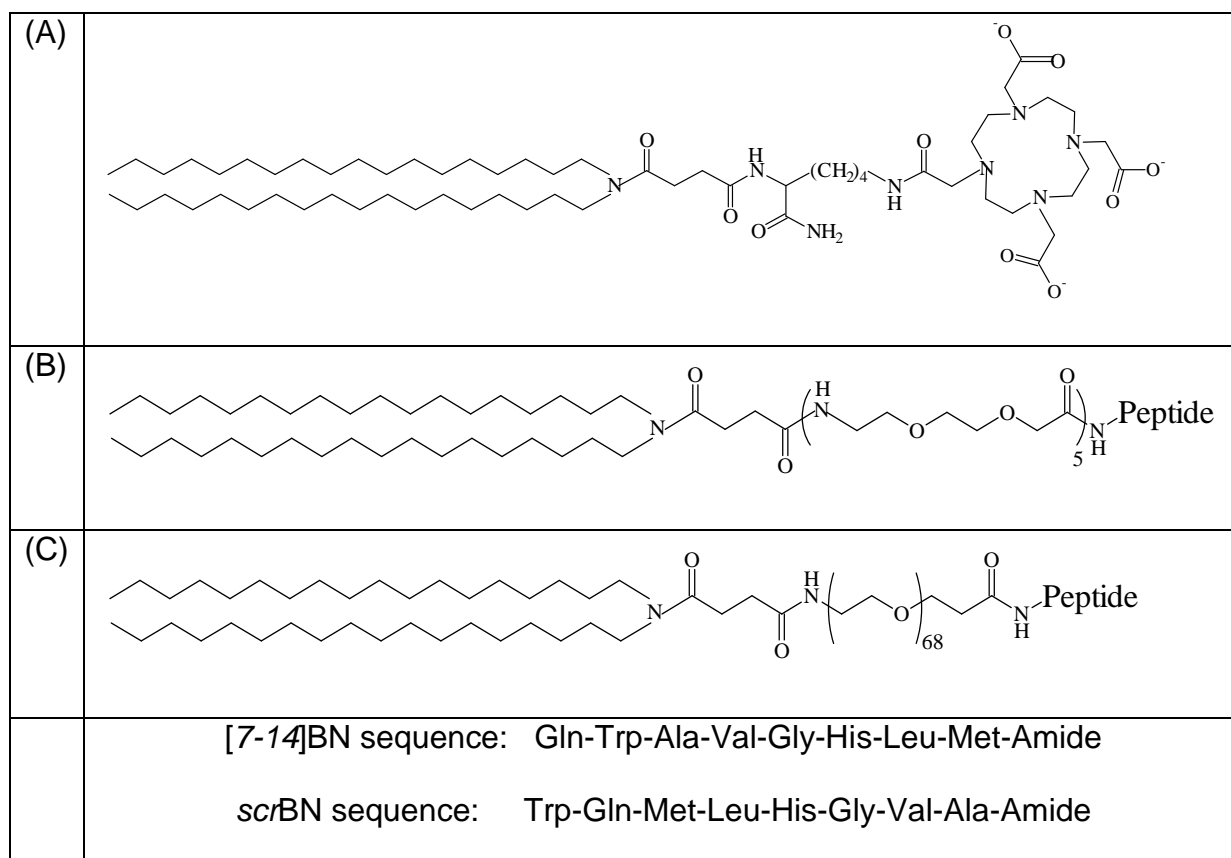


Figure 4.2: Schematic representation of amphiphilic monomers: (A)(C18)₂DOTA; (B) (C18)₂L5-[7-14]BN or (C18)₂L5-*scr*BN(*Sc*); (C)(C18)₂Peg3000-[7-14]BN or (C18)₂Peg3000-*scr*BN.

The synthesis of (C18)₂L5-[7-14]BN, (C18)₂Peg3000-[7-14]BN and the corresponding sequences in which [7-14]BN peptide was replaced by scrambled *scr*BN peptide was performed on solid phase by Fmoc/tBu chemistry according to standard solid phase peptide synthesis protocols, using Rink-amide MBHA resin as polymeric

Table 4.1: Critical micellar Concentration (cmc) values of binary systems obtained by using ANS and Pyr fluorescent probe.

Systems	CMC ANS (mol Kg ⁻¹)	CMC Pyr (mol Kg ⁻¹)	CMC mean
[7-14]BN-DTPAGlu	4.20E-06	4.60E-06	4.40E-06
[7-14]BN-DOTA	4.60E-06	3.70E-06	4.15E-06
(C18) ₂ DTPAGlu/(C18) ₂ L5-[7-14]BN	7.80E-06	5.60E-06	6.70E-06
(C18) ₂ DTPA/(C18) ₂ L5-[7-14]BN	5.40E-06	4.80E-06	5.10E-06
(C18) ₂ DOTA/(C18) ₂ L5-[7-14]BN	6.00E-06	5.10E-06	5.55E-06
(C18) ₂ DTPAGlu/(C18) ₂ Peg3000-[7-14]BN	5.00E-06	1.40E-06	3.20E-06
(C18) ₂ DTPA/(C18) ₂ Peg3000-[7-14]BN	6.00E-06	2.50E-06	4.25E-06
(C18) ₂ DOTA/(C18) ₂ Peg3000-[7-14]BN	-	-	-

4.2.3 Structural characterization

Figure 4.4a shows the scattering cross sections collected for the binary aqueous systems (C18)₂DOTA and for the ternary aqueous systems (C18)₂DOTA/(C18)₂L5-[7-14]BN.

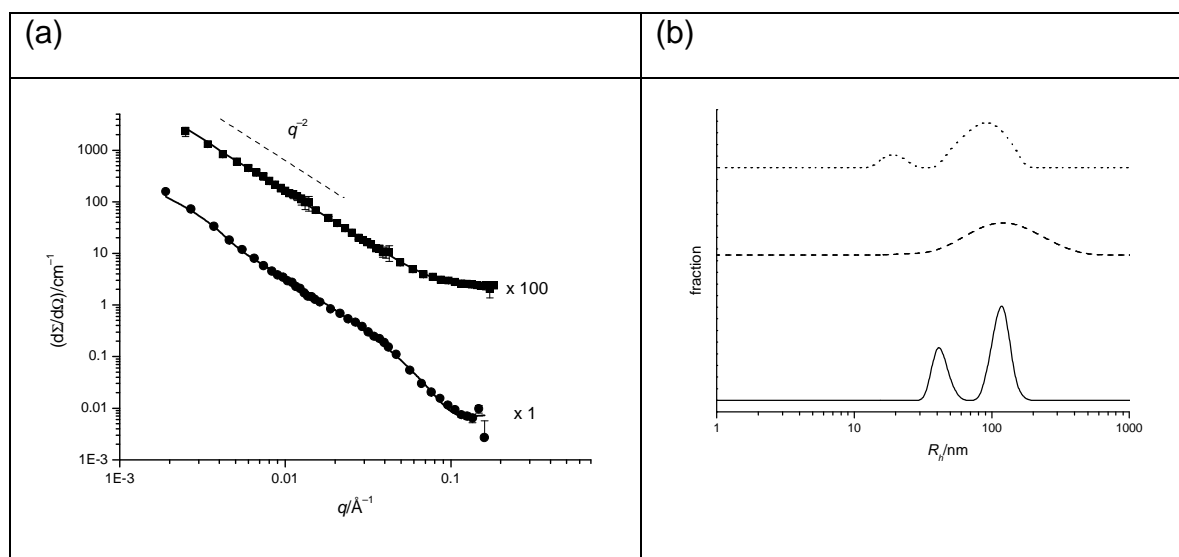


Figure 4.4: Structural characterization: (a) Scattering cross sections at 25°C of (C18)₂DOTA/D₂O (■) and (C18)₂DOTA/(C18)₂L5-[7-14]BN/D₂O (●). For a better visualization, data have been multiplied for a scale factor as indicated. Curves obtained through the fitting of equation 1 are also reported; (b) Hydrodynamical Radius distribution function obtained at 25°C by means of DLS measurements for the following systems: (C18)₂DOTA/H₂O (—), (C18)₂DOTA/(C18)₂L5-[7-14]BN/H₂O (---) and (C18)₂DOTA/(C18)₂Peg3000-[7-14]BN/H₂O (.....).

In figure 4.4b, examples of distribution functions obtained for hydrodynamical radii by means of DLS measurements are reported for aqueous systems (C18)₂DOTA, (C18)₂DOTA/(C18)₂L5-[7-14]BN and (C18)₂DOTA/(C18)₂Peg3000-[7-14]BN.

Inspection of figure 4.4a, reveals that, for both systems, the scattering cross sections $d\Sigma/d\Omega$, at high q , show a power law (q^{-2}) typical of bi-dimensional objects. Actually, as also shown by DLS, this scattering behavior can be ascribed to the presence of

large liposomal aggregates, whose Guinier regime falls almost completely in the very low q value, undetectable with the used SANS apparatus used. Thus, the aggregates presented in our systems have been modeled as a collection of randomly oriented planar sheets, for which the scattering cross sections can be expressed as

$$\frac{d\Sigma}{d\Omega} = 2\pi \Delta_p^2 \rho S d^2 \frac{1}{q^2} \frac{\sin^2\left(\frac{qd}{2}\right)}{\left(\frac{qd}{2}\right)^2} + \left(\frac{d\Sigma}{d\Omega}\right)_{\text{incoh}} \quad (1)$$

where Δ_p is the scattering length density difference between the scattering aggregates and the solvent, d is the plane thickness, S is the total surface per unit volume and $(d\Sigma/d\Omega)_{\text{incoh}}$ represents the incoherent contribution to the scattering cross section, mainly due to the presence of hydrogen nuclei. From a fitting of equation (1) to the experimental data it is possible to evaluate the thickness d of the liposome double layer of the system analyzed. These values are collected in Table 1 together with the values obtained from DLS experiments. Concerning this latter technique, the distribution function obtained for the hydrodynamic radii shows the presence of two diffusive modes for (C18)₂DOTA and (C18)₂DOTA/(C18)₂Peg3000-[7-14]BN aqueous systems, whereas a single mode is present for (C18)₂DOTA/(C18)₂L5-[7-14]BN system. Diffusion coefficients D , obtained through the regularized inverse Laplace transformation of the correlation functions, and hydrodynamic radii found through the Stokes – Einstein equation, provided that the solutions are highly diluted, are also reported in Table 4.2. The sizes obtained for the aggregates formed by the synthesized molecules are consistent with the dimensions of micelles and liposomes, that coexist for (C18)₂DOTA and (C18)₂DOTA/(C18)₂Peg3000-[7-14]BN aqueous systems, whereas for (C18)₂DOTA/(C18)₂L5-[7-14]BN system only large aggregates (liposomes) are present.

Table 4.2: Liposomal bilayer thickness (d), translational diffusion coefficient (D) and hydrodynamical radius (R_h) obtained for the systems investigated by means of SANS and DLS.

Aqueous System	d (Å)	D /cm ² s ⁻¹	R_h (nm)
(C18) ₂ DOTA	41 ± 2	(1.28±0.07)·10 ⁻⁸	190 ± 11
		(5.0±0.4) ·10 ⁻⁸	49 ± 4
(C18) ₂ DOTA/(C18) ₂ L5-[7-14]BN	41 ± 6	(1.2±0.1) ·10 ⁻⁸	200 ± 20
(C18) ₂ DOTA/(C18) ₂ Peg3000-[7-14]BN	$n.m$ ^[a]	(1.15±0.04) ·10 ⁻⁸	211±7
		(1.15±0.05) ·10 ⁻⁷	21±2

^a not measured.

However, in contrast with DLS results, the presence of micellar structures has not been detected in SANS cross sections profile. It is worthy to note that this circumstance does not imply the absolute absence of the smaller aggregates but can be ascribed to the ratio of the two populations that indicates a very large amount of liposomes, thus hiding the contribution of smaller micelles to the cross section

scattering. Inspection of Table 4.2 allows inferring that the thicknesses of the bilayers are substantially constant, around 41 Å, in the two analyzed systems. The low relative amount of the (C18)₂L5-[7-14]BN compared to the (C18)₂DOTA in the 10/90 mixed aggregates does not have a strong influence on the thickness of the double layers. Moreover the three supramolecular aggregates, independently from the presence of the peptide containing monomer in the final composition, show similar shape and size with a hydrodynamic radius R_q around 200 nm. A schematic view of the liposomal aggregates is reported in Figure 4.5.

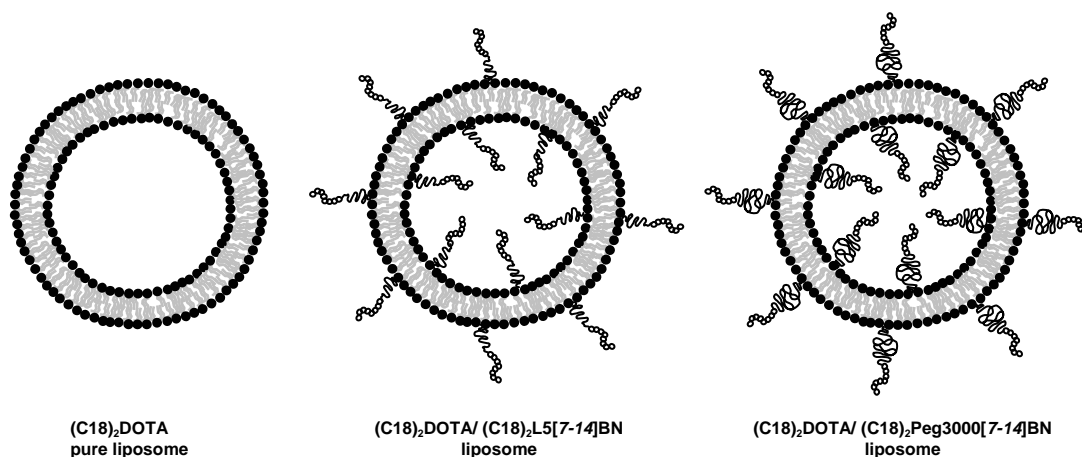


Figure 4.5: Schematic view of pure and mixed liposomal aggregates. In all cases, independently from the presence of 10% in peptide monomer in the final composition, liposomes show hydrodynamic radius, R_h , around 200 nm and bilayer, d , thickness of 4 nm.

As it concerns the micellar aggregates found, in low amount, in (C18)₂DOTA and (C18)₂DOTA/(C18)₂Peg3000-[7-14]BN samples, we note that DLS measurements are not able to provide the shape and the detailed dimensions of these objects. However, a simple calculation on the synthesized molecules, by assuming an all-trans conformation, provides a linear length of $\sim 40 \div 60$ Å, quite far from the hydrodynamical radius found for the micellar structures, probably due to the formation of elongated structures like rod-like or worm-like micelles.

Finally, SANS measurements carried out on mixed aggregates containing the monomer in which [7-14]BN peptide is replaced with the scramble peptide sequence (*scr*BN), don't show, as expected, significant structural modifications.

4.2.4 *In vitro* studies

Binding and internalization assays of ¹¹¹In-DOTA-βAla-[7-14]BN and ¹¹¹In-DOTA-βAla-*scr*BN peptide conjugates were performed on PC-3 cell lines at 37 °C, at different time points (0.5, 1.0, 2.0 and 4.0 h). Blocking studies performed using large excess of [Tyr⁴]-BN demonstrated that the uptake was receptor mediated. As shown in Figure 4.6A and in agreement with previous reports in the literature, ¹⁴⁶ high and specific binding and internalization of ¹¹¹In-DOTA-βAla-[7-14]BN peptide (8.98 ± 0.49 % at 4h) was found, while the scrambled peptide shows almost no binding and internalization. Receptor-mediated cellular uptake kinetics of mixed aggregates ((C18)₂DOTA/(C18)₂L5-[7-14]BN and (C18)₂DOTA/(C18)₂Peg3000-[7-14]BN) was evaluated in a similar fashion. The corresponding mixed aggregates in which the BN

peptide is replaced by a scrambled sequence ((C18)₂L5-*scr*BN or (C18)₂Peg3000-*scr*BN) and aggregates containing only (C18)₂DOTA were used as negative controls. Radiolabeling of the aggregates was performed at 2×10^{-4} M concentration. Trace amounts of ¹¹¹InCl₃ and up to 100 μCi were added to the aggregate formulation after addition of an equal volume of 0.4 N sodium acetate buffer. Confirmation of incorporation of the radioactive label into the aggregates was obtained by gel filtration. Specific preferential binding to PC-3 cells of mixed aggregates containing the five units of AdOO (L5 spacer) between the BN peptide sequence and the hydrophobic chains was observed ($10.3 \pm 0.82\%$ at 4h, Figure 4.6B), compared to the same aggregates in which the BN peptide was replaced by a scrambled sequence ($5.92 \pm 0.78\%$ at 4h) and to the (C18)₂DOTA aggregates ($1.63 \pm 0.14\%$ at 4h). Moreover, binding experiments of mixed aggregates (C18)₂DOTA/(C18)₂L5[7-14]BN were also performed after pre-incubation of cells with the [Tyr⁴]-BN blocking reagent. Surprisingly, under these experimental conditions liposomes containing (C18)₂DOTA alone show higher binding, with levels comparable to those obtained with the BN containing mixed aggregates (data not shown). We speculated that the hydrophobic residues on the N-terminus of the peptide may be encapsulated in the liposome bilayer during incubation with the cells. This hypothesis was confirmed by fluorescence spectroscopy experiments in which a solution containing (C18)₂DOTA aggregates was incubated, under stirring by vortex for 1 minute, with a small amount of [Tyr⁴]-BN (1 mg). 100 μl of the final solution were separated by gel filtration. The presence in the first gel-filtration fractions of a peak at 350 nm, corresponding to the fluorescence emission of the Trp residue in [Tyr⁴]-BN, confirms encapsulation of the [Tyr⁴]-BN in the aggregates. These results indicate that the [Tyr⁴]-BN peptide is unsuitable as receptor blocking reagent in the experiments with aggregates.

As shown in figure 4.6B, mixed aggregates show progressively increasing cell associated radioactivity over time (60 min vs. 240 min), regardless of which peptide is contained on the surface. Conversely, (C18)₂DOTA containing aggregates show no change in the levels of cell associated activity over time. This phenomenon could be related to the presence of the oxoethylene moieties in the L5 linker that, as previously reported for pegylated liposomes, favors accumulation of aggregates on tumor cells. By using similar binding experiments, we investigated the behavior of (C18)₂DOTA / (C18)₂Peg3000[7-14]BN. The cell associated radioactivity, as shown in Figure 4.6C, is lower compared to the values found for the aggregates containing the L5 spacer in the peptide monomer. We also observed similar values of cell associated radioactivity at all time points investigated for the two aggregates containing either the receptor specific [7-14]BN or the scrambled control peptides. For example, at 4h we found $5.20 \pm 0.39\%$ and $4.89 \pm 0.35\%$, respectively. Even if these values are higher compared to the (C18)₂DOTA aggregates ($1.63 \pm 0.14\%$ at 4h), there is no apparent specificity in binding and internalization due to the bioactive peptide sequence. The presence of the Peg3000 unit on the external liposomal surface may mask the peptide and prevent receptor binding. Moreover, the presence of Peg3000 increases non specific binding to tumor cells compared to the (C18)₂DOTA containing aggregates. These results indicate that aggregates containing a spacer with only five residues of AdOO yield higher accumulation and superior specific interaction with the PC3 cells compared to aggregates containing the longer Peg3000 spacer. Therefore, the (C18)₂DOTA/(C18)₂L5[7-14]BN mixed aggregate was chosen for experiments in an animal model, using the corresponding aggregate containing the *scr*BN peptide as negative control.

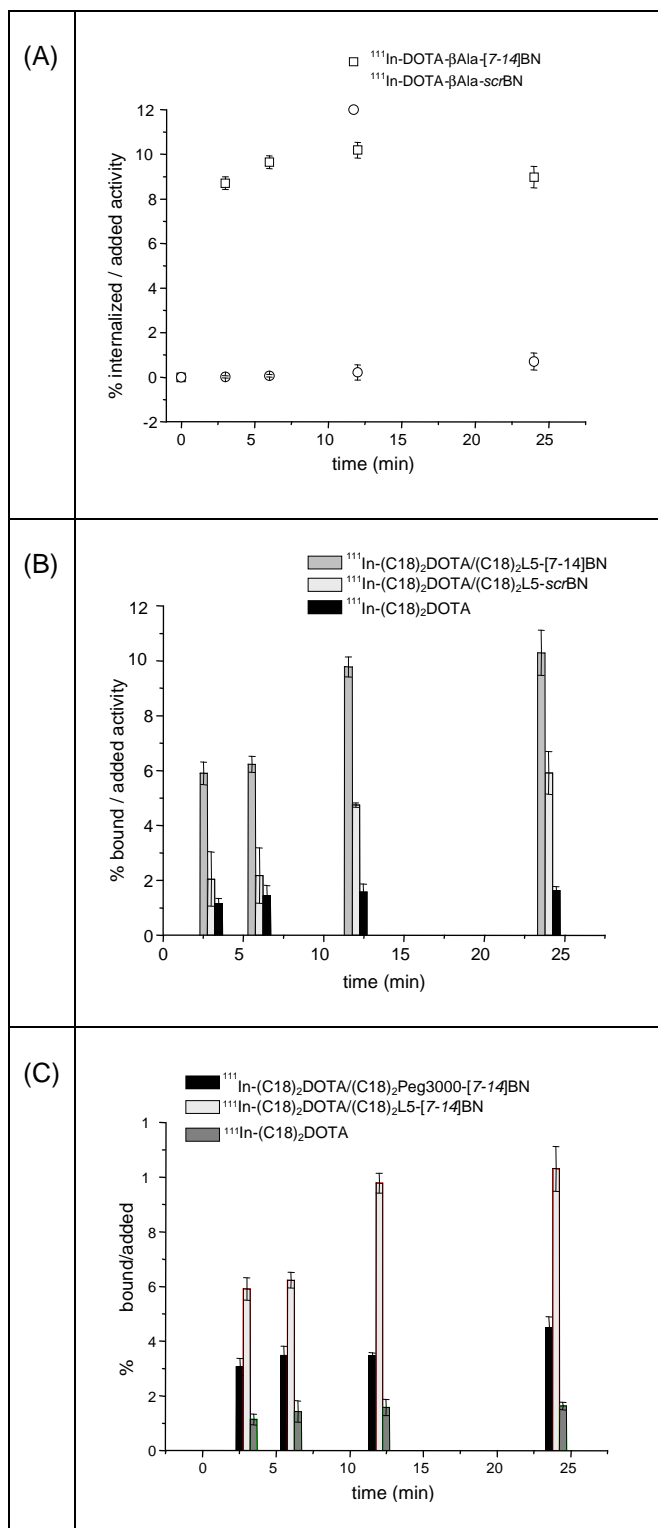


Figure 4.6: Binding assays on PC-3 cell lines overexpressing the GRP at 37 °C, at different time points (0.5, 1.0, 2.0 and 4.0h): (A) binding of $^{111}\text{InDOTA-}\beta\text{Ala-[7-14]BN}$ in comparison with $^{111}\text{InDOTA-}\beta\text{Ala-scrBN}$ radiolabeled peptides; (B) binding of ^{111}In -labeled aggregates $(\text{C18})_2\text{DOTA} / (\text{C18})_2\text{L5-[7-14]BN}$ (90/10) with respect to the corresponding aggregates in which the BN peptide is replaced by the BN scrambled peptide and to the $(\text{C18})_2\text{DOTA}$ pure aggregate; (C) binding of ^{111}In -labeled aggregates $(\text{C18})_2\text{DOTA}/(\text{C18})_2\text{Peg3000-[7-14]BN}$ in comparison with $(\text{C18})_2\text{DOTA}/(\text{C18})_2\text{L5-[7-14]BN}$ aggregates and with the $(\text{C18})_2\text{DOTA}$ aggregate.

4.2.5 *In Vivo* studies

In vivo biological behavior of ^{111}In -(C18)₂DOTA/(C18)₂L5[7-14]BN and ^{111}In -(C18)₂DOTA/(C18)₂L5[7-14]scrBN aggregates was evaluated after intravenous injection into GRPR positive tumor bearing mice (PC-3 xenografts). Figure 4.7c shows results of these experiments. Time activity curves of blood radioactivity concentration (Figure 4.7a) show fairly long circulation times of the aggregates. This is expected and desired as the intended application of these aggregates is drug delivery that requires high blood concentration of drugs for prolonged periods of time. The observed circulating half-lives of 4-5 h are in agreement with published reports on similar aggregates¹⁴⁷ and are the equivalent of 2-3 day half lives in humans.¹⁴⁸ Biodistribution at 48 h (Figure 4.7b) indicates that most radioactivity is in the liver whereas lower levels are obtained in the other organs. Among the other organs, tumors show relatively higher concentrations and the GRPR targeting ^{111}In -(C18)₂DOTA/(C18)₂L5-[7-14]BN aggregates show higher concentration in the PC-3 tumors compared to the scrambled peptide containing control aggregates. There is a slight increase in concentration of the GRPR targeting aggregate in the tumors compared to control at the 48 h time point evaluated (2.4% ID/g versus 1.6 % ID/g), this finding justifies further evaluation of this approach. It is noteworthy to point out that the overall accumulation of a potential drug carried by the aggregates to the target tumor is not only dependent on concentration of the aggregate in the tumor at the single time point but is also dependent on aggregate concentration as a function of time. Thus the integral of drug concentration in the tumor versus time is likely to benefit greatly from the targeting ability of the liposomes although this aspect needs to be specifically addressed in future experiments.

Figure 4.7c shows gamma camera images at different times after injection of ^{111}In -(C18)₂DOTA/(C18)₂L5-[7-14]BN containing aggregates. The images confirm the high uptake in liver and spleen and clearly show accumulation in the receptor positive tumors. There is similar contrast among the different organs at the three time points, indicating that the relative differences in concentration of the compound in normal organs and in the tumor is maintained throughout the 48 h observation period.

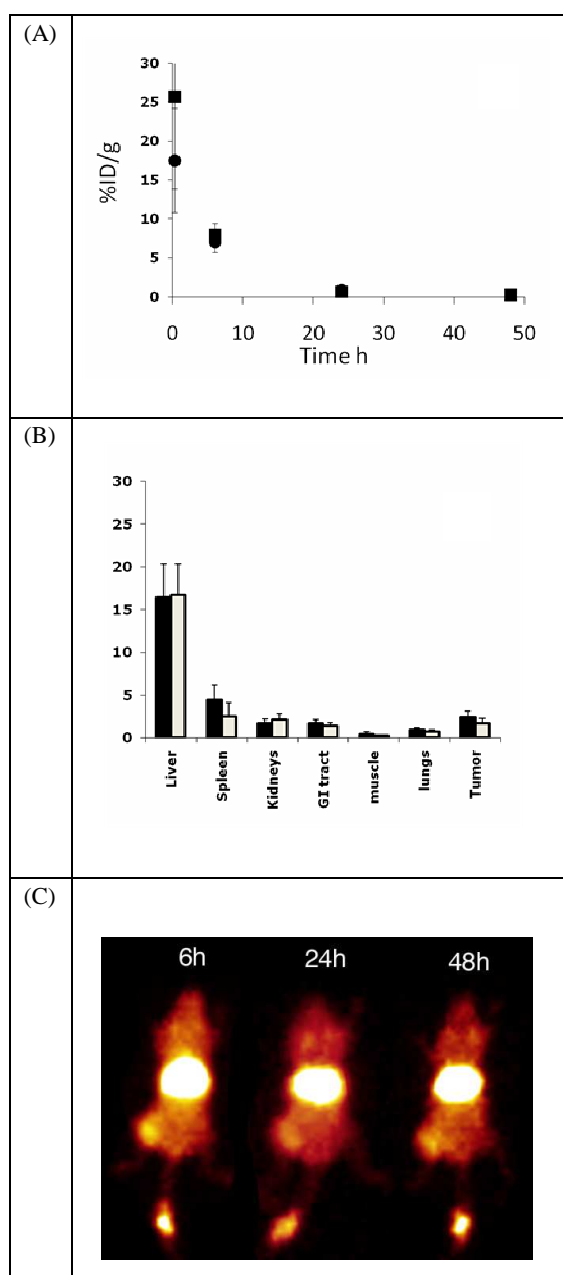


Figure 4.7: Animal studies. (A) Blood time activity curve following intravenous injection of $^{111}\text{In}-(\text{C18})_2\text{DOTA}/(\text{C18})_2\text{L5}-[7-14]\text{BN}$ aggregates (squares) and $^{111}\text{In}-(\text{C18})_2\text{DOTA}/(\text{C18})_2\text{L5}-[7-14]\text{scrBN}$ aggregates (circles). Error bars = SD. Blood clearance of radioactivity is slow and similar for the two aggregates. (B) Organ biodistribution at 48 h after injection of $^{111}\text{In}-(\text{C18})_2\text{DOTA}/(\text{C18})_2\text{L5}-[7-14]\text{BN}$ aggregates (black bars) and $^{111}\text{In}-(\text{C18})_2\text{DOTA}/(\text{C18})_2\text{L5}-[7-14]\text{scrBN}$ aggregates (white bars). Error bars = SD. There is high liver concentration of both aggregates. Uptake in other organs is similar for the two compounds. Higher uptake is observed for $^{111}\text{In}-(\text{C18})_2\text{DOTA}/(\text{C18})_2\text{L5}-[7-14]\text{scrBN}$ aggregates in the GRPR positive tumors. (C) Gamma camera images (ventral view) at different times after injection of $^{111}\text{In}-(\text{C18})_2\text{DOTA}/(\text{C18})_2\text{L5}-[7-14]\text{scrBN}$ aggregates. Highest uptake is observed in liver although activity in spleen as well as in the tumor located in the right flank are clearly visible over background. Relative concentration of radioactivity in the different organs does remains relatively constant over the 48 h observation period.

4.3 Experimental Section: Bombesin

4.3.1 Materials

Protected N^α-Fmoc-amino acid derivatives, coupling reagents and Rink amide *p*-methylbenzhydrylamine MBHA resin, Fmoc-8-amino-3,6-dioxaoctanoic acid (Fmoc-AdOO-OH), Fmoc-21-amino-4,7,10,13,16,19-hexaoxaheneicosanoic acid (Fmoc-AhOH-OH), DTPAGlu(OtBu)₅, DOTA(OtBu)₃-OH, Lys[DOTA(OtBu)₃]-OH derivative, [¹¹¹In]Cl₃ were purchased as reported in the paragraph 3.3.1 α-(9-Fluorenylmethyloxycarbonyl) amino-ω-carboxy poly(ethylene glycol) (Fmoc-NH-Peg3000-COOH) and Fmoc-4-(2-aminoethyl)-1-carboxymethyl-piperazine dihydrochloride (Fmoc-Acp•2HCl) were purchased by Iris Biotech GmbH (Marktredwitz, Germany). N,N-dioctadecylsuccinamic acid was synthesized according to literature (26). [¹¹¹In]Cl₃ was purchased from Mallinckrodt Med. All solutions were prepared as reported in the paragraph 3.3.1 The pH of all solutions was kept constant at 7.4. Analytical and Preparative HPLCs, LC-MS analyses and UV measurements were performed as described previously. The fluorescences studies, DLS and SANS measurements were performed as previously described.

4.3.2 Peptide Conjugate Synthesis

Peptide syntheses were carried out in solid-phase under standard Fmoc strategy. Rink-amide MBHA resin (0.78 mmol/g, 0.5 mmol scale, 0.640 g) was used. The elongations of the [7-14]BN, scrBN and 6-14[Acp⁶,Nleu⁸]BN peptides were achieved by sequential addition of Fmoc-AA-OH. Fmoc-AdOO-OH and Fmoc-NH-Peg3000-COOH linkers were coupled manually in DMF by using an excess of 2 equivalents. Instead Fmoc•Acp linker was coupled manually in DCM/DMF (50/50) by using an excess of 2 equivalents, the coupling was performed for over night. N,N-dioctadecylsuccinamic acid (0.5 mmol scale, 0.622 g) coupling was carried out as described in the paragraph 3.3.1. For the synthesis of the (C18)₂-(AhOH)-Lys(DTPAGlu)-(AhOH)₂-[7-14]BN ([7-14]BN-DTPAGlu), (C18)₂-(AhOH)-Lys(DOTA)-(AhOH)₂-[7-14]BN ([7-14]BN-DOTA), (C18)₂-(AhOH)-Lys(DTPAGlu)-(AhOH)₂-scrBN (scrBN-DTPAGlu), and (C18)₂-(AhOH)-Lys(DTPAGlu)-(AhOH)₂-6-14 [Acp⁶,Nleu⁸]BN (6-14 [Acp⁶,Nleu⁸]BN-DTPAGlu), after Fmoc removal from the N-terminal end of the peptide derivative, 1,250 g (0.50 mmol) of Dde-Lys(Fmoc)-OH, activated by a stoichiometric amount of PyBop and HOBt and two equivalents of DIPEA in DMF, were coupled by stirring the the resin slurry suspension for 60 min. The solution was filtered and the resin was washed with three portions of DMF. After removal of the Fmoc group on side chain of lysine residue, the chelating agent (DTPAGlu pentaester or DOTA trisester) was linked, through its free carboxyl function, to the ε-NH₂ of the lysine residue. This coupling step was performed using two equivalents of the chelating agent, HATU and four equivalents of DIPEA in DMF as a solvent. The coupling time, compared with the classical solid-phase peptide synthesis protocol, was increased up to 120 min. The resin was washed three times with DMF, then, the 1-(4,4-dimethyl-2,6-dioxo-cyclohexylidene)3-methylbutyl group (Dde) was removed by treatment with DMF/Hydrazine mixture (98 : 2). The peptide-resin was stirred with 3.0 mL of this solution for 10 min. The treatment was repeated twice, and the reaction was monitored by the qualitative Kaiser test. On N-terminal moiety, the Fmoc-AhOH-OH linker was coupled following the same procedure above described. After the removal of N-terminal Fmoc protecting group, N,N-dioctadecylsuccinamic

acid (0.622 g, 0.5 mmol) was coupled performed the same procedure above described in the paragraph 3.1. The peptide derivatives were cleaved from the solid support by suspending the resin in 10 mL of TFA/TIS/H₂O (95.5/2/2.5) mixture for 120 min. During this step all the amino acid side chains and the carboxylic groups of the chelating moiety were simultaneously freed from their protecting groups. Free peptide derivatives were worked up as described in the chapter 3.2.

DOTA-βAla-[7-14]BN and DOTA-βAla-scrBN: *Rt* = 19.1 min; *MW* = 1525 amu; $[M+H^+] = 1526.0$ amu.

(C18)₂L5-[7-14]BN and (C18)₂L5-scrBN: *Rt* = 22.50 min; *MW* = 2264 amu; $[M+2H^+]/2 = 1133.0$ amu.

(C18)₂Peg3000-[7-14]BN and (C18)₂Peg3000-scrBN: *Rt* = 21.9 min; *MW* = 4544 amu; $[M+3H^+]/3 = 1515.7$ amu, $[M+2H^++Na^+]/3 = 1523.0$ amu.

(C18)₂L5-6-14[Acp⁶,Nle⁸]BN: *Rt* = 23.90 min; *MW* = 2417 amu; $[M+2H^+]/2 = 1209.5$ amu.

(C18)₂-(AhOH)-Lys(DTPAGlu)-(AhOH)₂-[7-14]BN, [7-14]BN-DTPAGlu: *Rt* = 41.0 min; *MW* = 3116 amu.

(C18)₂-(AhOH)-Lys(DOTA)-(AhOH)₂-[7-14]BN, [7-14]BN-DOTA: *Rt* = 39.0 min; *MW* = 3062 amu.

(C18)₂-(AhOH)-Lys(DTPAGlu)-(AhOH)₂-scrBN, scrBN-DTPAGlu: *Rt* = 41.0 min; *MW* = 3116 amu.

(C18)₂-(AhOH)-Lys(DTPAGlu)-(AhOH)₂-6-14[Acp⁶,Nle⁸]BN, 6-14[Acp⁶,Nle⁸]BN-DTPAGlu: *Rt* = 37.50 min; *MW* = 3277 amu;

4.3.3 Aggregates Preparation

All solutions of [7-14]BN-DOTA and [7-14]BN-DTPAGlu, and the mixed aggregates peptide containing monomer and the chelating agent containing monomer in ratio molar (10:90) were prepared as described in the chapter 3.2. At same way was determined the solution concentrations and the preparation of the solutions for SANS measurements.

4.3.4 Preparation of the Radiotracers

The DOTA-βAla-[7-14]BN and DOTA-βAla-scrBN radiopeptides were prepared according to Wild et al.¹⁴⁹ Briefly, 10 μg of peptide in 250 μL of sodium acetate buffer (0.4 mol/L, pH 5.0) were incubated with ¹¹¹InCl₃ (3 to 5 μCi) for 30 min at 95°C and then excess of ^{nat}InCl₃ × 5H₂O was added to afford structurally characterized homogenous ligands. Radiolabeling of the aggregates was performed at final concentration of 2 × 10⁻⁴ M. Trace amounts of ¹¹¹InCl₃ (100 μCi) were added to 1 mL of the aggregates and sodium acetate buffer (0.4 mol/L, pH 5.0) was added to reach a final volume of 2 mL. The mixture was incubated for 30 min at 90°C. Confirmation of

incorporation of the label into the aggregates was obtained by gel filtration on Sephadex G-50 pre packed columns (Pharmacia Biotech).

4.3.5 In vitro studies

PC-3 cells were seeded into 6-well plates wherein they remained overnight ($0.8-1.0 \times 10^6$ cells per well). On the day of the experiment the medium was removed, the cells were washed twice with fresh medium (DMEM with 1% fetal bovine serum, pH 7.4) and incubated for 1h at 37°C. Internalization experiments of the ^{111}In -labeled peptides were performed as indicated in literature.¹⁵⁰ Approximately 0.08 μCi of $^{111}\text{natIn}$ -labeled peptide (0.25 pmol) were added to the medium and the cells were incubated (in triplicates) for 0.5, 1, 2 and 4 h at 37°C, 5% CO_2 . A 1000 fold excess of [Tyr⁴]-BN was used to determine non specific internalization. At each time point the internalization was stopped by removing the medium followed by washing the cells with ice-cold solution of phosphate-buffered saline (PBS, pH 7.4). Cells were then treated 5 min (twice) with glycine buffer (0.05 mol/L glycine solution, pH adjusted to 2.8 with 1 mol/L HCl) to distinguish between cell surface-bound (acid releasable) and internalized (acid resistant) radioligand. Finally, the cells were detached from the plates by incubating with 1 mol/L NaOH for 10 min at 37°C.

An amount of 0.5 μCi (100 μL) per well ^{111}In -labeled aggregates to a final concentration of 2×10^{-4} M were added to the medium and the cells were incubated (in triplicates) for 0.5, 1, 2 and 4 h at 37°C, 5% CO_2 . Afterwards, the binding buffer was aspirated and the cells were washed twice with ice-cold phosphate-buffered saline (PBS, pH 7.4); this represented the unbound fraction. The cells were then collected with 1 N NaOH; this corresponded to the bound fraction. The calculations of the in vitro experiments were done by measuring the radioactivity of each collected fraction in a γ -counter (Cobra II; Packard Instrument Co.) related to the standards.

4.3.6 In vivo studies

Animal experiments were carried out on 6 week old female CD1 nude mice (Charles River Italia). Mice bearing xenografts of PC-3 cells were generated as previously described.³⁰ Briefly, 100 μL of the cell suspensions at a density of $2-3 \times 10^7 \text{ mL}^{-1}$ in PBS were injected the flank of mice (weight 17–23 g). Biodistribution and imaging experiments were performed two weeks after implanting cells (tumor sizes were between 0.5 and 1 g). Procedures involving animals and their care were in conformity with institutional guidelines that comply with national and international laws and policies. Approximately 100 μCi of ^{111}In -labeled aggregate preparation (C18)₂DOTA/(C18)₂L5-[7-14]BN and the corresponding aggregates in which the BN peptide is replaced by the scrambled peptide) were injected into the lateral tail vein of each mouse (n = 5). Imaging was performed at different times after injection, following administration of an intraperitoneal anesthetic on a clinical gamma camera equipped with a medium energy collimator. Venous orbital sinus samples were also collected at different times to obtain blood time activity curves. The animals were killed 48 h after injection, imaged and subsequently dissected in order to quantitatively determine organ concentrations of radioactivity by weighing and counting each dissected organ. Dilutions of the injected compound were simultaneously counted for accurate determination of the injected dose. The relative amount of radioactivity in the organs was calculated and expressed as percentage of the injected dose/gram tissue (%ID/g) normalized to a 20 g mouse.

5. Supramolecular aggregates labeled with Cholecystokinin

5.1 Introduction

The cholecystokinin (CCK) peptides have been implicated in various regulatory functions: as neurotransmitters in the brain and in the regulation of various functions of the gastrointestinal tract; primarily at the level of the stomach, pancreas, and gallbladder.¹⁵¹ In addition, they can act as physiological growth factors in most parts of the gastrointestinal tract and also as stimulatory growth factors in several neoplasms, such as colon and gastric cancers.^{152, 153}

The actions of the CCK are mediated by two different receptor types, called CCK_A-R and CCK_B-R receptors, respectively.¹⁵⁴

Most of the studies focus on the binding mode of the C-terminal cholecystokinin octapeptide amide (CCK 26-33 or CCK8) that displays high affinity for both receptors, even if the sulphated form of CCK8 (with a sulphate moiety on the Tyr27 side chain) is 1000-fold more active than the non-sulphated CCK8 in binding to CCK_A-R. The NMR structure of the complex CCK8 with the 47-residue N-terminal extracellular arm of the CCK_A-R, suggests that CCK8 binds to CCK_A-R with the C-terminus within the seven-helical bundle of the GPCR and the N-terminal side projecting out between the trans-membrane loops 1 and 7 and specifically interacting with N-terminus of CCK_A-R (Figure 5.1).

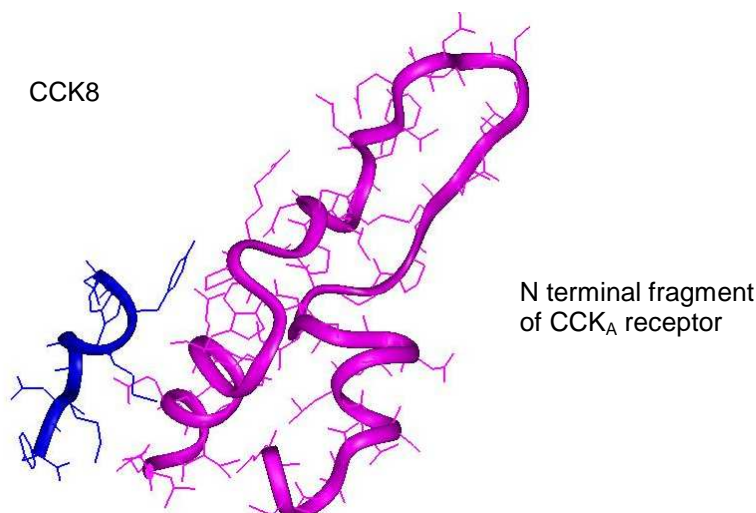


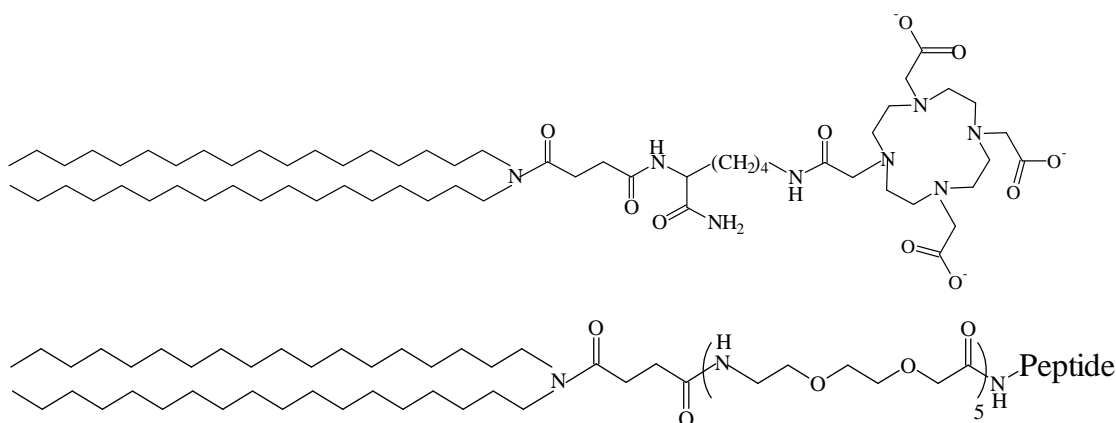
Figure 5.1: Interaction between the CCK8 peptide and the CCK_A-47 residue N-terminal fragment.

This study suggests that modifications on the N-end of CCK8 obtained by introducing chelating agents, their metal complexes and other substituents should not affect the interaction with CCK_A-R.¹⁵⁵ The design of the amphiphilic molecules was carried out as the previous reported monomers introducing on N-terminus ethoxilic linkers and two units of eighteen alkyl carbon.

5.2 Results & Discussion

5.2.1 Monomer Synthesis and Aggregate Preparation

The CCK8 peptide conjugate $(C18)_2L5CCK8$ was also synthesized on solid phase following the same procedures as above reported previous (see paragraph 3.3.2).¹¹⁷ A CCK8 fluorescent derivative (FITC- β Ala-Gly-CCK8) was also synthesized and used to verify CCK receptor expression on the selected cells. In this case a β -alanine residue was introduced between the FITC chromophore group and the CCK8 N-terminus to avoid fluoresceine elimination by the Edman degradation mechanism.¹⁵⁶ The assembly of pure and mixed aggregates was obtained by combining, in a 10:90 molar ratio, the $(C18)_2L5CCK8$ and the $(C18)_2DOTA$ monomers (Figure 5.2). The drug loading content (*DLC*), defined as the weight percentage of doxorubicin in the aggregates), and the releasing properties of the liposomal aggregates were studied by using the cytotoxic doxorubicin as drug model.



Peptide sequence: Gly-Glu-Tyr-Met-Gly-Trp-Met-Glu-Phe-Amide

Figure 5.2: Schematic representation of $(C18)_2DOTA$ and $(C18)_2L5CCK8$ amphiphiles. The CCK8 peptide sequence is reported using the amino acid three-letter code.

The mixed aggregate in which a small amount (10%) of amphiphilic peptide derivative is added to the $(C18)_2DOTA$ monomer, preserves the same liposomal structure and dimension, as already experienced for mixed aggregates based on similar synthetic amphiphilic monomers.

5.2.2 Doxorubicin loading and release from liposomes

Cytotoxic doxorubicin (DOX) was loaded in the liposomes by using the well-assessed procedures based on ammonium ion gradient. Doxorubicin solution was incubated under stirring for 12 h at 4°C. Subsequently, unloaded doxorubicin was removed by Sephadex G50 column pre-equilibrated with HBS. The weight drug/weight lipid ratio chosen for the loading experiments was based on the value reported for Doxil, in which a 0.127 weight drug/weight lipid ratio is found. The doxorubicin loading content was calculated by fluorescence measurements at 590 nm for subtraction the amount

of free doxorubicin, eluted by gel filtration, from the total amount of loaded doxorubicin. A calibration curve was constructed using different concentrations of free DOX in HBS. The *DLC* was above 95% of the total; and the corresponding weight drug/weight lipid ratio, observed on these experimental conditions, is 0.134. The release profile of DOX from liposomes (DOTA-DOX and CCK8/DOTA-DOX) was studied within 96 h, using a dialysis membrane immersed in HEPES buffer (pH 7.4) at 37 °C temperature. Transfer of released DOX through dialysis membrane to buffer solution was assumed to take place rapidly, and the release of DOX from its liposomal vehicle to medium was assumed to be the rate-limiting step in this process. The amount of DOX released was estimated by UV-Vis spectroscopy at 480 nm and the releasing profiles for the two liposomes are reported in Figure 5.3, as percentage of the total encapsulated doxorubicin. No significant difference was observed between DOTA-DOX and CCK8/DOTA-DOX liposomes.

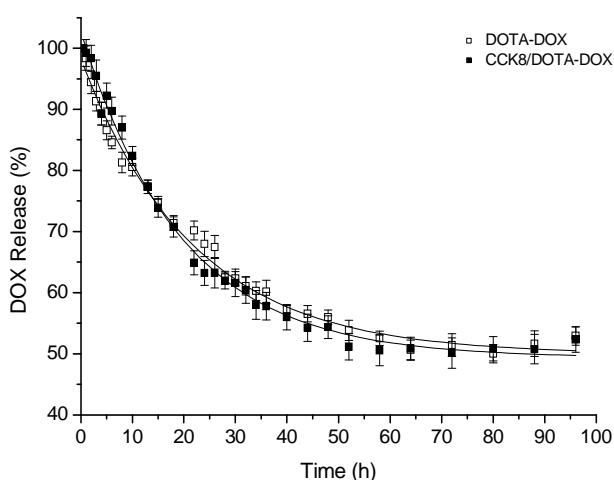


Figure 5.3: Release of DOX by CCK8/DOTA-DOX, and DOTA-DOX liposomes. The amount of DOX released was estimated by UV-Vis spectroscopy at 480 nm.

5.2.3 Cellular uptake and *in vitro* cytotoxicity of liposomal DOX

The expression of CCK₂-R on HuVEC and A431 cells was analyzed by flow cytometric assays. The cells were incubated with FITC-βAla-Gly-CCK8 peptide and FITC alone, which was used as negative control. Experiments were performed at 4°C, in order to block non-specific binding. Results indicate significant expression of CCK₂-R, the difference in expression was approximately two-fold increased for A431 cells with respect to HuVEC cells (Figure 5.4). Specific binding between CCK₂-R and FITC-βAla-Gly-CCK8 was also demonstrated by performing competition experiments in which an excess of unlabeled CCK8 peptide was added.

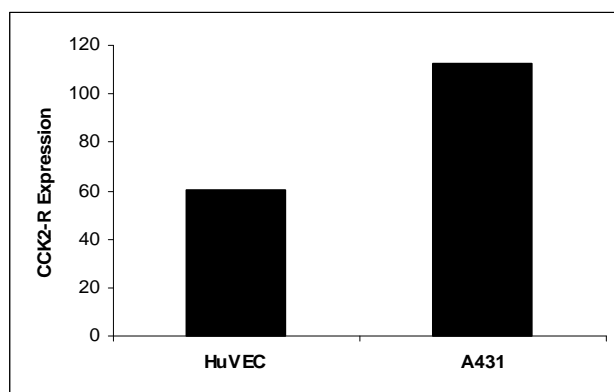


Figure 5.4: Relative expression of CCK₂-R as determined by FACS analysis for HuVEC and A431 cells. The cells (10⁶ cells/ml) were incubated with 80 nM FITC-βAla-Gly-CCK8 for 1 h at 4°C. Cells treated with 80 nM FITC were used as negative control. The results are expressed as relative fluorescence, i.e. mean fluorescence of the sample minus the mean fluorescence of the corresponding control. Measurements were performed three times and typical results are shown.

The cellular uptake of the targeted liposomal doxorubicin formulation (CCK8/DOTA-DOX) with respect to the self-assembled liposomal non-specific doxorubicin (DOTA-DOX) was estimated by using flow cytometry analysis based on DOX fluorescence. Experiment on free doxorubicin and empty aggregates were also performed as control. As shown in Table 5.1 and Figure. 5.5, under the same concentration (1 μg doxorubicin/ml) the cell associated DOX on A431 and HuVEC cells for CCK8/DOTA-DOX was respectively 70 and 8 fold higher than for DOTA-DOX treated cells. This result indicates that bioactive peptide in CCK8/DOTA-DOX is able to enhance the DOX uptake into the carcinoma cells *in vitro* compared to DOTA-DOX.

Table 5.1 Uptake of liposomal DOX in normal and transformed cells

DOX formulation	relative fluorescence	
	A431	HuVEC
CCK8/DOTA-DOX	8.63 ± 1.08	3.16 ± 0.78
DOTA-DOX	0.12 ± 0.03	0.36 ± 0.20
free DOX	23.71 ± 1.86	28.40 ± 3.90

Values are expressed as relative fluorescence intensity i.e. mean of fluorescence minus the mean of fluorescence of control.

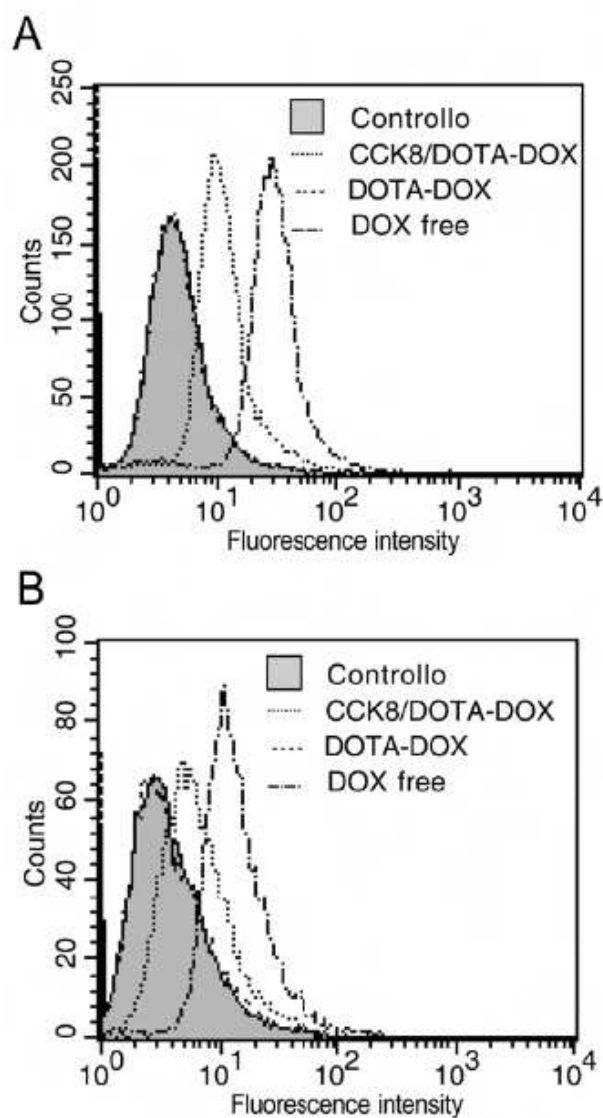


Figure 5.6: Flow cytometric analysis of association of liposomal DOX and free DOX with human cells. A431 cells (A) and HuVEC cells (B) at a density of 1×10^6 cells/ml were incubated with CCK8/DOXA-DOX, DOXA-DOX, and free DOX at a final concentration of $1 \mu\text{g}$ DOX/ml for 1 h at 4°C . Untreated cells were used as negative control. Histograms were obtained from a single experiment and were representative of three similar experiments.

The higher levels of DOX in tumour cells treated with CCK8/DOXA-DOX were not caused by the augmented leakage of DOX because the DOX release for CCK8/DOXA-DOX was very similar to that for DOXA-DOX as shown in Figure. 5.3. As expected the highest amount of cell associated fluorescence was observed with free DOX. The effect of liposomal DOX on cytotoxicity of carcinoma cells was also assessed. A431 cells were exposed to liposomal formulation for 8 h and the cell viability was measured by MTT assays (Figure. 5.7). Incubation with CCK8/DOXA-DOX showed significantly lower cell survival compared to DOXA-DOX treated cells, in presence of drug amounts ranged between 250 and 1000 ng/ml. On the other hand, liposomal DOX below 100 ng/ml concentration showed no significant differences on cell survival. In experiments performed with free DOX, 50% cell killing

was observed with 30 ng/ml of drug. This result suggests a lower toxicity of the liposomal cytotoxic drug with respect to the free-drug.

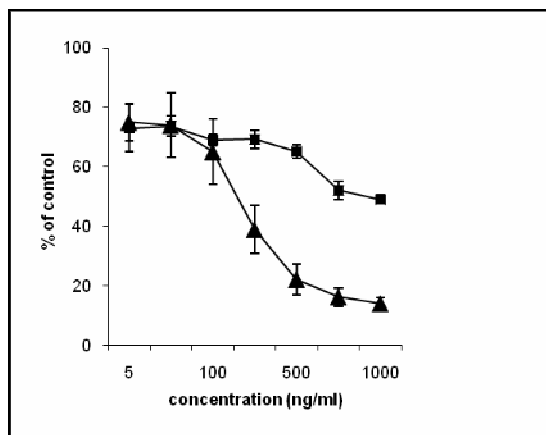


Figure 5.7: Cytotoxicity of liposomal DOX against human carcinoma cells. A431 cells (3000 cells/well) were incubated with CCK8/DOX-DOX (▲) and DOTA-DOX (■) at different concentration ranging between 0 and 1000 ng/ml at 37°C. After 8 h the medium was removed and after additional 72 h an MTT assay was performed. Data are expressed as percent of control. Each value is the mean \pm SEM of 3 experiments performed in triplicate.

The increased potency of CCK8/DOX-DOX with respect to DOTA-DOX can be fully attributed to DOX because control experiments with empty liposome had no significant effect on cell viability as confirmed by viability assessment through phase-contrast microscopy (Figure.5.8).

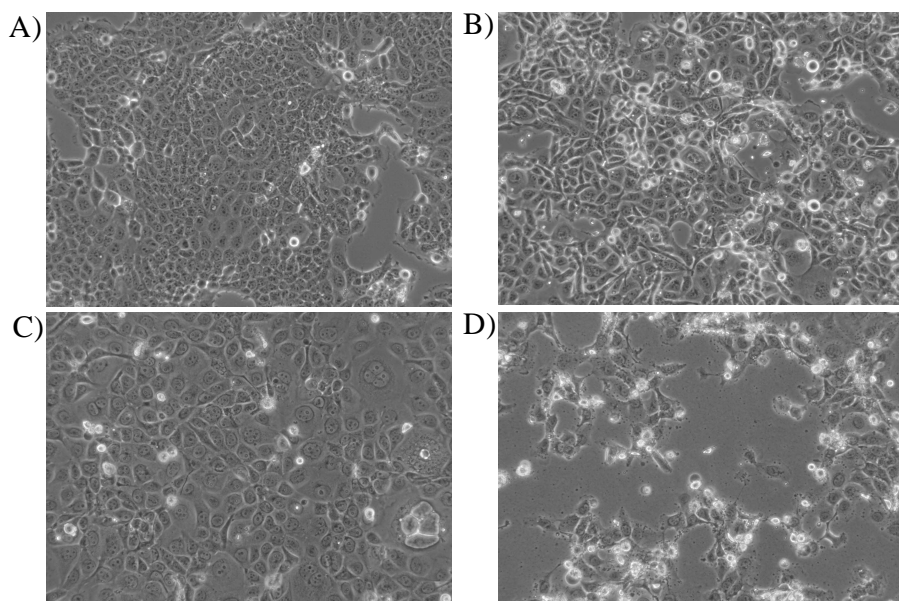


Figure 5.8: Phase-contrast microscopy of A431 untreated (A), incubated with CCK8/DOX (B), CCK8/DOX-DOX (C) and free DOX (D). After 24 h at 37°C cells were examined by phase contrast microscopy and photographs were taken through a 10X objective.

5.3 Experimental Section: CCK8

5.3.1 Materials

Protected N^α-Fmoc-amino acid derivatives, coupling reagents, Rink amide MBHA resin, Fmoc-8-amino-3,6-dioxaoctanoic acid (Fmoc-AdOO-OH), DOTA chelating agent (1,4,7,10-Tetraazacyclododecane-1,4,7,10-tetracetic acid), were purchased as reported in the paragraph 3.3.1. The N,N-dioctadecylsuccinamic acid was synthesized according to literature (Schmitt et al., 1994). Doxorubicin hydrochloride (commercial name of (8S,10S)-10-(4-amino-5-hydroxy-6-methyl-tetrahydro-2H-pyran-2-yloxy)-6,8,11-trihydroxy-8-(2-hydroxyacetyl)-1-methoxy 7,8,9,10 -tetrahydro-tetracene-5,12-dione) and Fluorescein 5-isothiocyanate (FITC isomer I) 3-(4,5-Dimethyl-2-thiazolyl)-2,5-diphenyl-2H-tetrazolium bromide (MTT), isopropanol, bovine serum albumin (BSA), phosphate buffered saline (PBS) were purchased from Sigma-Aldrich (Milan, Italy). Dulbecco eagle medium modified (DMEM), fetal calf serum (FCS), L-Glutamine, endothelial basal medium (EBM-2) and growth factor were purchase from Lonza (Milano, Italy). All other chemicals were commercially available by Sigma-Aldrich or Fluka (Buchs, Switzerland) or LabScan (Stillorgan, Dublin, Ireland) and were used as received unless otherwise stated. The (C₁₈H₃₇)₂CONHLys-(DOTA)CONH₂ ((C18)₂DOTA) monomer was synthesized as previously described. Analytical and Preparative HPLCs, LC-MS analyses and UV measurements were performed as described in the paragraph 3.3.1. DLS measurements were carried out by miniDAWN TREOS Wyatt Technology (CA, USA).

5.3.2 Peptide conjugate synthesis

The (C₁₈H₃₇)₂NCO(CH₂)₂CO(AdOO)₅-G-CCK8 (C18)₂L5CCK8 monomer was synthesized in solid-phase under standard conditions using Fmoc strategy ¹¹⁷ as described in the paragraph 3.1 for the (C18)₂L5-Octreotide.

(C₁₈H₃₇)₂NCO(CH₂)₂CO(AdOO)₅-G-CCK8 ((C18)₂L5CCK8): R_t = 26.2 min; MW = 2243 amu; m/z = 2244 amu.

FITC-βAla-Gly-CCK8 was synthesized by solid phase methods under standard conditions by using the Fmoc strategy and a Rink amide MBHA resin (0.78 mmol g⁻¹ 1.0 mmol scale, 1.28 g) ¹¹⁷ using 433A Applied Biosystems automatic peptide synthesizer. On the N terminus of βAla-Gly-CCK8 peptide, still on the resin, 2 equivalents of fluoresceine 5-isothiocyanate (FITC), 2 equivalents of HATU, and 4 equivalents of DIPEA in DMF were added, in order to achieve FITC-βAla-Gly-CCK8. The reaction was carried out overnight and the coupling was monitored by the qualitative Kaiser test. The cleavage from the resin was obtained in TFA containing 2.5% (v/v) water and 2.0% (v/v) TIS stirring the mixture for 2 h at room temperature. The crude product was precipitated at 0 °C by adding diethylether drop wise. It was washed several times with small portions of cold diethyl ether. The product was purified by RP-HPLC and identified by mass spectra (electrospray ionization ESI).

FITC-βAla-Gly-CCK8: MS (ESI⁺): m/z (%): 1581 (100) [M-H⁺].

5.3.3 Aggregate formulation and DLS characterization

(C18)₂DOTA self-assembled and of (C18)₂DOTA/(C18)₂L5CCK8 mixed aggregates in 90/10 molar ratio were prepared as reported in the paragraph 3.3.1. The concentration of peptide containing solutions was determined by absorbance ($\epsilon_{280} = 6845 \text{ M}^{-1}\text{cm}^{-1}$). This value was calculated according to the Edelhoch method,¹³³ taking into account contributions from tyrosine and tryptophan present in the primary structure, which amount to 1215 and 5630 $\text{M}^{-1}\text{cm}^{-1}$, respectively.¹³⁴

Liposomes were prepared in at final concentration of 0.5 Mm with the isotonic HBS [Hepes (4-2-hydroxyethyl-piperazino-ethanesulfonic acid pH 7.4) Buffered Saline], (140 mM NaCl and 10 mM Hepes) by using the sonication and extrusion procedures as previously described. The aggregates were centrifuged at room temperature at 13,000 g for 10 min and then filtered through a polycarbonate membrane with 20 nm pore. The measurement was performed at 25°C. Scattered light intensities were measured by fixed detectors at up to 3 scattering angles ranging from 45° to 135°. The results were processed with the program Qels (Wyatt Technology).

5.3.4 Doxorubicin Loading

CCK8/DOTA-DOX and DOTA-DOX liposomal formulations were prepared by loading Doxorubicin·HCl in (C18)₂DOTA/(C18)₂L5CCK8 and (C18)₂DOTA supramolecular aggregates, respectively. DOX was remote-loaded via an ammonium citrate gradient method and the free DOX was removed by gel-filtration.¹⁵⁷

Briefly, 1 mM liposomal solution, prepared as above reported, was passed on centrifugal filter device (Ultrafree-0,5) to remove the ammonium citrate solution. After centrifugation for 25 min at 13600 r.p.m., liposomes were recollected with isotonic HBS [Hepes (4-2-hydroxyethyl-piperazino-ethanesulfonic acid pH 7.4) Buffered Saline], (140 mM NaCl and 10 mM Hepes). Then, 0.176 mg of $1.0 \cdot 10^{-3}$ M doxorubicin solution were added to each milliliter of liposome solution. This suspension was stirred for 12 h at 4° C. Subsequently, unloaded doxo rubicin was removed by Sephadex G50 column pre-equilibrated with HBS (140 mM NaCl and 10 mM Hepes). The DOX concentration and *DLC* were determined by using fluorescence spectroscopy. The excitation wavelength of Doxorubicin was set at 480 nm.

5.3.5 Doxorubicin release

The in vitro DOX release from liposomes was measured using a dialysis method. DOX-loaded liposomes were passed over a centrifugal filter device (Ultrafree-0,5), immediately before their use, to remove any free DOX from the solution. 1.5 mL of Doxorubicin containing aggregates (CCK8/DOTA-DOX and DOTA-DOX) previously prepared were put into a dialysis bag (MW cutoff = 3500), placed into 15 mL of the media and incubated under stirring for 96 h at 37°C. Two milliliter of the dialyzed solution was taken, at various time points, to measure the drug content in the dialyzed solution and the same volume of fresh buffer solution was replenished immediately. The concentration of released DOX was analyzed by UV spectrophotometer at 480 nm.

5.3.6 Cell culture

The human epidermoid carcinoma cell line A431 overexpressing the CCK₂-R by stable transfection¹⁵⁸ kindly provided by Dr. L. Aloj (Istituto Nazionale Tumori, Fondazione G. Pascale, Napoli, Italy) was cultured as exponential growing subconfluent monolayer on 100-mm plates in DMEM supplemented with 10% FCS, 2 mM L-glutamine and 250 µg/ml G418 in a humidified atmosphere containing 5% CO₂ at 37°C. The endothelial cells (HuVEC) were purchased from Lonza seeded on T-25 primary flask (Beckton Dickinson) and maintained in EBM-2 supplemented with growth factor.

5.3.7 Flow cytometric analysis

Flow cytometry studies were conducted to measure the expression level of CCK₂-R in A431 and HuVEC and to compare free DOX, DOTA-DOX and CCK8/DOTA-DOX uptake. Cells were washed with PBS, harvested using 0.02% EDTA/PBS and suspended at a density of 1 x 10⁶/mL.

The expression level of CCK₂-R was measured using 80 nM FITC-βAla-Gly-CCK8 peptide. Cells exposed to FITC alone (80 nM) were used as negative control. To compare liposomal uptake, aliquots of the cell suspension were incubated with CCK8/DOTA-DOX and DOTA-DOX, at equivalent doxorubicin concentration of 1 µg/mL. Untreated cells were used as negative control, while free DOX (1 µg/mL) treated cells were used as positive control. After 1 h at 4 °C, cells were washed three times with cold 0.1% BSA/PBS (pH 7.4) and analyzed with a flow cytometer equipped with a 488 nm argon laser (FACScan, Becton Dickinson, CA, USA). A total of 20,000 and 10,000 events per sample were collected for A431 and HuVEC cells, respectively. Values of fluorescence intensity were obtained from histogram statistic of CellQuest software.

5.3.8 Cytotoxicity assay

Cytotoxicity of CCK8/DOTA-DOX, DOTA-DOX and free DOX was determined with MTT assays.¹⁵⁹ Briefly, 3000 A431 cells were placed in each well in 96-well plates and incubated overnight to allow cell attachment. The culture medium was removed and cells were incubated with increasing concentration of each compound at concentration ranging between 0 and 1000 ng/mL. After 8 h the medium was removed and the cells were incubated for additionally 72 h in fresh medium, during the last 2 h plates were incubated with 10 µl of MTT at 5 mg/mL. Finally, media was removed and 100 µl of 0.1 N HCl in isopropanol was added to all wells and mixed thoroughly. The absorbance was measured with a BioRad 680 microtiter plate reader (BioRad, BioRad, Corston, UK) using a wavelength of 590 nm. Cell treated with liposomes without DOX were used as positive control. The mean value ± SEM of cell viability for each treatment was expressed as the percentage of viable cells relative to the control. The experiment was performed at least 3 times, and triplicate wells were used in each experiment. For each treatment, the IC₅₀ value was estimated by plotting the percentage of viable cells *versus* log DOX concentration.

6. Conclusions

New supramolecular aggregates able to drive contrast agents and/or drugs on tumour cells have been obtained and fully characterized for their structure and their *in vitro* and *in vivo* behaviour.

The new mixed supramolecular aggregates were obtained by assembling together two synthetic amphiphilic monomers. The more abundant monomer, used to drive the aggregation process, is an anionic surfactant. It contains two C18 alkyl chains that allow the formation of supramolecular aggregates in water solution, a lysine residue acting as spacer, and a chelating agent. Cyclic (DOTA) or branched (DTPA, DTPAGlu) chelating agents have been used; they are able to coordinate radioactive metal ions such as $^{111}\text{In(III)}$ or $^{67/68}\text{Ga(III)}$, allowing to follow the *in vivo* biodistribution of the aggregates by using the nuclear medicine techniques, or the paramagnetic Gd(III) ion to obtain MRI contrast agents.

The other, bioactive, amphiphilic monomer contains the same hydrophobic moiety with two C18 alkyl chains, and a bioactive peptide able to address the aggregates on specific biological targets such as membrane receptors overexpressed by cancer cells. The peptide is spaced by the lipophilic moiety through ethoxylic spacers of different length, introduced between the peptide N-terminus and the hydrocarbon chains.

Three different, well known, bioactive peptides have been used: the C-terminal cholecystinin octapeptide amide (CCK8), the C-terminal bombesin sequence ([7-14]BN), and the somatostatin analog Octreotide. All of them are able to recognize overexpressed membrane receptors in a wide number of tumours. Moreover they can be efficiently modified on their N-terminus, because the active region for receptor binding is on the C-terminal end.

Aggregates were structurally characterized by using fluorescence spectroscopy and scattering techniques such as DLS (Dynamic Light Scattering) and SANS (Small Angle Neutron Scattering). The results suggest that the two monomers co-assemble in water solution to give supramolecular aggregates with different shape and size. Small spherical micelles, elongated micelles, open bilayers and liposomes have been found and characterized. Several factors (pH, ionic strength, molar ratio between monomers, aggregation method, charge on the chelating agent, length of the spacer, etc.) influence the aggregate shape and size. All these factors have been studied in order to find the better conditions to obtain supramolecular aggregates with the desired shape and size.

Aggregates in which gadolinium ions are complexed by the chelating agent have been tested for MRI applications. They are able to drive a great number of paramagnetic gadolinium ions on the biological target, and each gadolinium complex in the aggregate presents higher values of relaxivity parameters respect to isolated gadolinium complexes. These achievements can overcome the well know problems linked to the contrast agent concentration. In particular, new supramolecular systems derivatized with octreotide seem very promising target-selective MRI contrast agents: the bioactive octreotide peptides remain well exposed on the aggregate hydrophilic surface, as demonstrated by the UV absorbance and fluorescence behaviour of tryptophan residue, while each gadolinium complex presents high relaxivity value.

The efficiency of target selective supramolecular aggregates in binding the transmembrane receptors was confirmed by *in vitro* and *in vivo* investigation using flow cytometry and Nuclear Medicine techniques. These techniques were employed to evaluate aggregate cellular uptake. Moreover the specificity and the cytotoxicity

were validated by *in vitro* studies. These tests were performed with bombesin labeled aggregates.

In vitro data show specific binding of the $^{111}\text{In}-(\text{C}18)_2\text{DOTA}/(\text{C}18)_2\text{L}5-[7-14]\text{BN}$ containing aggregates in receptor expressing cells. Instead, the presence of Peg3000 unit on the external liposomal surface, could hide the peptide and prevent the receptor binding. In vivo experiments using $^{111}\text{In}-(\text{C}18)_2\text{DOTA}/(\text{C}18)_2\text{L}5-[7-14]\text{BN}$ show the expected biological behavior of aggregates of such size and molecular composition and preliminarily confirm the ability to specifically target and concentrate in receptor expressing xenografts. Further work will delineate to what extent therapeutic efficacy can be increased by such an approach in the animal model currently presented.

Finally, the CCK8 labeled systems were tested as drug carriers. The $(\text{C}18)_2\text{DOTA}/(\text{C}18)_2\text{L}5\text{-G-CCK}8$ liposomes were filled with doxorubicin, one of the most employed cytotoxic chemiotherapeutic drug. In vitro biological assays confirm that these liposomes are promising candidates to act as target-selective vehicle for simultaneous delivery of a drug (in the inner compartment) and a contrast agent (on the aggregate surface, for its visualization).

7. Techniques

In this chapter it will be described the principal techniques used to synthesize and characterize the micelle and vesicle aggregates.

In the following section are reported

- (1) Solid Phase Peptide Synthesis (SPPS), the base principles for the syntheses of the monomers;
- (2) Fluorescence, method employed to measure the critical micellar concentrations (cmc);
- (3) SANS and DLS, techniques used for define the shape and the size of the aggregates;
- (4) Cytometry Flow, technique employed to evaluate the cellular uptake of the aggregates as tools for drug delivery.

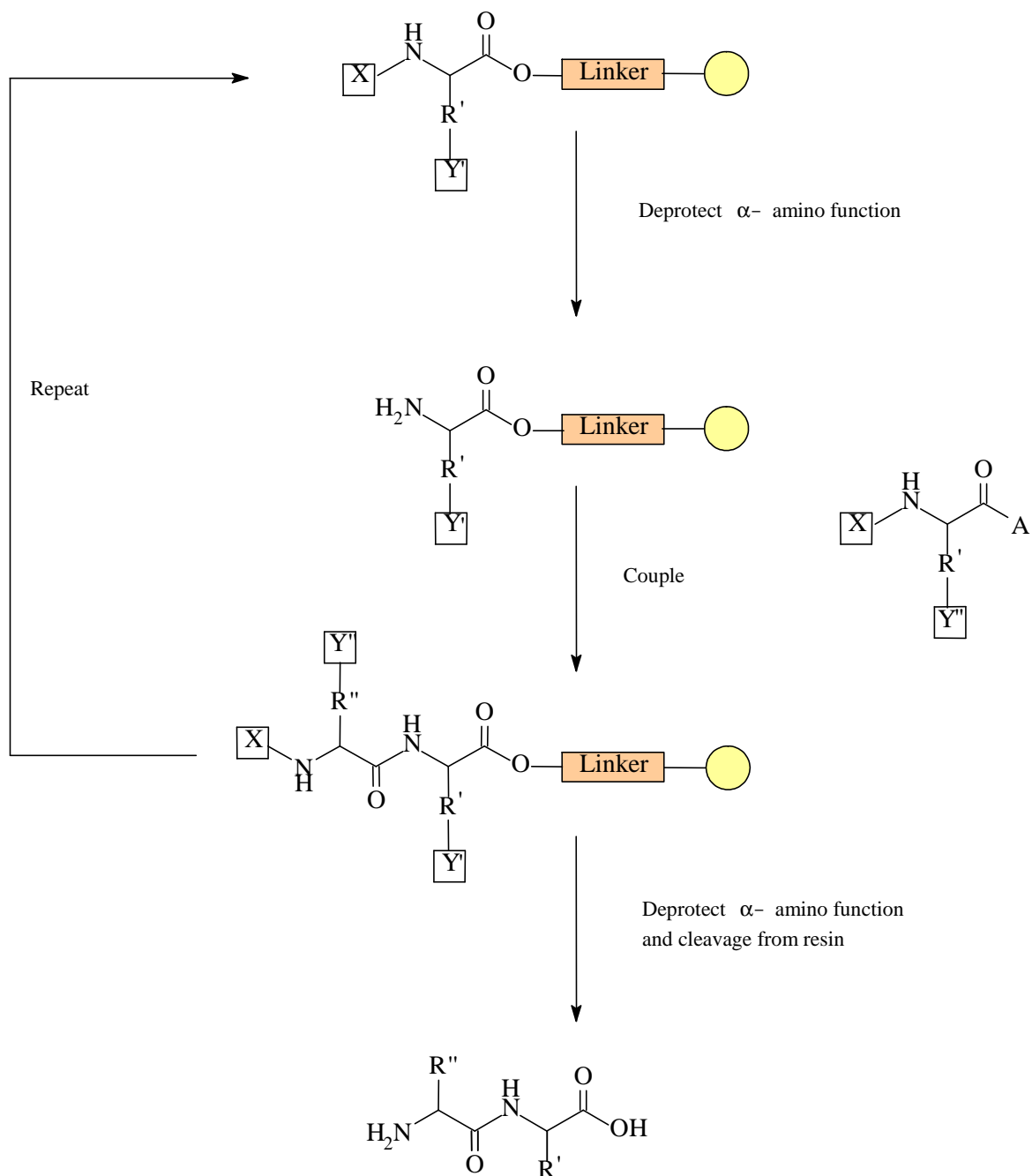
7.1 Solid phase peptide Synthesis (SPPS).

The peptide syntheses were performed by the solid phase peptide synthesis (SPPS) approach using the Fmoc/tBu chemistry (Figure 7.1.1).¹¹⁷ Following this strategy the peptide chain and the amino acid reagent are in different phase. The resin is insoluble in the most of the solvents for this reason the growing peptide chain firmly attached to a completely insoluble solid particle, can be filtered and washed free of reagents and by-products. This greatly simplifies the manipulation and shortens the time required for the synthesis of the peptide. The resin possesses a porous gel structure which allowed ready penetration of reagents, an especially in the presence of swelling solvents. These supports are chemically robust and are compatible with a wide range of reaction conditions. There are several kinds of resin, with different properties.

The Rink Amide MBHA resin¹⁶⁰ was selected for the syntheses of several monomers, because, after cleavage, this support releases the peptide amide on the C-terminal carboxyl group (Figure 7.1.2.A) like in natural form. The C-terminal amino acid is attached to a cross-linked polystyrene resin via an acid labile bond with a linker molecule. The H-Thr(tBu)-ol-(2-chlorotriyl) resin was selected for the syntheses of octreotide monomers, because, after cleavage, this support releases the peptide alcohol on the C-terminal carboxyl group (Figure 7.1.2.B). The coupling of N^α-protected amino acids in solid phase synthesis is typically carried out in DMF or NMP with pre-formed active esters or using activation reagents which generate *in situ* benzotriazolyl esters. In order to drive the acylation to completion an excess of activated amino acid derivative is utilized, typically 2-10 times the resin functionality.

The excess used depends on the nature of the activated species and on the resin loading and avoid volume of the reaction vessel employed. Highly reactive species are generating *in situ* using activating reagents like BOP, PyBOP, HBTU, TBTU and HATU. In the Figure 7.1.3 are reported two activating groups usually employed in peptidic synthesis. The N^α-terminus amino acid function is protected with the Fmoc group, which is stable in acid, but removable, by treatment with 20-50% v/v piperidine in DMF. The mechanism of the Fmoc deprotection reaction is shown in Figure 7.1.4. On the other hand, any side chain functional groups are protected with base stable, acid labile groups.

Generally, side-chain protecting groups and resin-linkage are chosen such that protecting groups are removed and the assembled peptide released under the same conditions.



X= Temporary amino protecting group
 Y=Permanent side-chain protecting group
 A= Carboxyl activating group

Figure 7.1.1: The solid phase peptide synthesis (SPPS) principle.

The C-terminal residue is anchored to a TFA-labile linkage agent. The side-chain functionalities are protected with TFA-labile protecting groups. In Fmoc peptidic synthesis, the cleavage from the resin and global side chain deprotection are

effected with a solution of trifluoroacetic acid (95%). Optimum cleavage conditions are very much dependent on the individual amino acid residues present, their number and sequence, the side-chain protecting group, and the type of linker attached to the resin. Some scavengers such as thioanisole, ethanedithiole, cresole, p-methyl-indole, triisopropylsilane can be used to improve the cleavage.

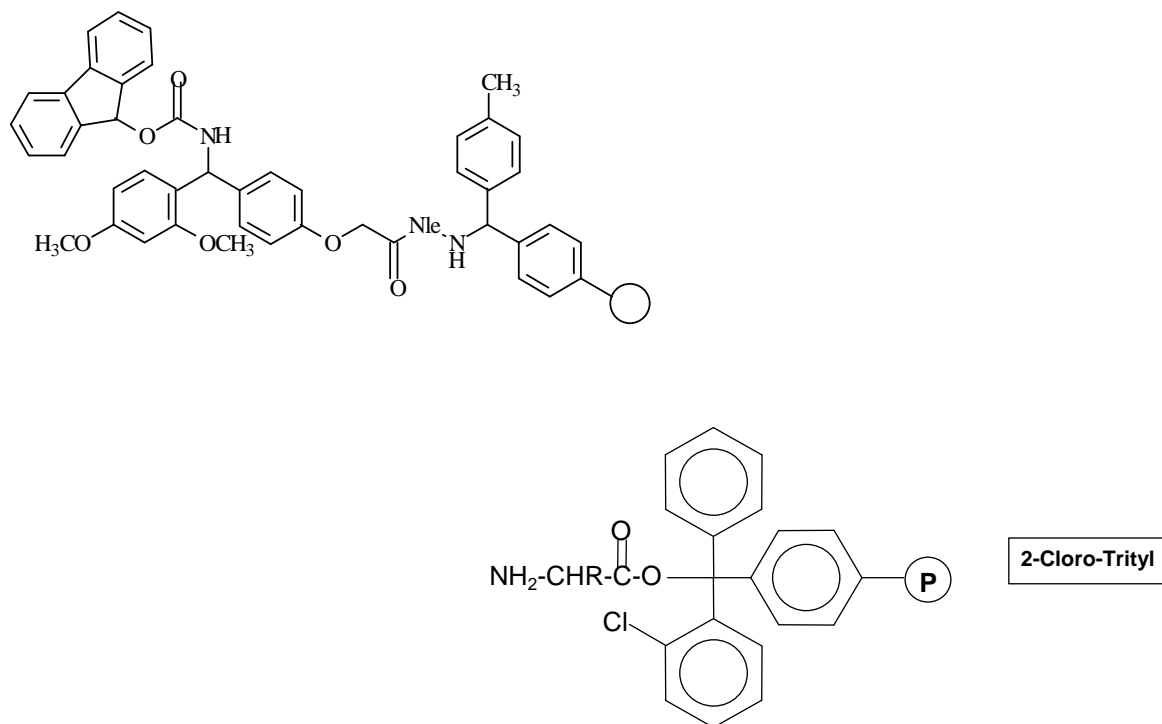


Figure 7.1.2: Rink Amide MBHA resin and H-Thr(tBu)-ol-(2-chlorotrityl) resin.

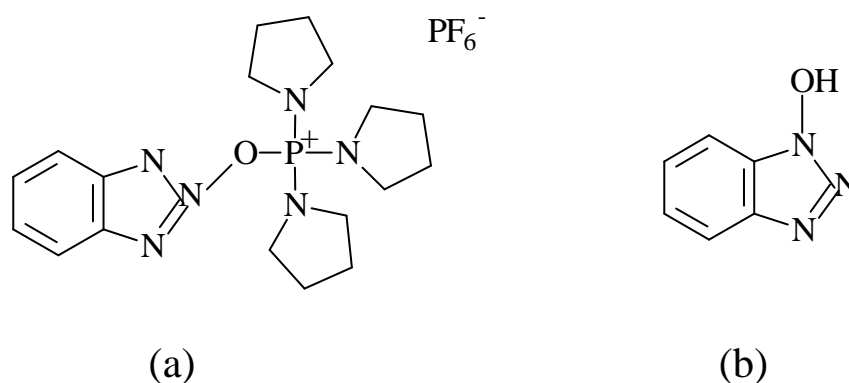


Figure 7.1.3: Schematic representation of two activating agents: (a) benzotriazol-1-yl-oxy-tris-pyrrolidino-phosphonium; (b) 1-hydroxybenzotriazole.

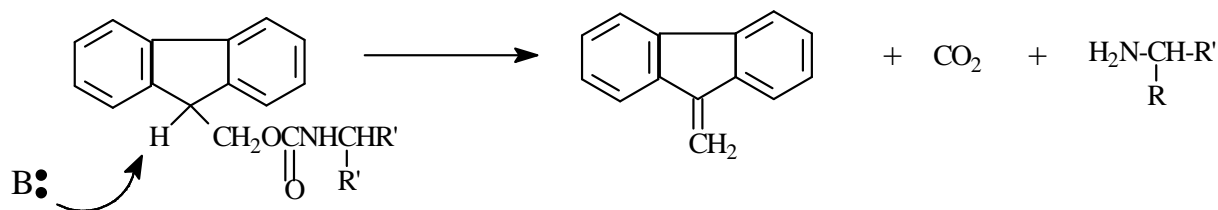


Figure 7.1.4: Mechanism of N^α-Fmoc protecting group remotion reaction.

In manual synthesis, it is standard practice to check the completeness of the coupling reaction before proceeding to the next step in the synthesis cycle. For this purpose, a number of sensitive tests have been developed to detect the presence of residual amine on the solid support. The most widely used qualitative test for the presence or absence of free amino groups is the Kaiser test.

7.2 Fluorescence

Luminescence is the emission of light from any substance and occurs from electronically excited states. The luminescence is formally divided into two categories, *fluorescence* and *phosphorescence*, depending on the nature of the excited states. In excited singlet states, the electron in the excited orbital is paired (of opposite spin) to the second electron in the ground-state orbital. Consequently, return to the ground state is spin-allowed and occurs rapidly by emission of a photon (10 ns). Phosphorescence, instead, is emission of light from triplet excited states, in which the electron in the excited orbital has the same spin orientation as the ground state electron.¹⁶¹ Transitions to the ground state are forbidden and the emission rates are slow (10⁻³-10⁰s), so that phosphorescence lifetimes are typically millisecond to second. The processes which occur between the absorption and the emission of the light are usually illustrated by a Jabłoński diagram. A typical Jabłoński diagram is shown in Figure 7.2.1. The singlet ground, first and second electronic states are depicted by S₀, S₁ and S₂, respectively. At each of this electronic energy levels the fluorephores can exist in a number of vibrational energy levels, denoted by 0,1,2 etc.

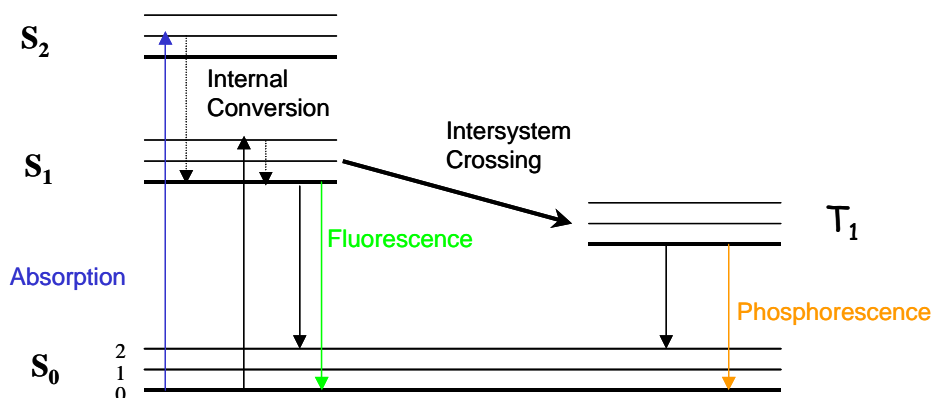


Figure 7.2.1: One form of Jabloński diagram.

At room temperature, thermal energy is not adequate to significantly populate the excited vibrational states. Absorption typically occurs from molecules with the lowest vibrational energy. The larger energy difference between the S_0 and S_1 excited states is too large for thermal population of S_1 , and it is for this reason we use the light and not heat to induce fluorescence. A fluorophore is usually excited to some higher vibrational level of either S_1 or S_2 . The molecules rapidly relax to the lowest vibrational level of S_1 . This process is called 'internal conversion' and, generally occurs in 10^{-12} s or less. Since fluorescence lifetimes are typically near 10^{-8} s, internal conversion is generally complete prior to emission. Hence, fluorescence emission generally results from a thermally equilibrated excited state, that is, the lowest-energy vibrational state of S_1 .

Return to the ground state typically occurs to a higher excited vibrational ground-state level, which then (10^{-12} s) reaches thermal equilibrium (Figure 7.2.1). Molecules in the S_1 state can also undergo a spin conversion to the first triplet state, T_1 . Emission from T_1 is termed phosphorescence and is, generally, shifted to longer wavelengths (lower energy) relative to the fluorescence. Conversion of S_1 to T_1 is called 'intersystem crossing'. Transition from T_1 to the singlet ground state is forbidden, and rate constant for triplet emission is several orders of magnitude smaller than those for fluorescence. Because of this rapid relaxation, emission spectra are usually independent of the excitation wavelength (Kasha's rule). Examination of the Jabloński diagram (Figure 7.2.1) reveals that the energy of the emission is typically less than that of absorption. Hence, fluorescence typically occurs at lower energy or longer wavelengths. Moreover, according to the Franck-Condon principle, all electronic transitions are vertical, that is, they occur without change in the position of the nuclei. As a result, if a particular transition probability (Franck-Condon factor) between zeros and second vibrational levels is largest in absorption, the reciprocal transition is also most probable in emission (Figure 7.2.2).

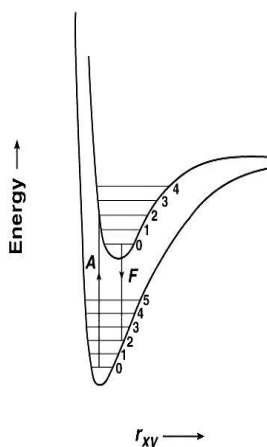
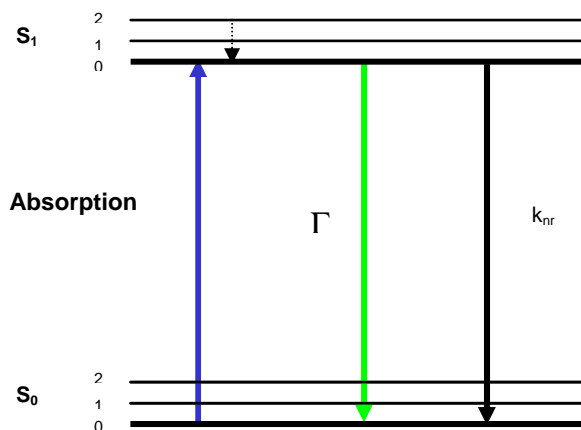


Figure 7.2.2: Franck-Condon factors

Fluorescence lifetime and quantum yield are perhaps the most important characteristics of a fluorophore. The quantum yield is the number of emitted photons relative to the number of absorbed photons. The lifetime is also important, as the lifetime determines the time available for the fluorophore to interact with or diffuse in its environment, and hence the information available from its emission. The meaning of the quantum yield and lifetime is best represented by a simplified Jabloński diagram (Figure 7.2.3). In this diagram we are interested in the emissive rate of the fluorophore (Γ) and its rate of non radioactive decay to S_0 (k_{nr}). The fluorescence quantum yield is the ratio of the number of photons emitted to the number absorbed. The process governed by the rate constant Γ and k_{nr} both depopulate the excited state. The fraction of fluorophores which decay through the emission, and hence the quantum yield, is given by:



$$Q = \frac{\Gamma}{\Gamma + k_{nr}} \quad (7.2.1)$$

Figure 7.2.3: A simplified Jabloński diagram

For the fluorophore illustrated in Figure 6.2.3 the lifetime is:

$$\tau = \frac{1}{\Gamma + k_{nr}} \quad (7.2.2)$$

The lifetime of the fluorophore in absence of nonradioactive processes is called intrinsic or natural lifetime and is given by:

$$\tau_n = 1/\Gamma \quad (7.2.3)$$

In principle, the natural lifetime τ_n can be calculated from the absorption spectra, extinction coefficient, and emission spectra of fluorophore.

Moreover, τ_n can be calculated from the measured lifetime (τ) and quantum yield:

$$\tau_n = \tau/Q \quad (7.2.4)$$

The intensity of the fluorescent radiation at the wavelength λ depends from the concentration (c) and the molar extinction coefficient (ϵ) of the sample:

$$I_f = kI_0(1 - 10^{-\epsilon lc}) \quad (7.2.5)$$

where I_0 is the intensity of the incident light at the wavelength $\lambda' < \lambda$, generating fluorescence, and k is a constant, which depends from the instrumentation.

7.2.1 Fluorescence Quenching

The intensity of fluorescence can be decreased by a wide variety of processes. Such decreases in intensity are called quenching. It can occur by different mechanisms. '*Collisional or dynamic quenching*' occurs when the excited-state fluorophore is deactivated upon contact with some other molecule in solution, which is called the quencher. In this case the fluorophore is returned to the ground state during a diffusive encounter with the quencher. The molecule is not altered in the process.



In the eq. 7.2.6 P is the probe and Q the quencher.

For collisional quenching, the decrease in intensity is described by Stearn-Volmer equation:

$$\frac{F_0}{F} = 1 + K[Q] = 1 + k_q \tau_0 [Q] \quad (7.2.7)$$

In this expression K is the Stern-Volmer quenching constant, k_q is the bimolecular quenching constant, τ_0 is the unquenched lifetime, and $[Q]$ is the quencher concentration.

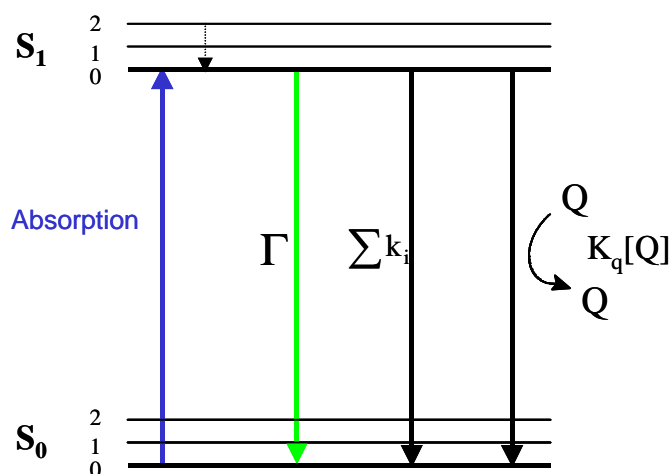


Figure 7.2.4: Jablonski diagram with collisional quenching and fluorescence resonance energy transfer (FRET). The term $\sum k_i$ is used to represent non radioactive paths to the ground state besides quenching and FRET.

Besides *dynamic quenching*, fluorescence quenching, can occur by a variety of the processes. Fluorophores can form nonfluorescent complexes with quenchers. This process is referred to as '*static quenching*' since it occurs in the ground state and does not rely on diffusion or molecular collisions.



For the static quenching the fluorescence intensity upon quencher concentration is easily described by the following equation:

$$\frac{F_0}{F} = 1 + K_S[Q] \quad (7.2.9)$$

Where F_0/F is the fraction of fluorescence that remains, $[Q]$ is the concentration of the quencher and $K_S = [F-Q]/[F][Q]$. Quenching can also occur by a variety of trivial, nonmolecular, mechanisms, such as attenuation of the incident light by the fluorophore itself or other absorbing species.

7.3 Dynamic Light Scattering (DLS)

The dynamic light scattering (DLS) is a technique widely used to study the dynamical properties of colloidal dispersions. In a DLS experiment the fluctuations of the scattered light intensity are measured as a function of time at a constant scattering angle. These intensity fluctuations occur because the particles in solution are in constant motion, the Brownian motion. The analysis of the intensity fluctuations allows the determination of the distribution of diffusion coefficients of the particles, which are converted then into a size distribution using established theories. In DLS the temporal variation of the intensity is measured and is represented usually through the so-called intensity autocorrelation function. Since, in general, it is not convenient to deal with a large intensity values as function of time, one reduces the intensity fluctuations to the autocorrelation function $G^{(2)}(t)$. The intensity correlation function measures the correlation between the intensity value $I(t)$ at a generic time (t) and the intensity value $I(t + t_d)$ being t_d the time delay.

$$G^{(2)}(t) = \lim_{T \rightarrow \infty} \frac{1}{T} \int_0^T I(q, t') I(q, t' + t) dt'$$

where $I(q, 0)$ and $I(q, t)$ are the intensities of the scattered light at delay time $t=0$ and $t=t$, respectively.

Its normalized value, $g^{(2)}(t)$, is defined by :

$$g^{(2)}(t) = \frac{G^{(2)}(t)}{G^{(2)}(0)}$$

where $G^{(2)}(0)$ is the time-averaged value of the square intensity, i.e. $[I(t)^2]$. The models used in the fitting procedures are expressed with respect to the normalized time correlation function of the electric field, $g^{(1)}(t)$, because the time correlation function of scattered light is not simply related to the motion of the molecules.

$$g^{(1)}(t) = \frac{[E^*(Q, 0)E(q, t)]}{[E^*(Q, 0)E(q, 0)]}$$

The two normalized time correlation functions are related by Siegert's relationship:

$$g^{(2)}(t) - 1 = \beta |g^{(1)}(t)|^2$$

where $\beta (\geq 1)$ is the coherence factor, which accounts for deviation from ideal correlation and depends on the experimental geometry.

For a monodisperse system, $g^{(1)}(t)$ will decay as a single exponential function with a characteristic relaxation time τ :

$$g^{(1)}(t) = \exp(-t/\tau)$$

whereas for a polydisperse system $g^{(1)}(t)$ will be multiexponential and may be expressed as a Laplace transformation of a distribution of relaxation times, $A(\tau)$:

$$g^{(1)}(t) = \int_{-\infty}^{+\infty} \tau A(\tau) \exp(-t/\tau) d \ln \tau$$

where $\tau = \Gamma^{-1}$ and Γ is the relaxation or frequency rate.

The relaxation time distribution $\tau A(\tau)$ is obtained by regularized inverse Laplace

transformation (RILT) of the measured intensity correlation function using calculation algorithms. In the analyses in this work, algorithms of two commercial programs have been used: REPES incorporated in the GENDIST analysis package and RILT incorporated ALV-5000/E software.

The relaxation rate Γ is obtained from the first moment of the relaxation time distribution, and from its value is possible to estimate the apparent translational diffusion coefficient D , through this relation:

$$D = \lim_{q \rightarrow 0} \Gamma/q^2$$

where q is the absolute value of the scattering vector ($q = 4 \pi n_0 \sin (\theta/2)/\lambda$, where n_0 is the refractive index of the solvent, in this work is water, λ is the incident wavelength and θ is the scattering angle).

D is, thus, obtained from the slope of Γ as a function of q^2 , where Γ is measured at different scattering angles.

The diffusion coefficient D obtained in a DLS experiment is believed to be the mutual diffusion coefficient. The Brownian motion generates concentration fluctuations that in turn produce a chemical potential gradient and the associated flow is proportional to this gradient through a coefficient called the mutual diffusion coefficient, which can be described by Fick's second law:

$$D = \frac{1}{6\pi\eta R} [\delta\pi/\delta c]$$

where π is the osmotic pressure of the dispersion and c is the concentration of the solute.

In particular for infinite dilute dispersions:

$$\pi = cK_B T \rightarrow (\delta\pi/\delta c) = K_B T$$

D reduces to the self-diffusion coefficient D_0 and we obtain the Stokes-Einstein equation:

$$D = \frac{K_B T}{6\pi\eta R}$$

7.4 Small angle neutron scattering (SANS)

SANS is a small angle scattering technique that exploits the wave-particle duality of the neutron and its unique nuclear properties to provide information about the size (length scale varies from 1 to 1000 nm) and shape of molecules and their assemblies. In SANS, the scattering vector q is used to describe the relationship between the incident and the scatter wavevectors. Its module, q , is the independent variable in a SANS experiment and has magnitude $q = 2\pi \sin(\theta/2)/\lambda$ and dimensions of $(\text{length})^{-1}$. By combining q with the Bragg law of diffraction, one obtains the simple and useful relationship: $d = 2\pi/q$, from which the molecular-level length scale (d) at any accessible q can be obtained. The dependent variable in a SANS experiment is the differential scattering cross-section, $(d\Sigma/d\Omega)$, improperly also called intensity of scattering $I(q)$. Scattering cross section $d\Sigma/d\Omega$ contains information on interactions, size and shapes of aggregates present in the system, and can be expressed for a collection of monodisperse bodies as

$$d\Sigma/d\Omega(q) = n_p P(q) S(q) + (d\sigma/d\Omega)_{\text{inch}} \quad 7.4.1$$

where n_p represents the number density of the scattering object present in the system, $P(q)$ and $S(q)$ are respectively the form and the structure factor of the scattering particles, whereas $(d\Sigma/d\Omega)_{\text{inch}}$ takes into account for the incoherent contribution to the cross section measured, mainly due to the presence of hydrogenated molecules. The form factor contains information on the shape of the scattering objects, whereas the structure factor accounts for inter-particle correlations and is normally important for concentrated or charged systems. Provided that solutions are quite dilutes ($c < 10^{-3}$ mol kg $^{-1}$) the structure function $S(q)$ can be approximated to the unity, and the scattering cross section is reduced to

$$d\Sigma/d\Omega(q) = n_p P(q) + (d\sigma/d\Omega)_{\text{inch}} \quad 7.4.2$$

Microstructural parameters of the aggregates have been obtained by applying the appropriate model to the experimental SANS data. Experimental data have shown in the analyzed systems the existence of cylindrical micelles and/or the presence of vesicular aggregates.

Scattering from cylindrical structures is characterized by a region where the $d\Sigma/d\Omega \sim q^{-1}$ power law dependence holds. The single particle form factor for such micelles can be written as

$$P(q) = (\rho_c - \rho_0)^2 \pi R^2 l \int \frac{\sin^2(ql/2\cos\varphi) [j_1(qR\sin\varphi)]^2}{(q/2\cos\varphi)^2 (qR\sin\varphi)} \sin\varphi d\varphi \quad 7.4.3$$

where l is the length of the cylinders, R the radius of the base, whereas j_1 is the first order Bessel function and $\rho_c - \rho_0$ the scattering length density difference between the cylinders and the solvent.

Vesicular aggregates cannot be observed in their completeness since the Guinier region of such objects falls almost completely in the USANS domain. As consequence the SANS region is characterized by a power law $d\Sigma/d\Omega \sim q^{-2}$ due to the scattering of vesicular double layer. Indeed the q range spanned by the SANS

measurements is such to allow regarding the vesicles as randomly oriented planar sheets for which the form factor can be expressed by

$$P(q) = 2\pi (\rho_c - \rho_0)^2 S d^2 \frac{1 \sin^2(qd/2)}{q^2 (qd/2)^2} \quad 7.4.4$$

where d is the plane thickness, and S is the plain surface per unit volume. Scattering from solutions containing cylindrical structures has been analyzed by using eqs 7.4.2 and 7.4.3, whereas in the systems containing vesicles aggregates, eqs 7.4.2 and 7.4.4 have been used. Systems containing both the objects have been treated assuming each kind of aggregate scattered independently from the other and expressing the cross section as the sum of the form factors weighted for two scale factors (K_{cyl} , K_{sheets}) the relative number density of the objects

$$d\Sigma/d\Omega (q) = n_p K_{cyl} P_{cyl} (q) + K_{sheets} P_{sheets} + (d\sigma/d\Omega)_{incoh} \quad 7.4.5$$

and treating the scale factors as adjustable parameters.

7.4 Flow Cytometry

Flow cytometry is a technology that allows a single cell to be measured for a variety of characteristics, determined by looking at how they flow in liquid [1]. Instruments used for this can gather information about cells by measuring visible and fluorescent light emissions, allowing cell sorting based on physical, biochemical and antigenic traits. A flow cytometer, sometimes called a Fluorescence Activated Cell Sorter (FACS), has several key components [2] (Figure 7.4):

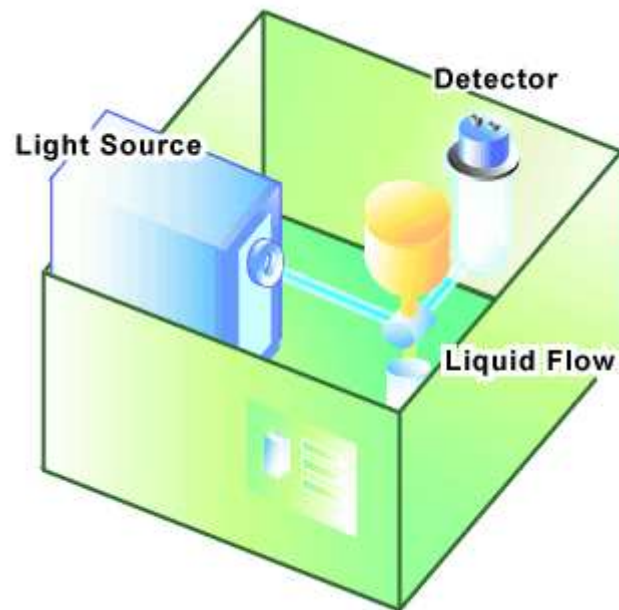


Figure 7.4: A rendition of a flow cytometer: **1.** A light or excitation source, typically a laser that emits light at a particular wavelength; **2.** A liquid flow that moves the suspended cells through the instrument and past the laser; and **3.** A detector, in this case a photomultiplier tube, which is able to measure the brief flashes of light emitted as cells flow past the laser beam.

In a flow cytometer, single cells move past the excitation source and the light hitting the cells is either scattered or absorbed and then re-emitted (fluorescence). This scattered or re-emitted light is collected by the detector (Figure 7.4).

7.4.1 Light Scatter

Scattered light is a consequence of a light beam making contact with a cell, resulting in either reflected or refracted light reaching the detector. The pattern of light scattering is dependent on cell size and shape, giving relative measures of these cellular characteristics as cells flow through the beam. This can be quite useful, as cells can be sorted on the basis of size or shape to different collection tubes using a technique called electrostatic deflection, which employs charged plates to change the path of the cell (Figure 7.4.1).

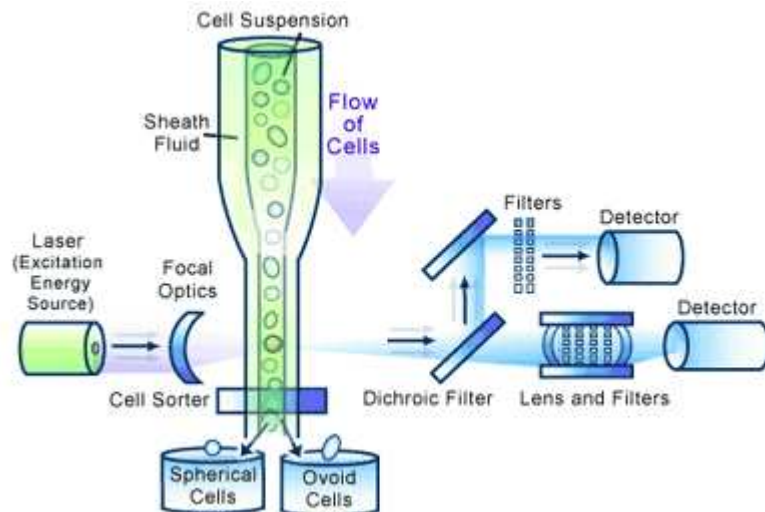


Figure 7.4.1 A schematic of fluorescence detection by a flow cytometer and a schematic of cell sorting by a flow cytometer.

7.4.2 Fluorescence

Fluorescence-based detection depends on the absorption of light by the cell and the subsequent re-emission of this light at a different frequency. Flow cytometers make use of this technology by employing filters to block the original light source from reaching the detector, while the fluorescence emission is allowed through for detection, which allows only a very low background of stray light to reach the detector. In flow cytometry experiments, fluorescence is often achieved by the deliberate labeling of a cellular component using a fluorescent marker, usually a type of dye. These dyes fluoresce only when light of the appropriate wavelength (specified by the frequency of the laser) hits them, causing the emission of secondary light at a different wavelength. Detection of the second wavelength is used as a measure of the presence of the dye on the cell and thus the component it is labeling. Various fluorescent dyes are commercially available and their emitted colors are reminiscent of the reds and greens seen in fireworks. The most common fluorescent dyes are Texas-Red, fluorescein isothiocyanate (FITC) and phycoerythrin (PE). Table 1 shows some of the different fluorochromes, their excitation and emission wavelengths, and their emission color.

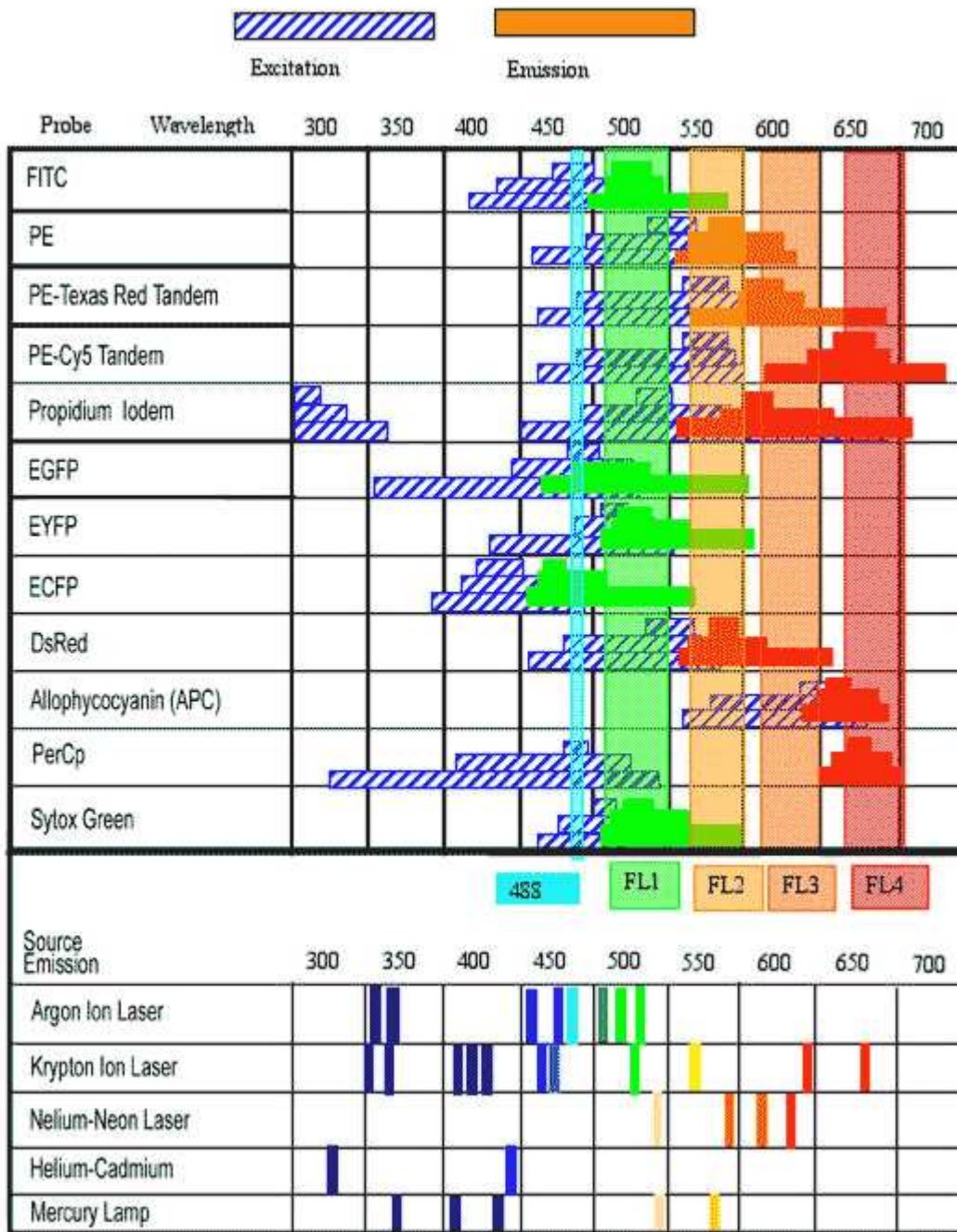


Table 7.4.2. Common fluorescent dyes.

7.4.3 Display and Interpretation of Flow Cytometry Data

The amount a cell scatters or fluoresces light is measured by the detector and subsequently need to be displayed for interpretation. These profiles of cells are normally displayed as dot plots or histograms. Dot plot displays use two parameters to graph the data generated by flow analysis, with each dot representing the passage of one cell through the detector. The X- and Y-axes measure the different emissions, displaying a dot for each of the cells that show that particular emission. In Figure 7.4.3, the dot blot shows an example where two populations of cells have been

analyzed by flow cytometry. A cell of a particular population type will show up as a dot in the quadrant of the dot plot designated for that population.

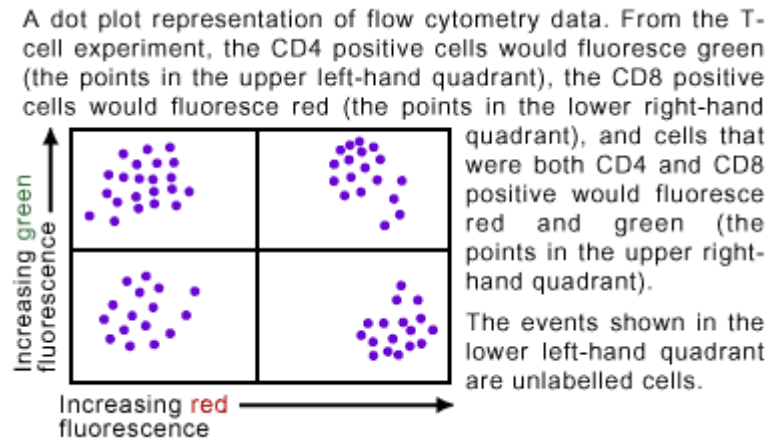


Figure 7.4.3: A Dot plot of flow cytometry data.

Histograms can also be used to display data from flow cytometry experiments. In these plots the X-axis shows the intensity of the detected signal and the Y-axis measures the number of events (cells) counted. Histograms often display the output of two (or more) samples using a single fluorochrome. In an experiment determining the presence or absence of a particular cell marker or a relative increase or decrease of a marker after experimental treatment, a histogram shows the shift in the fluorescence intensity of the sampled cells (Figure 7.4.4).

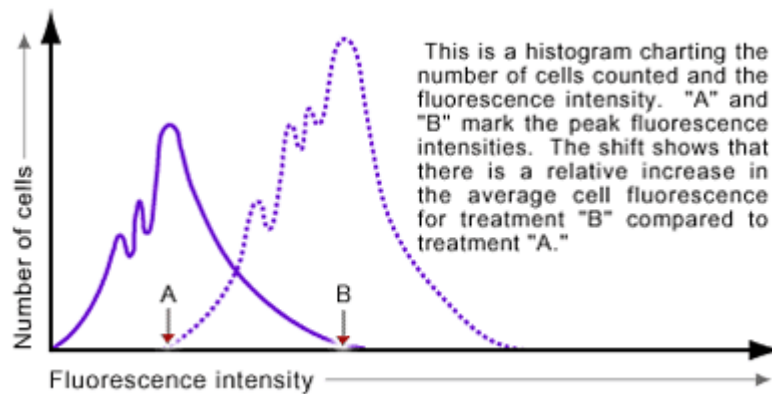


Figure 7.4.4: A histogram of flow cytometry data.

Acknowledgements

I am grateful to Prof. L. Paduano and Dr. G. Mangiapia of the University of Naples "Federico II" for SANS measurement. I want thank Prof.S.Aime and Dr. E.Gianolio of the University of Turin relaxivity measurement. Moreover I want thank Dr. R. Palumbo of the CNR of Naples for biological assaies.

My greater thanks are for Prof. G. Morelli, Dr. D. Tesauro and Dr. A. Accardo for critical assessment of the results obtained during all doctorate.

References

- [1]. Allen, T. M.; *Nature Rev. Drug Discov.*, **2002**, 2, 750.
- [2]. Jain, R. K.; *Nature Med.*, **1998**, 4, 657.
- [3]. Srivinas, P.R.; Barker, P.; Srovastava, S.; *Lab. Invest.*; **2002**, 82, 662.
- [4]. Koo, O.M.; Rubistein, I.; Onyuksel, H.; *Nanomedicine* **2005**, 1, 193.
- [5]. Panyam, J.; Labhasetwar, V.; *Adv. Drug Deliv. Rev.*, **2003**, 55, 329.
- [6]. Sahoo, S.K.; Labhasetwar, V.; *Drug Discov Today.*, **2003**, 8, 1112.
- [7]. Langer, R.; *Science*, **2001**, 293, 58.
- [8]. Liu, Y.; Chen, X.; Xin, J.H.; *J Mater Sci*, **2006**, 41, 5399.
- [9]. Liu, Y.; Miyoshi, H.; Nakamura, M.; *J Controlled Release*, **2006**, 114, 89.
- [10]. Okuda, T.; Kawakami, S.; Akimoto, N.; Niidome, T.; Yamashita, F.; Hashida, M.; *J Controlled Release*, **2006**, 116, 330.
- [11]. Moghimi, S.M.; Szebeni, J.; *Prog Lipid Res*, **2003**, 42, 463.
- [12]. Kwekkeboom, D.; et al; *Journal of Nuclear Medicine*, **2000**, 41, 1704.
- [13]. Aloj, L.; Morelli, G.; *Curr. Pharm. Des.*, **2004**, 10, 3009.
- [14]. Lamberts, S.; Krenning, E.P.; Reubi, J.C.; *Endocr Rev*, **1991**, 12, 482.
- [15]. Patent U.S. 5,436,155; WO9714715; *Biochemical and Biophysical Research Communications*, **1999**, 258, 689.
- [16]. U.S. Patent WO9851337 and WO9835707.
- [17]. Degiorgio, V.; *Physics of amphiphiles: micelles, vesicles and microemulsions, Amsterdam*, **1985**.
- [18]. Wiener, E.C.; Brechbiel, M.W.; Brothers, H.; Magin, R.L.; Gansow, O.A.; Tomalia, D.A.; Lauterbur, P.C. *Magn. Res. Med.* **1994**, 3, 1.
- [19]. Andre, J.P.; Toth, E.; Fischer, H.; Seelig, A.; Macke, H.R.; Merbach, A.E. *Chem. Eur. J.* **1999**, 5, 2977.
- [20]. Torchilin, V.P.; *J. of Controlled release*, **2001**, 73, 137.
- [21]. Szoka, F.; Jr *Ann. Rev. Biophys. Bioeng.* **1980**, 9, 467.
- [22]. Torchilin, V.P.; *Eur. J. Pharm. and Biopharm.*, **2009**, 71, 431.
- [23]. Al-Jamal, W.T.; Kostaresol, K.; *Nanomedicine* (London, United Kingdom), **2007**, 2(1), 5.
- [24]. Torchilin, V.P.; *Nat. Rev. Cancer*, **2005**, 4, 145.
- [25]. Torchilin, V.P.; *J. Controlled Release*, **2001**, 73, 137.
- [26]. Ferrari M., *Nat. Rev. Cancer*, **2005**, 5, 161.
- [27]. Allen, T.M.; *Nat. Rev. Cancer*, **2002**, 2, 750.
- [28]. Mulder, W.J.M.; Strijkers, G.J.; Briley-Saebo, K.C.; Frias, J.C.; Aguinado, J.G.S.; Vudic, E.; Amirbekian, V.; Tang, C.; Chin, P.T.K.; Nicolay, K.; Fayad, Z.A.; *Magn Reson. Med.*, **2007**, 58, 1164.
- [29]. Accardo, A.; Tesauro, D.; Mangiapia, G.; Pedone, C.; Morelli, G.; *Biopolymers (Peptide Sciences)*, **2007**, 88, 121.
- [30]. Accardo, A.; Tesauro, D.; Aloj, L.; Tarallo, L.; Arra, C.; Mangiapia, G.; Vaccaro, M.; Pedone, C.; Paduano, L.; Morelli, G.; *ChemMedChem*, **2008**, 3, 602.
- [31]. Battey, J. F.; Way, J. M.; Corjay, M. H.; Shapira, H.; Kusano, K.; Harkins, R.; Wu, J. M.; Slattery, T.; Mann, E.; Feldman, R. I.; *Proc. Natl. Acad. Sci. U.S.A.* **1991**, 88, 399.

- [32]. Torchilin, V.P.; ed. *Nanoparticulates as Pharmaceutical Carriers*. London, UK Imperial College Press ; **2006**.
- [33]. Lasic, D.D.; *Liposomes: From Physics to Applications*. New York, NY : Elsevier ; **1993**.
- [34]. Torchilin, V.P.; *Nat Rev Drug Discov*, **2005**, 4, 145.
- [35]. Lipinski, C.A.; Lombardo, F.; Dominy, B.W. ; Feeney, P.J.; *Adv Drug Deliv Rev*, **2001**, 46, 26.
- [36]. Fernandez, A.M.; Van Derpoorten, K.; Dasnois, L.; Lebtahi, K.; Dubois, V.; Lobl, T.J.; Gangwar, S.; Oliyai, C.; Lewis, E.R.; Shochat, D.; Trouet, A.; *J Med Chem.*, **2001**, 44, 3750.
- [37]. Yalkowsky, S.H.; ed. *Techniques of Solubilization of Drugs*. New York, NY : M Dekker ; **1981**.
- [38]. Shabner, B.A.; Collings, J.M.; eds. *Cancer Chemotherapy: Principles and Practice*. Philadelphia, PA : JB Lippincott ; **1990**
- [39]. Yokogawa, K.; Nakashima, E.; Ishizaki, J.; Maeda, H.; Nagano, T.; *Pharm Res*, **1990**, 7, 691.
- [40]. Hagelucken, A.; Grunbaum, L.; Nurnberg, B.; Harhammer, R.; Schunack, W.; Seifert, R.; *Biochem Pharmacol*, **1994** 47, 1789.
- [41]. Yuan, F.; Dellian, M.; Fukumura, D.; Leunig, M.; Berk, D.A.; Torchilin, V.P.; Jain, R.K.; *Cancer Res.*, **1995**, 55, 3752.
- [42]. Allen, M.T.; Hansen, C.; Martin, F.; Redemann, C.; Yau-Young, A.; *Biochim. Biophys Acta*, **1991**, 1066, 29.
- [43]. Rose, P.G.; Smrekar, M.; Haba, P.; Fusco, N.; Rodriguez, M.; *Am. J. Clin. Oncol.*, **2008**, 31, 476.
- [44]. Weissleder, R.; Mahmood, U. *Molecular Imaging. Radiology* **2001**, 219, 316.
- [45]. Aime, S.; Cabella, C.; Colombatto, S.; Geninatti Crich, S.; Gianolio, E.; Maggioni, F. *J Magn Reson Imaging* **2002**, 16, 394.
- [46]. Morel, S.; Terreno, E.; Ugazio, E.; Aime, S.; Gasco, M.R. *European Journal of Pharmaceutics and Biopharmaceutics* **1998**, 45, 157.
- [47]. Anelli, P.L.; Lattuada, L.; Lorusso, V.; Schneider, M.; Tournier, H.; Uggeri, F.; *Magnetic Resonance Materials in Physics, Biology and Medicine* **2001**, 12, 114.
- [48]. Wiener, E.C.; Brechbiel, M.W.; Brothers, H.; Magin, R.L.; Gansow, O.A.; Tomalia, D.A.; Lauterbur, P.C. *Magn. Res. Med.* **1994**, 3, 1.
- [49]. Aime, S.; Botta, M.; Garino, E.; Geninatti Crich, S.; Giovenzana, G.; Pagliarin, R.; Palmisano, G.; Sisti M. *Chem. Eur. J.* **2000**, 6, 2609.
- [50]. Bligh, S.W.; Harding, C.T.; Sadler, P.J.; Bulman, R.A.; Bydder, G.M.; Pennock, J.M.; Kelly, J.D.; Latham, I.A.; Marriott, J.A. *Magn. Res. Med.* **1991**, 17, 516.
- [51]. Schmiedl, U.; Ogan, M.; Paajanen, H.; Marotti, M.; Crooks, L.; Brito, E.; Brasch, R.C. *Radiology*, **1987**, 162, 205.
- [52]. Liu, S.; Edward, D.S.; *Chem. Rev.* **1999**, 99, 2235.
- [53]. Torchilin, V.P.; *Advanced in Drug Delivery*, **2002**, 54, 235.
- [54]. Andre, J.P.; Toth, E.; Fischer, H.; Seelig, A.; Macke, H.R.; Merbach, A.E. *Chem. Eur. J.* **1999**, 5, 2977.
- [55]. Aime, S.; Botta, M.; Fasano, M.; Terreno, E. *Chem Rev.* **1998**, 27, 19.
- [56]. Lasic, D.D.; *Nature*, **1992**, 355, 279.
- [57]. R.J. Hunter (Ed.), *Introduction to Modern Colloid Science*, Oxford University Press, Oxford, UK, **1993**.

- [58]. Martinez-Coscolla, A.; Miralles-Loyola, E.; Garrigues, T.M.; Sirvent, D.; Salinas, E.; Casabo, V.G.; *Drug. Res.*, **1993**, *43*, 699.
- [59]. G.S. Kwon, K. Kataoka, *Adv. Drug Deliv. Rev.*, **1995**, *16*, 295.
- [60]. Tilcock, C.; Unger, E.; Cullis, P.; MacDougall, P.; *Radiology*, **1989**, *171*, 77.
- [61]. Kabalka, G.; Buonocore, E.; Hubner, K.; Moss, T.; Norley, N.; Huang, L.; *Radiology*, **1987**, *163*, 255.
- [62]. Grant, C.W.M.; Karlik, S.; Florio, E.A.; *Magn. Reson. Med.*, **1989**, *11*, 236.
- [63]. Unger, E.; Fritz, T.; Wu, G.; Shen, D.; Kulik, B.; New, T.; Crowell, M.; Wilke, N.; *J. Liposome Res.*, **1994**, *4*, 811.
- [64]. Unger, E.; Shen, D.K.; Wu, G.L.; Fritz, T.; *Magn. Reson. Med.*, **1991**, *22*, 304.
- [65]. Koenig, S.H.; Ahkong, Q.F.; Brown III, R.D.; Lafleur, M.; Spiller, M.; Unger, E.; Tilcock, C.; *Magn. Reson. Med.* **1992**, *23*, 275.
- [66]. Kabalka G.W.; Davis, M.A.; Buonocore, E.; Hubner, K.; Holmberg, E.; Huang, L.; *Invest. Radiol.*, **1990**, *25*, S63.
- [67]. Kabalka, G.W.; Buonocore, M.A.; Hubner, K.; Holmberg, E.; Huang, L.; *Magn. Reson. Med.* **1988**, *8*, 89.
- [68]. Torchilin, V.P.; *Advanced in Drug Delivery*, **2002**, *54*, 235.
- [69]. Lasic, D.D.; Martin, F.J.; *Stealth Liposomes* Boca Raton, FL : CRC Press ; **1995**.
- [70]. Torchilin, V.P.; Trubetskoy, V.S.; *Adv Drug Deliv Rev*, **1995**, *16*, 141.
- [71]. Lukyanov, A.N.; Hartner, W.C.; Torchilin, V.P.; *J Control Release*, **2004**, *94*, 187.
- [72]. Maeda, H.; Wu, J.; Sawa, T.; Matsumura, Y.; Hori, K.; *J Control Release*, **2000**, *65*, 271.
- [73]. Torchilin, V.P.; *J Microencapsul.*, **1998**, *15*, 19.
- [74]. Sapra, P.; Allen, T. M.; *Cancer Res.*, **2002**, *62*, 7190.
- [75]. Park, J.W.; Kirpotin, D.B.; Hong, K.; Shalaby, R.; Shao, Y.; Nielsen, U.B.; Marks, J.D.; Papahadjopoulos, D.; Benz, C.C.; *J. Control. Release*, **2001**, *74*, 95.
- [76]. Lukyanov, A.N.; Elbayoumi, T.A.; Chakilam, A.R.; Torchilin VP , *J. Control. Release*, **2004**, *100*, 135.
- [77]. Raffaghello, L.; Pagnan, G.; Pastorino, F.; Cosimo, E.; Brignole, C.; Marimpietri, D.; *Cancer Lett.*, **2003**, *197*, 151.
- [78]. Mastrobattista, E.; Gerben, G.A.; Bloois, L.; Filipe, A.C.S.; Jiskoot, W.; Storm, G.; *J. Biol. Chem.*, **2002**, *277*, 27135.
- [79]. Ni, S.; Stephenson, S.M.; Lee, R.; *J. Anticancer Res.*, **2002**, *22*, 2131.
- [80]. Pan, X.Q.; Wang, H.; Lee, R.J.; *Pharm. Res.*, **2003**, *20*, 417.
- [81]. Hatakeyama, H.; Akita, H.; Maruyama, K.; Suhara, T.; Harashima, H.; *Int. J. Pharm.*, **2004**, *281*, 25.
- [82]. Ishida, O.; Maruyama, K.; Tanahashi, H.; Iwatsuru, M.; Sasaki, K.; Eriguchi, M.; Yanagie, H.; *Pharm. Res*, **2001**, *18*, 1042.
- [83]. Drummond, D.C.; Hong, K.; Park, J.W.; Benz, C.C.; Kirpotin, D.B.; *Vitam. Horm.*, **2000**, *60*, 285.
- [84]. Dagar, S.; Krishnadas, A.; Rubinstein, I.; Blend, M.J.; Onyuksel, H.; *J. Control. Release*, **2003**, *91*, 123.

- [85]. Schiffelers, R. M.; Koning, G.A.; Hagen ten, T.L.M.; Fens, M.H.A.; Schraa, M.A.J.; Janssen, A.P.C.A.; Kok, R.J.; Molema, G.; Storm, G.; *J. Control. Release*, **2003**, *91*, 122.
- [86]. Lestina, B.J.; Sagnella, S. M.; Xu, Z.; Shive, M.S.; Richter, N.J.; Jayaseharan, J.; *J. Control. Release*, **2002**, *78*, 235.
- [87]. Mulder, W.J.M.; Strijkers, G.J.; Griffioen, A.W.; van Bloois, L.; Molema, G.; Storm, G.; Koning, G.; Nicolay, K.; *Bioconjugate Chem.*, **2004**, *15*, 799.
- [88]. Lattuada L.; Lux, G.; *Tetrahedron Lett.*, **2003**, *44*, 3893.
- [89]. Lipinski, M.J.; Amirbekian, V.; Frias, J.C.; Aguinado, J.G.S.; Mani, V.; Briley- Saebo, K.C.; Fuster, V.; Fallon, J.T.; Fisher, E.A.; Fayad, Z.A.; *Magn. Reson.Med.*; **2006**, *56*, 60.
- [90]. Amirbekian, V.; Lipinski, M.J.; Briley-Saebo, K.C.; Amirbekian, S.; Aguinado, J.G.S.; Weinreb, D.B.; Vucic, E.; Frias, J.C.; Hyafil, F.; Mani, V.; Fisher, E.A.; Fayad, Z.A.; *Proc. Natl. Acad. Sci.*, **2007**, *104*, 961.
- [91]. Li, K.C.P.; Bednarski, M.D.; *J Magn. Res. Imag.*, **2002**, *16*, 388.
- [92]. Sipkins, D.A.; Cheresch, D.A.; Kazemi, M.R.; Nevin, L.M.; Bednarski, M.D.; Li, K.C.P.; *Nat. Med.*, **1998**, *4*, 623.
- [93]. Sipkins, D.A.; Gijbels, K.; Tropper, F.D.; Bednarski, M.D.; Li, K.C.P.; Steinman, L.; *J. Neuroimmunol.*, **2000**, *104*, 1.
- [94]. Bull, S.R.; Guler, M.O.; Bras, R.E.; Maede, T.J.; Stupp, S.I.; *Nano Lett.*, **2005**, *5*, 1.
- [95]. Bull, S.R.; Guler, M.O.; Bras, R.E.; Venkatasubramanian, P.N.; Stupp, S.I.; Maede T.J.; *Bioconjugate Chem.*, **2005**, *16*, 1343.
- [96]. van Tilborg, G.A.F.; Mulder, W.J.M.; Deckers, N.; Storm, G.; Reutelingsperger C.P.M.; Strijkers, G.J.; Nicolay, K.; *Bioconjugate Chem.*, **2006**, *17*, 741.
- [97]. Schmieder, A.H.; Winter, P.M.; Caruthers, S.D.; Harris, T.D.; Williams, T.A.; Allen, J.S.; Lacy, E.K.; Zhang, H.; Scott, M.J.; Hu, G.; Robertson, J.D.; Wickline, S.A.; Lanza, G.M.; *Magn. Reson. Med.*, **2005**, *53*, 621.
- [98]. Van Tiborg G.A.F.; Mulder, W.J.M.; Deckers, N.; Storm, G.; Reutelingsperger, C.P.M.; Strijkers, G.J.; Nicolay, K.; *Bioconjugate Chem.*, **2006**, *17*, 741.
- [99]. Mulder, W.J.M.; Strijkers, G.J.; Habets, J.W.; Bleeker, E.J.W.; van der Schaft, D.W.J.; Storm, G.; Koning, G.A.; Griffioen, A.W.; Nicolay, K.; *FASEB J.*, **2005**, *19*, 2008.
- [100]. Brandwijk, R.J.M.G.E.; Mulder, W.J.M.; Nicolay, K.; Mayo, K.H.; Thijssen, V.L.J.L.; Griffioen, A.W.; *Bioconjugate Chem.*, **2007**, *18*, 785.
- [101]. Mulder, W.J.M.; Brandwijk, R.J.M.G.E.; Storm, G.; Chin, P.T.K.; Strijkers, G.J.; Donerà, C.D.M.; Nicolay, K.; Griffioen, A.W.; *Nano Lett.*, **2006**, *6*, 1.
- [102]. Ke, T.; Jeong, E.K.; Wang, X.; Feng, Y.; Parker, D.; Lu, Z.R.; *Int. J. Nanomed.*, **2007**, *2*, 191.
- [103]. Accardo, A.; Tesauro, D.; Roscigno, P.; Gianolio, E.; Paduano, L.; D'Errico, G.; Pedone, C.; Morelli, G.; *J. Am. Chem. Soc.*, **2004**, *126*, 3097.
- [104]. Mangiapia, G.; Accardo, A.; Lo Celso, F.; Tesauro, D.; Morelli, G.; Radulescu, A.; Paduano, L.; *J. Phys. Chem. B*, **2004**, *108*, 17611.
- [105]. Tesauro, D.; Accardo, A.; Gianolio, E.; Paduano, L.; Teixeira, J.; Schillen, K.; Aime, S.; Morelli, G.; *ChemBioChem*, **2007**, *8*, 950.

- [106]. Vaccaro, M.; Mangiapia, G.; Paduano, L.; Gianolio, E.; Accardo, A.; Tesauro, D.; *ChemPhysChem*, **2007**, *8*, 2526.
- [107]. Mierke, D.; Giragossian, C.; *Med. Res. Rev.*, **2001**, *21*, 450.
- [108]. Reubi, J.C.; Waser, B.; *Cancer Res.*, **1997**, *57*, 1377.
- [109]. Maeda, H.; *Adv Drug Deliv Rev.*, **2001**, *46*, 169.
- [110]. Skubitz, K.M.; *Cancer Invest.*, **2003**, *21*, 167.
- [111]. Harrington, K.J.; Lewanski, C.; Northcote, A.D.; Whittaker, A.; Peters, A.M.; Vile, R.G.; Stewart, J.S.W.; *Eur J Cancer*, **2001**, *37*, 2015.
- [112]. Patel, Y.; *Front Neuroendocrinol*, **1999**, *20*, 198
- [113]. Melacini, G.; Zhu, Q.; Goodman, M.; *Biochemistry*, **1997**, *36*, 1241.
- [114]. Pohl, E.; Heine, A.; Sheldrick, G.M.; Dauter, Z.; Wilson K. S.; Kallen, J.; Huber, W.; Pfaffli P.J.; *Acta Crystallogr. D Biol. Crystallogr.*, **1995**, *5*, 159.
- [115]. Wang, Q.; Graham, K.; Schauer, T.; Fietz, T.; Mohammed, A.; Liu, X.; Hoffend, J.; Haberkorn, U.; Eisenhut, M.; Mier, W.; *Nucl. Med. Biol.*, **2004**, *31*, 30.
- [116]. Torchilin, V.P.; Omelyanenko, V.G.; Papisov, M.I.; Bogdanov, A.J.; Trubetskoy, V.S.; Herron, J.N.; Gentry, C.A.; *Biochim. Biophys. Acta*, **1994**, *119*, 20.
- [117]. Chang, W.C.; White, P.D.; *Fmoc Solid Phase Peptide Synthesis*. Oxford University Press: New York, USA; **2000**.
- [118]. Diwu, Z.; Lu, Y.; Zhang, C.; Klaubert, D.H.; Haugland, R.P.; *Photochemistry and Photobiology*; **1997**, *66*, 431.
- [119]. Nakajima, A.; *Journal of Luminescence*, **1976**, *11*, 432.
- [120]. Vaccaro, M.; Mangiapia, G.; Paduano, L.; Gianolio, E.; Accardo, A.; Tesauro, D.; Morelli, G.; *ChemPhysChem.*, **2007**, *8*, 2538.
- [121]. Morag, O.; Ahmad, A.; Kamaly, N.; Perouzel, E.; Caussin, A.; Keller, M.; Herlihy, A.; Bell, J.; Miller, A.D.; Jorgensen, M.R.; *Org. Biomol. Chem.*, **2006**, *4*, 3497.
- [122]. Bauer, W.; Briner, U.; Doepfner, W.; *Life Sci.*, **1982**, *31*, 1140.
- [123]. Lackowicz, J.R.; *Principles of Fluorescence Spectroscopy*. Plenum Press: New York, **1983**.
- [124]. Caravan, P.; Ellison, J.J.; McMurry, T.J.; Lauffer, R.B.; *Chem. Rev. (Washington, DC)*, **1999**, *99*, 2352.
- [125]. Bloembergen, N.; Morgan, L.O.; *J. Chem. Phys.*, **1961**, *34*, 850.
- [126]. Lipari, G.; Szabo, A.; *J. Am. Chem. Soc.*, **1982**, *104*, 4559.
- [127]. Lipari, G.; Szabo, A.; *J. Am. Chem. Soc.*, **1982**, *104*, 4570.
- [128]. Anelli, P.L.; Fedeli, F.; Gazzotti, O.; Lattuada, L.; Lux, G.; Rebasti, F.; *Bioconjugate Chem.*, **1999**, *10*, 140.
- [129]. Schmitt, L.; Dietrich, C.; *J. Am. Chem. Soc.*, **1994**, *116*, 8491.
- [130]. Ellmann, G.L.; *Arch. Biochem. Biophys.*, **1959**, *82*, 77.
- [131]. Gadolinio libero
- [132]. Edelhoch, H.; *Biochemistry*, **1967**, *6*, 1954.
- [133]. Pace, C.N.; Vajdos, F.; Fee, L.; Grimsley, G.; Gray, T.; *Protein Sci.*, **1995**, *4*, 2423.
- [134]. K. S. Birdi, H. N. Singh and S. U. Dalsager, *J. Phys. Chem.* **1979**, *83*, 2737.
- [135]. De Vendittis, E.; Palumbo, G.; Parlato, G.; Bocchini, V.; *Analytical Biochemistry* **1981**, *115*, 286.

- [136]. Russell, T. P.; Lin, J. S.; Spooner, S.; Wignall, G. D.; *J. Appl. Crystallogr.*, **1988**, 21, (6), 638.
- [137]. Wignall, G. D.; Bates, F. S.; *J. Appl. Crystallogr.*, **1987**, 20(1), 40.
- [138]. Berne, B. J.; Pecora, R.; *Dynamic Light Scattering with applications to Chemistry, Biology and Physics. John Wiley & Sons: New York* **1976**.
- [139]. Fathi, Z.; Corjay, M. H.; Shapira, H.; Wada, E.; Benya, R.; Jensen, R.; Viallet, J.; Sausville, E. A.; Battey, J. F.; *J. Biol. Chem.*, **1993**, 268, 5984.
- [140]. Nagalla, S. R.; Barry, B. J.; Creswick, K. C.; Eden, P.; Taylor, J.T.; Spindel, E. R.; *Proc. Natl. Acad. Sci. U.S.A.*, **1995**, 92, 6209.
- [141]. Wada, E.; Way, J.; Shapira, H.; Kusano, K.; Lebacqz-Verheyden, A. M.; Coy, D.; Jensen, R.; Battey, J.; *Neuron*, **1991**, 6, 430.
- [142]. Markwalder, R.; Reubi, J.C.; *Cancer Res.*, **1999**, 59, 1159.
- [143]. Gugger, M.; Reubi, J.C.; *Am J Pathol.*, **1999**, 155, 2076.
- [144]. Fleischmann, A.; Waser, B.; Reubi, J.C.; *Cell Oncol.*, **2007**, 29, 433.
- [145]. Smith, C.J.; Volkert, W.A.; Hoffman, T.J.; *Nucl. Med. Biol.*, **2005**, 32, 740.
- [146]. Hua, F.; Cutler, C. S.; Hoffman, T.; Sieckman, G.; Volkert, W. A.; Jurisson, S. S.; *Nucl. Med. & Biol.*, **2002**, 29, 430.
- [147]. Alberts, D. S.; Muggia, F. M.; Carmichael, J.; Winer, E. P.; Jahanzeb, M.; Venook, A. P.; Skubitz, K. M.; Rivera, E.; Sparano, J. A.; Dibella, N. J.; Stewart, S. J.; Kavanagh, J. J.; Gabizon, A. A.; *Seminars in Oncology*, **2004**, 31(6, Suppl. 13), 90.
- [148]. Schneider, K.; Oltmanns, J.; Hassauer, M.; *Regulatory Toxicology and Pharmacology*, **2004**, 39(3), 347.
- [149]. Heppeler, A.; Froidevaux, S.; Maecke, H.R.; et al. (1999) *Chem Eur J* 5, 1981.
- [150]. Zhang, H.; Chen, J.; Waldherr, C.; Hinni, K.; Waser, B.; Reubi, J.C.; Maecke, H.R.; *Cancer Res.*, **2004**, 64, 6715.
- [151]. Walsh, J.H.; Gastrin. In: Walsh, J.H. and Dockray, G.J. (eds.), *Gut Peptides: Biochemistry and Physiology*, **1994**, 75.
- [152]. Smith, J.P. and Solomon, T.E. *Gastroenterology* **1988**, 95, 1541.
- [153]. Renfeld, J.F. and van Solinge, W.W. *Adv. Cancer. Res.* **1994**, 63, 295.
- [154]. Wank, S.A. *Am.J.Physiol.* **1998**, 274, G607.
- [155]. Pellegrini, M.; Mierke, D.F.; *Biochemistry*, **1999**, 38, 14783.
- [156]. Jullian, M.; Hernandez, A.; Maurras, A.; Puget, K.; Amblard, M.; Martinez, J.; Subra, G.; *Tetr. lett.* **2009**, 50, 263.
- [157]. Fritze, A.; Hens, F.; Kimpfler, A.; Schubert, R.; Peschka-Süss, R.; *Biochim Biophys Acta*, **2006**, 1758, 1640.
- [158]. Aloj, L.; Caraco, C.; Panico, M.; Zannetti, A.; Del Vecchio S.; Tesauro, D.; De Luca, S.; Arra, C.; Pedone, C.; Morelli, G.; Salvatore, M.; *J. Nucl. Med.*, **2004**, 45, 494.
- [159]. Denizot, F.; Lang, R.; *J. Immunol. Method*, **1986**, 89, 277.
- [160]. Rink, H.; *Tetrahedron Lett.*, **1987**, 28, 3787.
- [161]. Lakowicz, J.R.; *Principles of Fluorescence Spectroscopy*, II Ed., **1999**, Kluwer Academic, New York.

Abbreviations

AdOO	8-amino-3,6-dioxaoctanoic acid
AhOH	21-amino-4,7,10,13,16,19-hexaoxaheneicosanoic acid
ANS	8-anilinonaphtalene-1-sulfonate
BFC	Bifunctional chelator
BN	Bombesin
BSA	Bovine Serum Albumin
CCK	Cholecystokinin
CCK8	C-terminal octapeptide of cholecystokinin
CCK _A -R, CCK _B -R	Cholecystokinin receptor type A and B
Cmc	Critical micellar concentration
¹³ C NMR	Nuclear Magnetic Resonance
d	thickness radius
D	Self-diffusion coefficient
DCM	Dichloromethane
Dde	1-(4,4-Dimethyl-2,6-dioxocyclohex-1-ylidene)3-methyl-butyl
DIPEA	<i>N,N</i> diisopropylethylamine
DMF	<i>N,N</i> -dimethylformamide
<i>DLC</i>	Doxorubicin Loading Content
DLS	Dinamic Light Scattering
DOX	Doxorubicin
DOTA	1,4,7,10-Tetraazacyclododecane-1,4,7,10-tetracetic acid
DTPA	1,4,7,10-Tetraazacyclododecane-1,4,7,10-tetracetic acid diethylenetriaminepentaacetic acid
DTPAGlu	<i>N,N</i> -bis[2-[bis(carboxy-ethyl)amino]ethyl]-L-glutamic acid
FACS	Fluorescence Activated Cell Sorting
FITC	Fluorescein 5-isothiocyanate
Fmoc	9-fluorenylmethoxycarbonyl
GPCR	G-protein coupled receptor
GRPR	Gastrin-releasing peptide receptor
HATU	O-(7-azabenzotriazol-1-yl)-1,1,3,3 tetramethyluronium
HBS	Hepes Buffered Saline
¹ HNMR	Protonic nuclear magnetic resonance
HOBt	1-hydroxybenzotriazole
<i>I(Q)</i>	Scattering intensity
MRI	Magnetical Resonance Imaging
Mtt	4-methyltrityl
NMRD	Nuclear Magnetic Relaxation Dispersion
<i>n_w</i>	water molecules' number
PBS	Phosphate Buffer Saline
Peg	Poly(ethylene glycol)
Pip	Piperidine
<i>P(Q)</i>	Form factor
PyBop	benzotriazol-1-yl-oxy-tris-pyrrolidino-phosphonium
Pyr	Pyrene
<i>r_{1p}</i>	water proton relaxation value
<i>R_{1obs}</i>	Proton longitudinal relaxation rate
<i>R_{HY}</i>	Hydrodynamic radius
RP-HPLC	Reverse-phase High Pressure Liquid Cromatografy

R_t	Retention time
SANS	Small-Angle Neutron Scattering
$S(Q)$	Structure factor
SSTRs	somatostatin receptor subtypes
tBu	<i>tert</i> -Butyl
T1	Longitudinal relaxation time
T2	Transverse relaxation time
TFA	Trifluoroacetic acid
TIS	Triisopropylsilane
$Tl_3(CF_3CO_2)_3$	Thallium trifluoroacetate
τ_M	Residence lifetime
τ_R	Rorientational correlation time
τ_S	Electron spin relaxation time

Publication List

- 1). **Morisco Anna**, Accardo Antonella, Gianolio Eliana, Tesauo Diego, Benedetti Ettore and Morelli Giancarlo "Micelles derivatized with Octreotide as Potential Target Selective Contrast Agents in MRI", *J. Pept. Sci.* 2009; **15**: 242–250.
- 2). Antonella Accardo, Diego Tesauo, **Anna Morisco**, Gaetano Mangiapia, Mauro Vaccaro, Eliana Gianolio, Richard K. Heenan, Luigi Paduano and Giancarlo Morelli "Micelles Obtained by Aggregation of Gemini Surfactants Containing the CCK8 Peptide and a Gadolinium Complex", *J Biol Inorg Chem* (2009) 14:587–599.
- 3). Antonella Accardo, Rosalba Mansi, **Anna Morisco**, Gaetano Mangiapia, Luigi Paduano, Diego Tesauo, Aurel Radulescu, Michela Aurilio, Luigi Aloj, Claudio Arra, Giancarlo Morelli "Peptide modified nanocarriers for selective targeting of bombesin receptors", *Molecular Biosystems*, submitted.
- 4). **Anna Morisco**, Antonella Accardo, Diego Tesauo, Rosanna Palumbo and Giancarlo Morelli "CCK8 labeled supramolecular aggregates as doxorubicin carriers on tumor cells", *Journal of Pharmaceutical Sciences*, submitted.

Symposium Communications

- 1). Accardo, D. Tesauo, **A. Morisco**, C. Pedone and G. Morelli "Bioactive peptides as target-selective delivery tools of high relaxivity MRI contrast agents based on amphiphilic Gadolinium complexes" 11th Naples Workshop on bioactive peptides Napoli 24-27 maggio 2008.
- 2). **Morisco Anna**, Accardo Antonella, Gianolio Eliana, Tesauo Diego, Benedetti Ettore and Morelli Giancarlo "Micelles Derivatized with Octreotide as Potential Target Selective Contrast Agents in MRI" Scuola Nazionale di Chimica Bioinorganica 14-16 settembre 2008 Napoli.
- 3). **A. Morisco**, A. Accardo, E. Gianolio, D. Tesauo, E. Benedetti and G. Morelli "Micelles Derivatized with Octreotide and Gadolinium complexes as Potential target selective contrast agents in MRI" 8th workshop on Pharmaco Bio-Metals 24-26 ottobre 2008 Ravenna.
- 4). Diego Tesauo, Antonella Accardo, Carlo Pedone, **Anna Morisco**, Rosanna Palumbo, Giancarlo Morelli "Pt(II) complex anchored to CCK8 peptide as target selective cytotoxic agent

toward tumor cells” XXIII Congresso Nazionale della Società Chimica (SCI) 5-10 Luglio 2009 Sorrento.

- 5). **Anna Morisco**, Antonella Accardo, Diego Tesauro, Rosanna Palumbo, Giancarlo Morelli “CCK8 labeled supramolecular aggregates as doxorubicin carrier” XII Congress on the supramolecular chemistry 6-9 september 2009 Parma.
- 6). Antonella Accardo, **Anna Morisco**, Rosalba Mansi, Diego Tesauro, Gaetano Mangiapia, Luigi Aloj, Luigi Paduano, Giancarlo Morelli “Peptide labeled aggregates as nanocarriers to target cells overexpressing GRP receptors” XII Congress on the supramolecular chemistry 6-9 september 2009 Parma.
- 7). Diego Tesauro, Antonella Accardo, **Anna Morisco**, Giancarlo Morelli, Carlo Pedone “Pt(II) complexes vehicled by supramolecular aggregates labeled with bioactive peptides as target selective cytotoxic agents” 9th workshop on Pharmaco Bio-Metals 6-8 novembre 2009 Siena.

Micelles obtained by aggregation of gemini surfactants containing the CCK8 peptide and a gadolinium complex

Antonella Accardo · Diego Tesauro · Anna Morisco · Gaetano Mangiapia ·
Mauro Vaccaro · Eliana Gianolio · Richard K. Heenan · Luigi Paduano ·
Giancarlo Morelli

Received: 5 November 2008 / Accepted: 8 January 2009 / Published online: 3 February 2009
© SBIC 2009

Abstract Two gemini surfactants, [C18CysL5CCK8]₂ and [C18CysDTPAGlu]₂, containing, respectively, the CCK8 peptide and the DTPAGlu chelating agent or its gadolinium complex have been prepared by linking lipophilic chains through a disulfide bond between two cysteine residues. The two surfactants aggregate in water solution forming pure or mixed micelles, with a critical micellar concentration in the 5×10^{-6} – 5×10^{-5} mol kg⁻¹ range, as measured by fluorescence spectroscopy. As indicated by small-angle neutron scattering, the shape and size of the micelles are influenced by the temperature: increasing temperature leads to progressive reduction of the size of the

supramolecular aggregates. Cylindrical structures found at lower temperatures (10–40 °C) evolve into ellipsoidal micelles at 50–80 °C. Furthermore, the surface-exposed CCK8 peptide changes its conformation above a transition temperature of approximately 45 °C, going from a β -sheet to a random-coil structure, as indicated by circular dichroism measurements. The mixed aggregate obtained by coaggregation of the two gemini-based amphiphilic compounds, [C18CysDTPAGlu(Gd)]₂ and [C18CysL5CCK8]₂ in 70:30 molar ratio, represents the first example of a peptide-containing gemini surfactant as a potential target-selective contrast agent in MRI. In fact, it presents a high relaxivity value of the gadolinium complex, 21.5 mM⁻¹ s⁻¹, and the CCK8 bioactive peptide exposed on the external surface is therefore capable of selective targeting of the cholecystokinin receptors.

Electronic supplementary material The online version of this article (doi:10.1007/s00775-009-0472-1) contains supplementary material, which is available to authorized users.

A. Accardo · D. Tesauro · A. Morisco · G. Morelli (✉)
Department of Biological Sciences and IBB CNR,
CIRPeB, University of Naples “Federico II”,
Via Mezzocannone 16,
80134 Naples, Italy
e-mail: gmorelli@unina.it

G. Mangiapia · M. Vaccaro · L. Paduano (✉)
Department of Chemistry CSGI—Consorzio Interuniversitario
per lo Sviluppo dei Sistemi a Grande Interfase,
University of Naples “Federico II”,
Via Cynthia, 80126 Naples, Italy

E. Gianolio
Department of Chemistry I.F.M.,
Molecular Imaging Centre,
University of Turin,
Via Nizza 52, 10125 Turin, Italy

R. K. Heenan
ISIS-CLRC, Rutherford Appleton Laboratory,
Chilton, Oxfordshire OX11 0QX, UK

Keywords Peptide gemini surfactant ·
Amphiphilic gadolinium complexes · CCK8 peptide ·
Micelles · Small-angle neutron scattering

Introduction

Over the past two decades magnetic resonance imaging (MRI) has evolved into one of the most versatile and efficient noninvasive tools for clinical diagnosis [1, 2]. The advent of high magnetic fields, improved gradient coils, and pulse sequences has provided the means to obtain three-dimensional images of the internal part of the body at near cellular resolution [3]. The resolution of the image can be improved by administration of contrast agents. Stable complexes of gadolinium ion with polyaminocarboxylate ligands have been extensively used as paramagnetic contrast agents for MRI [4], because of their high

paramagnetism (seven unpaired electrons) and because of their favorable properties in terms of electronic relaxation [5]. The relative ability of a paramagnetic Gd(III) complex to act as an MRI contrast agent is expressed by its relaxivity, which measures the relaxation enhancement of water protons in solution containing the paramagnetic agent at 1 mM concentration [6]. Many efforts have been devoted to improving the relaxivity of Gd(III)-based contrast agents. As recognized early, high relaxivities can be achieved for slow-moving systems endowed with long rotational correlation times, fast exchange rates of the coordinated water molecules, and suitably long electronic relaxation rates of the unpaired electrons on the metal ion [1, 4].

On this basis several macromolecular systems have been designed in which the Gd(III) complexes are either covalently or noncovalently bound to high molecular weight substrates. Many supramolecular systems have been developed, such as dendrimers [7], polymers [8], proteins [9], water–gadofullerenes [10], and supramolecular amphiphilic aggregates such as micelles [11] and liposomes [12].

Among these carriers, micelles and liposomes, because of their easily controlled properties and good pharmacological characteristics, such as long blood retention, high tissue perfusion or excretion, are very promising candidates as contrast agents. The molecular targeting of supramolecular aggregates containing contrast agents might be accomplished by conjugating active recognition moieties, such as peptides [13] or antibodies [14], to their surface. For example, these bioactive markers could deliver the aggregates to membrane receptors overexpressed by cancerous cells [15].

We have recently developed mixed micellar aggregates containing a large number of gadolinium complexes and several units of a bioactive peptide, coupling together in the same contrast agent the high relaxivity due to the large number of paramagnetic complexes and the target specificity of the bioactive peptide [11, 16–18]. The CCK8 peptide (amino acid sequence Asp-Tyr-Met-Gly-Trp-Met-Asp-Phe-amide) is the C-terminal end of the peptide hormone cholecystokinin. This bioactive peptide should be able to deliver the aggregates on the cholecystokinin receptors CCK_A-R and/or CCK_B-R [19]. In this paper we describe new pure and mixed supramolecular structures in which both the amphiphilic monomers are represented by “gemini” surfactants. In general, as is well known, gemini surfactants are formed by the covalent linking of two “conventional” surfactants via a spacer [20, 21]. These surfactants have interesting features, such as low critical micellar concentration (cmc) values, which drastically reduce cytolytic action on the cell membrane. By manipulating the molecular architecture and the solution conditions, one can obtain a variety of supramolecular aggregates, such as vesicles and micelles. In the last few

years, Camilleri et al. proposed a novel class of peptide-based cationic gemini surfactants as nonviral gene-transfer vectors. These gemini surfactants include C12 saturated hydrocarbon “tails” and a short peptide “head group” with one or more basic amino acid residues. They were synthesized by starting from the reaction of L-cysteine with dibromoethane to form the bithioether [22, 23] or by using a spermine molecule as a linker [24]. We have developed a new synthetic procedure in the solid phase to easily obtain gemini-based peptide surfactants by introducing a cysteine residue in the peptide sequence. This strategy allows disulfur-bridge formation under mild oxidative conditions, reducing the number of purification steps. The new strategy was applied in the work reported here for the achievement of two gemini surfactants: one containing the bioactive sequence of the cholecystokinin peptide CCK8, [C18CysL5CCK8]₂, and the other one containing the chelating agent DTPAGlu or its gadolinium complex, DTPAGlu(Gd), [C18CysDTPAGlu(Gd)]₂ (see Fig. 1). We also report on the structural characterization and on the relaxivity behavior of supramolecular aggregates obtained by coassembling the two synthetic gemini surfactants at 70:30 molar ratio between the chelating monomer or its corresponding gadolinium complex and peptide monomer. Moreover, on the basis of recent reports in the literature which suggest conformational changes of the peptide upon temperature increase [25, 26] and to highlight the structural behavior of these aggregates as function of temperature [27, 28], we also performed structural investigations over a wide temperature range. These supramolecular aggregates represent the first example of peptide-containing gemini surfactants as potential target-selective contrast agents in MRI.

Results and discussion

Both gemini surfactants were synthesized by solid-phase methods using Rink amide 4-methylbenzhydrylamine (MBHA) resin as a polymeric support and 9-fluorenylmethoxycarbonyl(Fmoc)/*t*-Bu chemistry according to standard solid phase peptide synthesis protocols [29]. After the cleavage from the resin, the crude monotailed products were dissolved in an ammonium hydrogen carbonate solution (pH 8.0–8.5) and stirred at room temperature for 24 h [see Fig. S1 for liquid chromatography (LC)–mass spectrometry (MS) data of crude products]. The oxidation reactions were followed by using the colorimetric Ellmann test [30]. In Fig. 2 the ¹H NMR spectrum of C18Cys-DTPAGlu monomer in dimethyl-*d*₆ sulfoxide (DMSO-*d*₆) before its oxidation to the corresponding gemini surfactant is shown. The NMR spectrum confirms the high purity of the product, allowing a good yield of the oxidized gemini

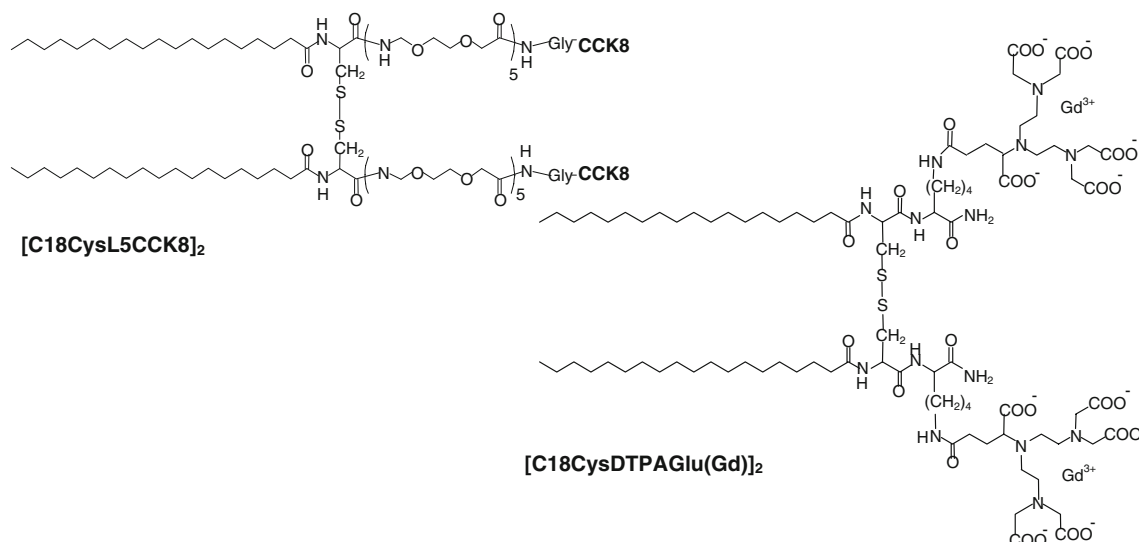
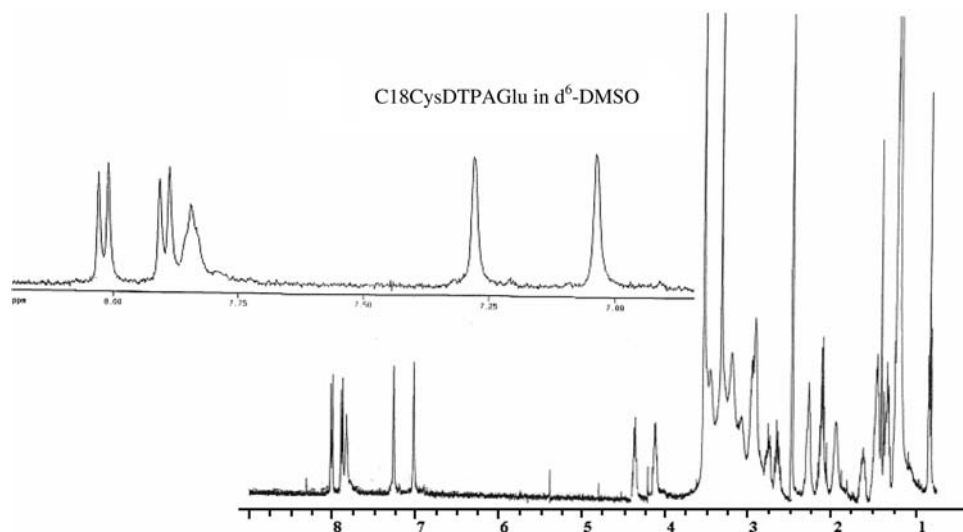


Fig. 1 $[C18CysDTPAGlu(Gd)]_2$ and $[C18CysL5CCK8]_2$ gemini amphiphilic monomers, obtained by connecting two identical moieties by a disulfide bond

Fig. 2 1H NMR spectrum of $C18CysDTPAGlu$ in dimethyl- d_6 sulfoxide



surfactant. As is clearly visible in the enlarged low-field region, the spectrum presents a broad signal (7.80 δ) corresponding to the 6NH -Lys proton, and two doublets related to 2NH amide protons of the Cys-Lys fragment. These signals (8.05 and 7.90 δ) are shifted at high field compared with the NH signal in random-coil peptide chains (8.40–8.30 δ). The $[C18CysL5CCK8]_2$ gemini surfactant was purified by preparative reversed-phase high-performance LC (HPLC) to a final HPLC purity of 90% and was isolated in 25% yield in lyophilized form. Analytical LC-MS data confirm the identity of the compound and its high purity. The gadolinium complex of $[C18CysDTPAGlu]_2$ was prepared by adding 2 equiv of $GdCl_3$ to a $[C18CysDTPAGlu]_2$ ligand solution at neutral pH and room temperature. To avoid the relaxivity contribution of free gadolinium ion, the excess was removed by filtering the

complex solution left at pH 10 for 24 h with a 0.2- μm syringe filter, as already reported for other chelating amphiphilic monomers [11]. The xylenol orange UV-spectrophotometric method was used to check for the absence of free $Gd(III)$ ions [31]. Self-assembling and mixed supramolecular aggregates were obtained by simply dissolving $[C18CysDTPAGlu]_2$ (or its corresponding gadolinium complex) and $[C18CysL5CCK8]_2$ gemini surfactants in phosphate buffer at pH 7.4.

Structural characterization

Fluorescence measurements

Cmc values of $[C18CysDTPAGlu]_2-H_2O$, $[C18CysDTPAGlu(Gd)]_2-H_2O$, and $[C18CysL5CCK8]_2-H_2O$ binary

systems and of [C18CysDTPAGlu]₂–[C18CysL5CCK8]₂–H₂O and [C18CysDTPAGlu(Gd)]₂–[C18CysL5CCK8]₂–H₂O ternary systems were determined by steady-state fluorescence spectroscopy by using, in separate experiments, two different probes: 8-anilinonaphthalene-1-sulfonate (ANS) and pyrene. The cmc measurements by two independent experiments allow minimization of the uncertainty in the calculated values. ANS and pyrene are both fluorescent probes that are poorly soluble in aqueous solution that change their emission spectrum depending on the polarity of the environment (hydrophobic or hydrophilic). The ANS fluorophore fluoresces at 480 nm only in a hydrophobic environment such as the inner micelle core [32]; thus, when the fluorescence intensity at 480 nm is plotted as a function of the amphiphile concentration, the breakpoint indicates the cmc value (see Fig. 3a, c, Table 1). In contrast, the pyrene molecule shows a more complex emission spectrum composed of five emission peaks (373, 379, 383, 389, and 393 nm). These peaks are affected by the polarity of the surrounding environment of the probe molecules. Specifically, it is considered that the

I_1/I_3 ratio of pyrene fluorescence is an index of the polarity of its environment. The values in hydrophobic solvents vary in the range 0.57–0.61, while in polar solvents the range is 1.25–2.00. In a micellar medium the observed values can be explained in terms of penetration of water into micelles and of the type of surfactant head group [33, 34].

As shown in Fig. 3b and d, the ratio between the intensities of the first (I_1) and the third (I_3) vibration bands of the pyrene emission spectrum remains constant (approximately 1.4–1.5) at monomer concentrations $c \leq 10^{-6}$ mol kg⁻¹, thus indicating the absence of micellar aggregates. At higher concentrations ($c > 10^{-6}$ mol kg⁻¹) I_1/I_3 decreases, thus indicating surfactant aggregation and pyrene migration from the aqueous environment into the hydrophobic core (or at the core–corona interface). Even though it has been reported that the polarity of the outer layer of the micelles could influence the pyrene emission [35], the cmc values obtained by using ANS and pyrene methods are in good agreement and indicate that all monomers in aqueous solution aggregate above a molal concentration in the

Fig. 3 a, c Fluorescence intensity of the 8-anilinonaphthalene-1-sulfonate fluorophore at 480 nm and **b, d** I_1/I_3 ratio of the pyrene vibration band versus surfactant concentration: [C18CysDTPAGlu]₂–H₂O (squares); [C18CysL5CCK8]₂–H₂O (open circles); [C18CysDTPAGlu(Gd)]₂–H₂O (filled circles); [C18CysDTPAGlu]₂–[C18CysL5CCK8]₂–H₂O (open triangles); [C18CysDTPAGlu(Gd)]₂–[C18CysL5CCK8]₂–H₂O (filled triangles). The data were multiplied by a scale factor for better comparison

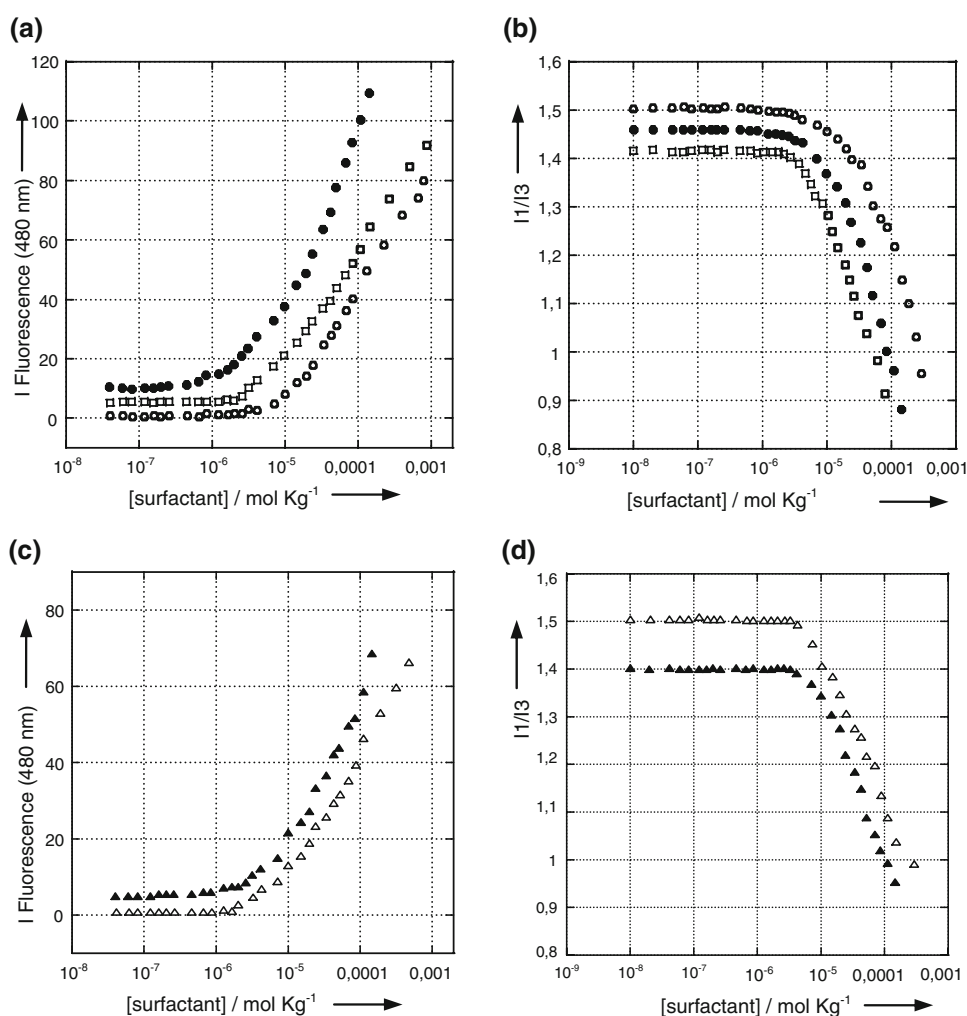


Table 1 Critical micellar concentration (*cmc*) values of supramolecular aggregates determined by steady-state fluorescence spectroscopy using 8-anilino-1-naphthalene-sulfonate (ANS) and pyrene as probes

System	ANS <i>cmc</i> (mol kg ⁻¹)	Pyrene <i>cmc</i> (mol kg ⁻¹)
[C18CysDTPAGlu] ₂ -H ₂ O	4.3 × 10 ⁻⁶	4.8 × 10 ⁻⁶
[C18CysDTPAGlu(Gd)] ₂ -H ₂ O	1.0 × 10 ⁻⁵	1.5 × 10 ⁻⁵
[C18CysL5CCK8] ₂ -H ₂ O	5.5 × 10 ⁻⁶	6.5 × 10 ⁻⁶
[C18CysDTPAGlu] ₂ - [C18CysL5CCK8] ₂ -H ₂ O	5.3 × 10 ⁻⁵	5.6 × 10 ⁻⁵
[C18CysDTPAGlu(Gd)] ₂ - [C18CysL5CCK8] ₂ -H ₂ O	8.0 × 10 ⁻⁶	8.0 × 10 ⁻⁶

See Fig. 1 for the molecular structures

5×10^{-6} – 5×10^{-5} mol kg⁻¹ range (see Table 1). These values are only slightly lower than the *cmc* values for the aggregates previously obtained by self-assembly of monotailed monomers (5×10^{-5} mol kg⁻¹) [11, 36]. This experimental result is apparently in disagreement with the well-known gemini surfactant properties, consisting of the ability of gemini surfactants to aggregate at *cmc* values lower than those of the monotailed monomers. In more detail, [C18CysDTPAGlu]₂ has a *cmc* value of approximately 4.6×10^{-6} mol kg⁻¹, while the corresponding monotailed monomer C18DTPAGlu has a *cmc* value of 5×10^{-5} mol kg⁻¹. These results can be explained taking into account the high electrostatic repulsion between the negative charges of the [C18CysDTPAGlu]₂ head groups. This monomer contains two DTPAGlu chelating agents in the same molecule, where each DTPAGlu moiety has five negative charges (COO⁻) at physiological pH, or two negative charges after gadolinium complexation. The *cmc* values are slightly higher than those found for double-tailed amphiphiles bearing only one charged DTPAGlu head group [16]. Hence, in the gemini compound two different effects are present: the higher tendency to aggregate with respect to the monotailed monomers, and the higher electrostatic repulsion between the head groups due to the negative charges of DTPAGlu moieties. The combination of these two effects produces (1) a slight stabilization of the gemini compound with a *cmc* value only 1 order of magnitude lower than for the monotailed monomer and (2) a slight loss in stability with respect to (C18)₂DTPAGlu. The *cmc* value (approximately 6×10^{-6} mol kg⁻¹) found for [C18CysL5CCK8]₂ monomer, in which there are no repulsion effects, is in agreement with the low expected values for gemini surfactants. In fact, the corresponding monotailed monomer (C18L5CCK8) did not show any tendency to aggregate under the same experimental conditions [36]. Moreover, fluorescence spectroscopy was used to confirm the presence of the bioactive peptide that is well exposed on the aggregate external surface: fluorescence at

approximately 360 nm of the tryptophan indole moiety (Fig. S2) is indicative of the presence of a tryptophan residue in a polar aqueous solvent, suggesting the presence of the entire CCK8 peptide in the micellar external environment.

Circular dichroism

The secondary peptide structures in pure aggregates formed by [C18CysL5CCK8]₂ and in [C18CysDTPAGlu]₂-[C18CysL5CCK8]₂ mixed aggregates [and the corresponding system in which the DTPAGlu chelating agent complexes the Gd(III) ion] were evaluated by circular dichroism (CD) spectroscopy. As was expected for short peptide sequences [37], and as previously reported [38, 39], the CCK8 octapeptide moiety does not undergo any folding process in water solution. On the other hand, in micellar aggregates obtained by self-assembly of (C18)₂L5CCK8, the peptide shows a classic β -sheet fold [40]. This result suggests that the hydrogen bonds among amino acids, well exposed on the external surface of the aggregates, promote intermolecular sheet-like structures that are stabilized by interactions between the alkyl chains. In the present case, according to the previous results, the CD spectrum of [C18CysL5CCK8]₂ reveals the characteristic shape of a β -sheet-type structure (Fig. 4). Upon heating the solution, the intensity of the CD spectra of the β -sheet structure signals (222 nm) decreases linearly, suggesting the breaking up of the interactions between peptides that are near each other. By plotting the intensity of the CD spectra at 222 nm as a function of temperature, one obtains a sigmoid curve composed of three temperature ranges: in the first one (from 10 °C to approximately 20 °C) the CD signal remains constant; in the second one (from approximately 20 °C to approximately 60 °C) there is a progressive decrease of the CD signal; and in the last one (from approximately 60 °C to 80 °C) the signal intensity remains constant. The maximum in the first derivative of the sigmoid curve indicates the transition temperature ($T_i \sim 45$ °C) at which the peptide structure changes from a β -sheet to a random-coil structure. The random-coil structure observed at 80 °C persists when the samples are cooled down. The peptide β -sheet conformation seems to be again obtained only below 20 °C, indicating a hysteresis phenomenon at the cooling rate used (1 °C min⁻¹). Similar structural behavior of the CCK8 peptide is observed in the case of the two mixed aggregates [C18CysDTPAGlu]₂-[C18CysL5CCK8]₂ and [C18CysDTPAGlu(Gd)]₂-[C18CysL5CCK8]₂, with T_i values in the same range (Fig. 5), and the presence of the hysteresis phenomenon. This result indicates that in mixed micelles, in which the two monomers [C18CysDTPAGlu]₂ and [C18CysL5CCK8]₂ are combined in 70:30 molar ratio, CCK8 molecules, notwithstanding their dilution in

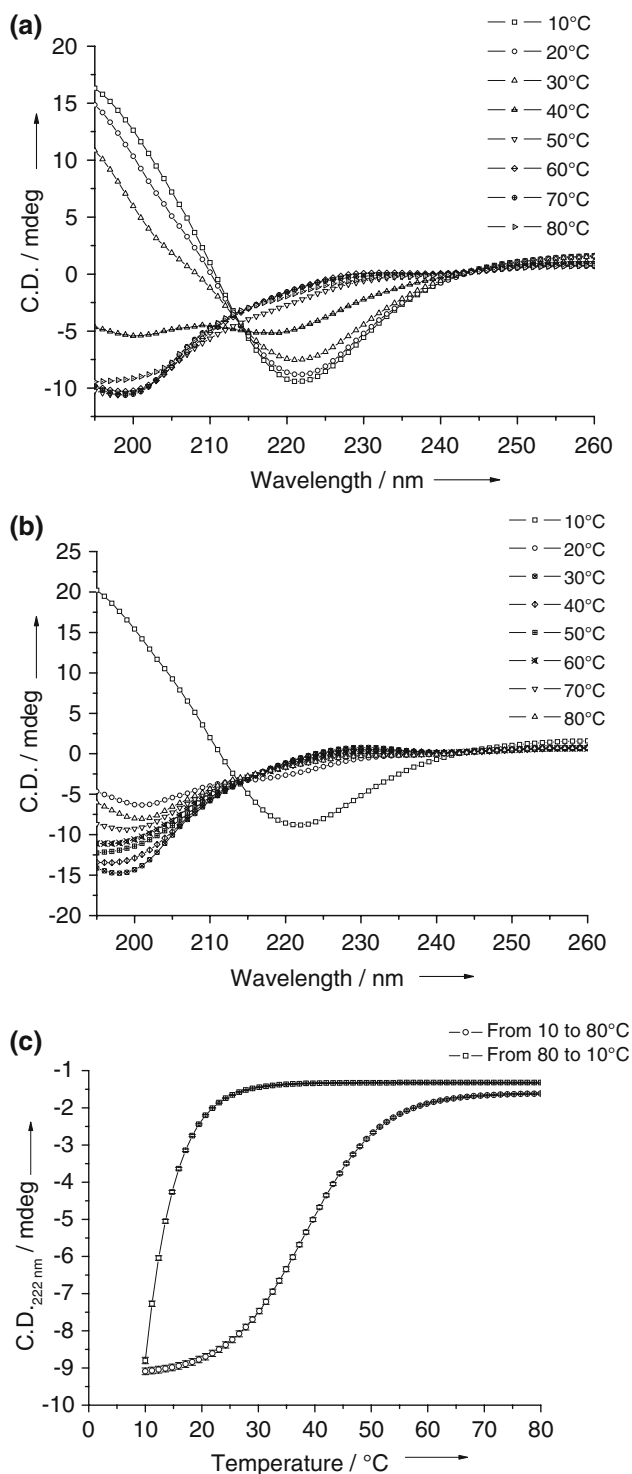


Fig. 4 Circular dichroism spectra of 1×10^{-4} M [C18CysL5-CCK8]₂ aggregate solution at pH 7.4: **a** aggregate solution heated from 10 to 80 °C; **b** aggregate solution cooled from 80 to 10 °C; **c** heating and cooling curves of the circular dichroism signal at 222 nm (from 10 to 80 °C and from 80 to 10 °C)

[C18CysDTPAGlu]₂ aggregates, are still close enough to each other to maintain hydrogen bonds among peptide chains.

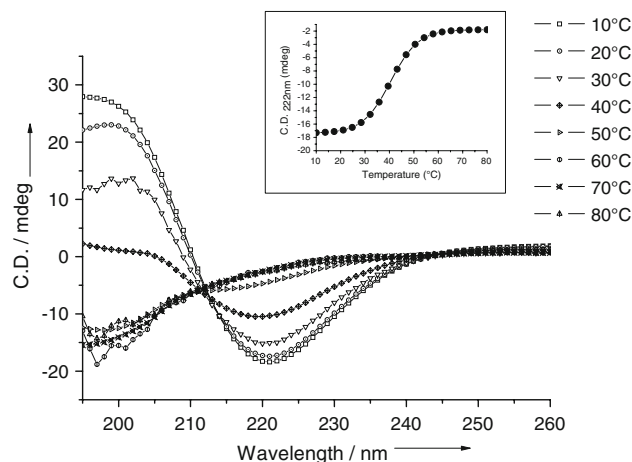


Fig. 5 Circular dichroism spectra of the [C18CysDTPAGlu(Gd)]₂–[C18CysL5CCK8]₂–H₂O ternary system (70:30 molar ratio, pH 7.4, 1×10^{-4} M concentration of the peptide-containing gemini surfactant) at different temperatures. The heating curve of the circular dichroism signal at 222 nm (from 10 to 80 °C) is shown in the inset

Small-angle neutron scattering

Small-angle neutron scattering (SANS) provides a direct probe of aggregate structure in dilute solutions. Figure 6 show the scattering cross sections collected for the [C18CysDTPAGlu(Gd)]₂ ($1.40 \text{ mmol kg}^{-1}$)–[C18CysL5-CCK8]₂ ($0.60 \text{ mmol kg}^{-1}$)–D₂O ternary system. The scattering cross sections for the [C18CysL5CCK8]₂ binary system and for the corresponding ternary systems containing [C18CysDTPAGlu]₂ are reported in Figs. S3 and S4. Figure 6a shows cross sections measured with temperature increasing, at 10, 40, 60, and 80 °C, and Fig. 6b shows cross sections measured with temperature decreasing, at 50, 20, and 10 °C. Inspection of the data shows some characteristic behavior for all the systems. The absence of a peak or depression of the signal at lower q suggests minimal, if any, intermicellar $S(q)$ interaction, as would be expected at these low concentrations in a 0.1 M buffer solution.

At 10 and 40 °C in Fig. 6a, the intensity for the initially prepared solutions scales with a $d\Sigma/d\Omega \propto q^{-1}$ power law characteristic of elongated structures (i.e., rod-like micelles). Owing to the lack of the Guinier regime for such temperatures, it is possible only to estimate that the length l of the cylinders should be greater than $2\pi/q_{\min}$, where q_{\min} is the smallest q value explored with the SANS measurements. The length of the rods is thus likely to be more than 700 Å. The radius of the cylindrical structures can be found from the axial Guinier equation for long, thin, rigid rods [41]:

$$\ln\left(q \frac{d\Sigma}{d\Omega}\right) = \ln(\phi(1-\phi)\pi R^2 \Delta^2 \rho) - \frac{q^2 R^2}{4}. \quad (1)$$

By fitting of Eq. 1 in the q range where $q \ll \pi/R$, cylindrical radii R of 19–24 Å were obtained, as reported in

Fig. 6 Scattering cross sections measured on heating (a) and cooling (b) the [C18CysDTPAGlu(Gd)]₂ (1.40 mmol kg⁻¹)–[C18CysL5CCK8]₂ (0.60 mmol kg⁻¹)–D₂O system, at the temperatures reported. To make the data more readable, cross sections were multiplied by a scale factor, as indicated

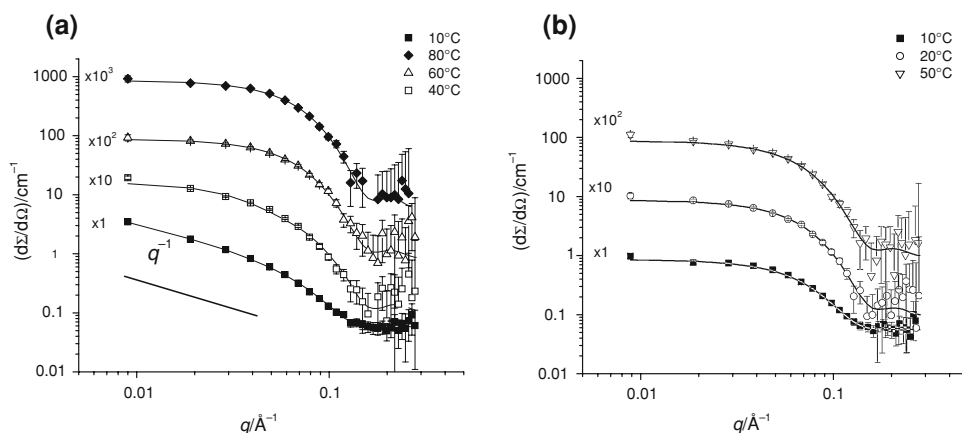


Table 2. It is worth noting that the flat background was taken into account for correct evaluation of the radius. Upon increasing the temperature above 40 °C, the aggregates change shape and the data suggest a form factor typical of ellipsoidal aggregates (see Figs. 6b, S3, S4). This behavior holds up to the highest temperature investigated (80 °C) and persists even when the samples are cooled down: the structural features seem to be preserved even if the initial temperature (10 °C) is again reached. Thus, we are in the presence of a hysteresis phenomenon. Scattering cross sections were modeled for a collection of monodisperse ellipsoidal micelles with an

aggregation number N_{agg} of surfactant molecules with volume v . When significant interactions among the aggregates can be excluded, the scattering cross sections $d\Sigma/d\Omega$ can be expressed as [42]

$$\frac{d\Sigma}{d\Omega} = n_p P(q) + \left(\frac{d\Sigma}{d\Omega} \right)_{incoh}, \quad (2)$$

where n_p is the number density of scattering bodies, $P(q)$ is the form factor of the bodies, and $(d\Sigma/d\Omega)_{incoh}$ is the incoherent scattering cross section. By modeling the micelles as uniform ellipsoids with semiaxes a , $b = c$, one can write the function $P(q)$ as

Table 2 Structural parameters obtained from fitting to small angle neutron scattering data at different temperatures

	10 °C	40 °C	50 °C	60 °C	80 °C	50 °C	20 °C	10 °C
[C18CysL5CCK8] ₂ (1.00 mmol kg ⁻¹)–D ₂ O								
N_{agg}	– ^a	– ^a	–	16 ± 1	15 ± 1	14 ± 1	14 ± 1	13 ± 1
R (Å)	21 ± 1	22 ± 1	–					
a (Å)			–	43 ± 2	42 ± 2	41 ± 2	41 ± 2	40 ± 2
$b = c$ (Å)			–	25 ± 1	25 ± 1	24 ± 1	24 ± 1	24 ± 1
[C18CysDTPAGlu(Gd)] ₂ (1.40 mmol kg ⁻¹)–[C18CysL5CCK8] ₂ (0.60 mmol kg ⁻¹)–D ₂ O								
N_{agg}	– ^a	– ^a	26 ± 1	22 ± 1	23 ± 1	22 ± 1	21 ± 1	21 ± 1
R (Å)	24 ± 1	23 ± 1						
a (Å)			57 ± 2	43 ± 2	46 ± 2	44 ± 2	44 ± 2	42 ± 2
$b = c$ (Å)			24 ± 1	25 ± 1	25 ± 1	25 ± 1	25 ± 1	25 ± 1
[C18CysDTPAGlu] ₂ (1.40 mmol kg ⁻¹)–[C18CysL5CCK8] ₂ (0.60 mmol kg ⁻¹)–D ₂ O								
N_{agg}	– ^a	– ^a	26 ± 1	25 ± 2	21 ± 1	21 ± 1	22 ± 1	23 ± 1
R (Å)	23 ± 1	19 ± 1						
a (Å)			57 ± 2	46 ± 2	44 ± 2	47 ± 2	46 ± 2	44 ± 2
$b = c$ (Å)			24 ± 1	24 ± 1	25 ± 1	24 ± 1	25 ± 1	26 ± 1

The equations used for the fitting are in the text. The radius (R) of cylindrical aggregates obtained at lower temperature is reported in the first two columns; the length of the semiaxis (a , $b = c$) of ellipsoidal micelles found at higher temperature and by cooling them to 10 °C is reported in the other columns

^a The aggregation number, N_{agg} , is not measurable in the case of cylindrical aggregates

$$P(q) = (\Delta\rho)^2 V^2 \int_0^1 F(q, \mu)^2 d\mu, \quad (3)$$

where $F(q, \mu)$ is the angle-dependent form factor for ellipsoidal micelles

$$F(q, \mu) = \frac{3j_1(u)}{u}, \quad (4)$$

with

$$u = q\sqrt{\mu^2 a^2 + (1 - \mu^2)b^2}, \quad (5)$$

where j_1 is the spherical Bessel function of first order, $V = 4/3\pi ab^2 = \nu N_{\text{agg}}$ is the micellar volume, and $\Delta\rho$ is the contrast existing between the micelles and the solvent. By using Eqs. 2, 3, 4, and 5, we obtained structural information on the aggregates present in the system and this is reported in Table 2.

Inspection of Table 2 reveals that micellar aggregates have elongated shapes with a cylindrical structure at lower temperatures and ellipsoidal shapes (with an axes ratio of approximately 2) at higher temperatures. The similar values observed for the radius of the cylindrical structures and for the minor semiaxis of the ellipsoidal structures suggest that the increase of the temperature leads to progressive shortening of the cylindrical structures to ellipsoidal micelles. Furthermore, the cooling of the systems again to 10 °C, once they have reached the maximum temperature investigated (80 °C), does not produce a significant change in the size and shape of the micelles.

Relaxivity measurements

The measured relaxivity value (r_{1p}) is defined, according to Eq. 6, as the paramagnetic contribution to the measured proton longitudinal relaxation rate ($R_{1\text{obs}}$) of a solution containing 1.0 mM concentration of the paramagnetic solute:

$$R_{1\text{obs}} = [\text{Gd}]r_{1p} + R_{1w}, \quad (6)$$

where R_{1w} is the diamagnetic contribution of pure water (0.38 s^{-1}). Relaxivity values at 20 MHz and 25 °C

(Table 3) were determined by mineralizing a 100- μl sample with 100 μl of 37% HCl at 120 °C overnight to determine the exact concentration of Gd(III) present in the solutions.

This mineralization process leads to a complete destruction of the gadolinium complex with the consequent release of free Gd(III) aquaion in the acidic solution. From the value of the observed relaxation rate ($R_{1\text{obs}}$) of this acidic solution, and knowing the relaxivity (r_{1p}) of Gd(III) aquaion in acidic conditions ($13.5 \text{ mM}^{-1} \text{ s}^{-1}$ at 20 MHz and 25 °C—GdCl₃ solutions whose concentrations were measured by inductively coupled plasma MS were used as standards, accuracy $\pm 0.1\%$) and the diamagnetic contribution (R_{1w}) in acidic conditions ($0.5 \text{ mM}^{-1} \text{ s}^{-1}$), we calculated the exact Gd(III) concentration using Eq. 6. Then, knowing the GdL concentration (opportunistically corrected for the 1:1 acidic dilution) and measuring $R_{1\text{obs}}$ of the aggregate-containing sample solutions, we calculated the relaxivity values of the two systems considered using again Eq. 6. The relaxivity measurements were performed on samples at a concentration much higher than the cmc: under these conditions, the contribution of monomeric species is negligible, and only aggregates are responsible for the measured relaxivity values. All the relaxometric characterization was conducted at 25 °C, that is, in the temperature conditions for which micelles have a rod-like cylindrical shape. The relaxivity values determined at 25 °C and 20 MHz are 18.4 and $21.5 \text{ mM}^{-1} \text{ s}^{-1}$ for pure and mixed micelles respectively. These values are in accordance with those of other similar gadolinium-containing micellar systems, as almost all the $q = 1$ (one inner-sphere water molecule) gadolinium-based micelles have relaxivity values in the range $18\text{--}23 \text{ mM}^{-1} \text{ s}^{-1}$ (20 MHz, 25 °C) [43–45]. To reach high relaxivity values, a very important parameter to account for is the exchange lifetime of the coordinated water molecule (τ_M) of a Gd(III) complex. The analysis of the temperature dependence of the transverse relaxation rate of the metal-bound ¹⁷O water resonance may be considered the method of choice for the determination of τ_M values [46, 47]. The τ_M value determined for the [C18CysDTPA-Glu(Gd)]₂ self-assembling aggregate at 25 °C and neutral pH was 152 ns. In the case of the [C18CysDTPAGlu(Gd)]₂–

Table 3 Principal relaxometric parameters measured at pH 7.4, 25 °C, and 20 MHz, calculated from fitting the nuclear magnetic relaxation dispersion (τ_R , Δ^2 , τ_V) and ¹⁷O NMR (τ_M) data as described in the text

System	r_{1p} ($\text{mM}^{-1} \text{ s}^{-1}$)	τ_M (ns)	τ_R (ns)			Δ^2 ($\times 10^{18} \text{ s}^{-2}$)	τ_V (ps)
			τ_1	S	τ_g		
[C18CysDTPAGlu(Gd)] ₂ –H ₂ O	18.4	152	0.190	0.49	3.20	7.65	57.3
[C18CysDTPAGlu(Gd)] ₂ –[C18CysL5CCK8] ₂ –H ₂ O	21.5	152 ^a	0.533	0.41	3.20	9.09	50.0

^a The exchange lifetime of the peptide-containing system was assumed to be similar to that of the corresponding system not containing the peptide

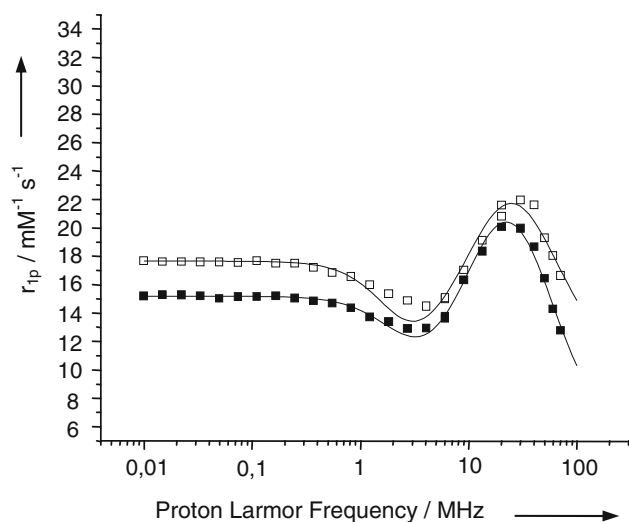


Fig. 7 Nuclear magnetic resonance dispersion profiles of [C18CysDTPAGlu(Gd)]₂ (filled squares) and [C18CysDTPAGlu(Gd)]₂–[C18CysL5CCK8]₂ (open squares) obtained at pH 7.4 and 25 °C, normalized to 1 mM concentration of Gd(III) ion. The curves through the data points were calculated with the parameters reported in Table 3

[C18CysL5CCK8]₂ mixed aggregate the τ_M value was assumed to be the same as that of the pure [C18CysDTPAGlu(Gd)]₂. From a quantitative analysis of the nuclear magnetic relaxation dispersion (NMRD) profiles it is possible to determine the reorientational correlation time (τ_R), which is related to the size of the system investigated. The NMRD profiles of [C18CysDTPAGlu(Gd)]₂ and [C18CysDTPAGlu(Gd)]₂–[C18CysL5CCK8]₂ at 25 °C are reported in Fig. 7. For the micellar systems, the data were analyzed using the Solomon–Bloembergen–Morgan model modified according to the Lipari–Szabo approach [48, 49]. This approach distinguishes between two independent motions: a rapid local motion governed by a correlation time defined as τ_1 and a slower global motion with a correlation time defined as τ_g . Data resulting from the fitting of the NMRD profiles are reported in Table 3. The analysis of experimental data gave the same value for τ_g of the two gadolinium-containing systems, that is, only slightly higher than the values reported for other gadolinium-based micellar systems [46].

The two systems differ substantially in the value of τ_1 as it seems that in mixed micelles containing the CCK8 amphiphilic moiety the internal motility of gadolinium-containing units is reduced. Clearly the complexes give rise to a system with a slower molecular tumbling in comparison with isolated gadolinium complexes. Anyway, the resulting relaxivity appears still lower than the expected values as internal motions are faster than the overall tumbling of the micellar system. According to the recent theory of Nicolle et al. [50], a relaxivity value lower than the theoretic one can be also ascribed to the interactions between nearby paramagnetic centers in micellar systems

which increase the transverse electronic relaxation of the electron spins of Gd(III) and, therefore, reduce the attainable water proton relaxivity. In this case, the proximity between Gd(III) centers is not only given by micellar assembly but also by the dimeric nature of the amphiphilic units.

Conclusion

The new gemini surfactants [C18CysL5CCK8]₂ and [C18CysDTPAGlu]₂ or its gadolinium complex [C18CysDTPAGlu(Gd)]₂ were prepared following a new efficient synthetic strategy. According to this strategy, amphiphilic monomers are synthesized using solid-phase methods, and after purification they are linked together through a disulfide bond between two cysteine residues, to give the corresponding gemini surfactants.

Gadolinium-based paramagnetic supramolecular aggregates derivatized with bioactive peptides, acting as selective contrast agents, have already been developed, by us and others, using different synthetic approaches [51, 52]. They are capable of visualizing neovascularization and angiogenic processes targeting $\alpha_v\beta_3$ integrins or tumor proliferation and metastasis, targeting cellular receptors overexpressed by cancer cells. The choice of synthetic strategy depends on whether coupling is performed before or after assembly of the supramolecular aggregate. The obvious goal of each approach is to achieve high coupling efficiency, but with the ligand retaining full binding affinity for its target receptor. The coupling of a ligand after the aggregate has been assembled involves the introduction of suitable activated functional groups onto the terminus of one of the aggregate components. Labeling procedures, based on the use of amphiphilic peptides that assemble together with amphiphilic gadolinium complexes in the peptide-labeled supramolecular aggregates, are very effective and have been used by us to have CCK8-labeled paramagnetic micelles and liposomes [11, 16–18]. The supramolecular aggregates reported here were structurally identified as cylindrical or ellipsoidal micelles. The shape and size of the micelles are influenced by the temperature: at lower temperatures micellar aggregates have elongated shapes with a cylindrical structure, while at higher temperatures ellipsoidal shapes are found. It seems that the increase of the temperature leads to progressive shortening of the cylindrical structures to ellipsoidal micelles. Likewise, the surface-exposed CCK8 peptide changes its conformation on increasing the temperature, going from a β -sheet to a random-coil structure. Even if there is any evidence that the two phenomena are related, the similarity of the transition temperatures of the two processes as well as the amplitude of the hysteresis indicate a possible

cooperation between the aggregate structure transition and the peptide conformation variation. The aggregates obtained by coaggregation of the two gemini-surfactant-based amphiphilic compounds, [C18CysDTPAGlu(Gd)]₂ and [C18CysL5CCK8]₂ in 70:30 molar ratio, represent the first example of peptide-containing gemini surfactants as potential target-selective contrast agents in MRI. The high relaxivity value, 21.5 mM⁻¹ s⁻¹, and the presence of CCK8 bioactive peptide exposed on the external surface of the micellar aggregate make this compound very attractive as an MRI contrast agent for in vivo visualization of tumor cells overexpressing the cholecystokinin receptors [53].

Materials and methods

Materials

Protected *N*^ε-Fmoc-amino acid derivatives, coupling reagents and Rink amide MBHA resin were purchased from Calbiochem-Novabiochem (Laufelfingen, Switzerland). Fmoc-8-amino-3,6-dioxaoctanoic acid (Fmoc-AdOO-OH) was purchased from Neosystem (Strasbourg, France). The DTPAGlu pentaester, *N,N*-bis[2-[bis[2-(1,1-dimethylethoxy)-2-oxoethyl]-amino]ethyl]-L-glutamic acid 1-(1,1-dimethylethyl)ester, was prepared according to the experimental procedure reported in the literature [54]. All other chemicals were commercially available from Sigma-Aldrich, Fluka (Buchs, Switzerland), or LabScan (Stillorgan, Dublin, Ireland) and were used as received unless stated otherwise. All solutions were prepared by weight using doubly distilled water. Samples to be measured by SANS techniques were prepared using D₂O (Sigma-Aldrich, purity better than 99.8%). The pH of all solutions was kept constant at 7.4. Preparative HPLCs were carried out using an LC8 Shimadzu HPLC system (Shimadzu, Kyoto, Japan) equipped with a UV lambda-Max model 481 detector using a Phenomenex (Torrance, CA, USA) C4 column (300 Å, 250 mm × 21.20 mm, 5 μm) eluted with H₂O/0.1% trifluoroacetic acid (TFA) (solvent A) and CH₃CN/0.1% TFA (solvent B) from 20 to 95% over 25 min at 20 mL min⁻¹ flow rate. LC-MS analysis was performed using a Thermo Electron (Waltham, MA, USA) Finnigan system.

[C18CysL5CCK8]₂

Peptide synthesis was carried out in the solid phase with a standard Fmoc strategy [29], by using an Applied Biosystems 433A automatic synthesizer. Rink amide MBHA resin (0.78 mmol g⁻¹, 0.5 mmol scale, 0.640 g) was used. The elongation of the G-CCK8 peptide was achieved by

sequential addition of Fmoc-amino acids with benzotriazol-1-yl-oxy-tris(pyrrolidinophosphonium) (PyBop)/1-hydroxybenzotriazole (HOBt) and *N,N*-diisopropylethylamine (DIPEA) (1:1:2) as coupling reagents, in dimethylformamide (DMF) in preactivation mode. The mixture was stirred for 1 h and after filtration the corresponding colorimetric test (Kaiser test) indicated the completion of the coupling. All couplings were performed twice for 1 h, by using an excess of 4 equiv for the single amino acid derivative. Fmoc deprotections were obtained using a 30% solution of piperidine in DMF. When the peptide synthesis was complete, the Fmoc N-terminal protecting group was removed and the five residues of Fmoc-AdOO-OH were condensed, step by step, according to the single coupling procedure by using an excess of 2 equiv. Then, the resin was washed and the terminal Fmoc protection was removed. A 1.171-g (2.0-mmol) amount of FmocCys(triphenylmethyl)-OH was coupled on the resin under stirring. The solution was filtered, the resin washed with three portions of DMF, and the Fmoc protecting group of the cysteine residue removed. To obtain the lipophylic monomer, 0.596 g (2.0 mmol) of nonaooctanoic acid was coupled on the linker-peptide N-terminus by using 1.040 g (2.0 mmol) of PyBop, 0.270 g (2.0 mmol) of HOBt, and 0.668 mL (4.0 mmol) of DIPEA in 4 mL of a 1:1 mixture of DMF and dichloromethane (DCM). The coupling time was 1 h under stirring at room temperature. For deprotection and cleavage, the fully protected resin was treated with a TFA solution containing triisopropylsilane (TIS) (2.0%) and water (2.5%) as scavengers. The free peptide derivative was precipitated in cold ethyl ether (Et₂O) and lyophilized from a H₂O/CH₃CN solution. The analytic LC-MS analysis confirmed the identity of the product. C₁₈H₃₇CO-Cys-(AdOO)₅-G-CCK8 (C18CysL5CCK8): *R*_t = 20.65 min; [M + 3H]^{+/3} = 741 amu (molecular weight 2,228).

The intramolecular disulfur bond between cysteine residues was obtained by reaction of the crude product (0.1 mmol; 223 mg) dissolved in 100 mL of 0.1 M ammonium hydrogen carbonate (pH 8.0–8.5) at room temperature for 24 h. The air-oxidation reaction was monitored by the colorimetric Ellmann test [30]. The identification of the oxidized product was confirmed by LC-MS analysis. The crude compound was purified by reversed-phase HPLC. Fractions were characterized by LC-MS analysis to assess purity and molecular weight. Pure fractions were pooled and lyophilized. The total amount of the oxidized gemini product was 550 mg, corresponding to a final yield of 25%. LC-MS characterization confirmed the identity of the oxidized gemini product. [C₁₈H₃₇CO-Cys-(AdOO)₅-G-CCK8]₂; *R*_t = 26.76 min; [M + 3H]^{+/3} = 1,485 amu (molecular weight 4,456).

[C18CysDTPAGlu]₂

Fmoc-Lys(Mtt)-OH (624.79 mg, 1.00 mmol), where Mtt is (4-methylphenyl)diphenylmethyl, activated by 1 equiv of PyBop and HOBt and 2 equiv of DIPEA in DMF was coupled twice to Rink amide MBHA resin (0.78 mmol/g, 0.250 mmol scale, 0.320 g) by stirring the slurry suspension for 1 h. The solution was filtered and the resin washed with three portions of DMF and three portions of DCM. The Mtt protecting group was removed by treatment with 2.0 mL of a DCM/TIS/TFA (94:5:1) mixture. The treatment was repeated several times until the solution became colorless. The resin was washed with DMF and then the DTPAGlu pentaester chelating agent was linked, through its free carboxyl function, to the α -NH₂ of the lysine residue. This coupling step was performed using 2.0 equiv of DTPAGlu pentaester and *O*-(7-azabenzotriazol-1-yl)-1,1,3,3-tetramethyluronium, and 4 equiv of DIPEA in DMF as the solvent. The coupling time, compared with that for the classic solid phase peptide synthesis protocol, was increased up to 2 h and the reaction was tested for completion by the Kaiser test. After removal of the Fmoc protecting group by 30% piperidine in DMF, and the coupling of the cysteine residue under standard conditions, the coupling of nona octanoic acid was performed in a DCM/DMF (1:1) mixture according to the previously described conditions. For deprotection and cleavage, the fully protected fragment was treated with TFA containing TIS (2.0%) and water (2.5%). The crude product was precipitated at 0 °C, washed several times with small portions of water, and recrystallized from methanol and water. The product was characterized by ¹H NMR spectroscopy and electrospray spectrometry.

C₁₈H₃₇CONHCysLys(DTPAGlu)CONH₂ (C18CysDTPAGlu): ¹H MMR (chemical shifts δ , tetramethylsilane as the internal standard, DMSO-*d*₆ as the solvent) 4.4 (m, α CH Cys), 4.1 (m, 1H, α CH Lys), 3.5 (overlapped, 1H, α CH Glu), 3.3 (s, 8H, NCH₂COOH), 2.7–2.8 (m, 8H, RNCH₂CH₂NR), 2.14 (m 2H, C(O)CH₂CH₂R), 1.87 (m, γ CH₂ Lys), 1.76 (m, 2H, δ CH₂ Lys), 1.65 (m, 2H, β CH₂ Lys), 1.5 (overlapped, 2H, RCH₂CH₃), 1.1–1.3 (m, 30 H, 15 CH₂), 0.8 (t, 3H, 1 CH₃). [M + H]⁺ = 976 amu (molecular weight 975).

The intramolecular disulfide bond reaction between the cysteine residues was carried out under the same conditions as described above in the case of C18CysL5CCK8, and the identity of the product was confirmed by LC-MS analysis.

[C₁₈H₃₇COCysLys(DTPAGlu)CONH₂]₂: R_t = 27.15 min; [M + H]⁺ = 1,950 amu (molecular weight 1,949).

Preparation of gadolinium complexes

The preparation of gadolinium complexes was carried out by adding 2 equiv of GdCl₃ to an aqueous solution of the

[C18CysDTPAGlu]₂ ligand at neutral pH and room temperature. The formation of the complexes was followed by measuring the solvent proton relaxation rate (1/*T*₁). The excess of uncomplexed Gd(III) ions, which yields a variation of the observed relaxation rate, was removed by filtering the complex solution left at pH 10 for 24 h with a 0.2- μ m syringe filter, as already reported for other chelating amphiphilic monomers [11]. A xylenol orange UV-spectrophotometric method was used to check for the absence of free Gd(III) ions [31].

Solution preparation

Stock solutions of [C18CysDTPAGlu]₂, [C18CysDTPAGlu(Gd)]₂, and [C18CysL5CCK8]₂ binary systems and [C18CysDTPAGlu]₂–[C18CysL5CCK8]₂ and [C18CysDTPAGlu(Gd)]₂–[C18CysL5CCK8]₂ ternary systems were prepared in 0.1 M phosphate buffer at pH 7.4. Solutions were stirred at room temperature until complete dissolution of the monomers and were then filtered through a 0.45- μ m filter. All mixed solutions were prepared at 70:30 molar ratio between [C18CysDTPAGlu]₂ or [C18CysDTPAGlu(Gd)]₂ and [C18CysL5CCK8]₂.

UV spectroscopy

The concentrations of solutions containing peptide surfactant were determined by absorbance measurement using a JASCO V-5505 UV–vis spectrophotometer equipped with a JASCO ETC.-505T Peltier temperature controller with a 1-cm quartz cuvette (Hellma). A molar absorptivity (ϵ_{280}) of 6,845 M⁻¹ cm⁻¹ was used for CCK8; this value was calculated according to the Edelhoof method [55], taking into account contributions from tyrosine and tryptophan present in the primary structure, which amount to 1,215 and 5,630 M⁻¹ cm⁻¹, respectively [56].

Fluorescence spectroscopy

Cmc values of aggregates were obtained by fluorescence spectroscopy. Emission spectra were recorded at room temperature using a JASCO model FP-750 spectrofluorimeter in 1.0 cm path length quartz cell. Equal excitation and emission bandwidths were used throughout the experiments, with a recording speed of 125 nm min⁻¹ and automatic selection of the time constant. The cmc values were measured by using ANS and pyrene as fluorescent probes. A stock solution of pyrene (*c* = 1.0 × 10⁻³ M) was prepared by adding a known weight of the compound to 20 wt% ethanol in water. The small amount of ethanol in the pyrene solution does not affect the spectral and self-aggregation behavior of amphiphiles. Small aliquots of 1 × 10⁻⁴ M aggregate solution, dissolved in 0.10 M phosphate buffer,

pH 7.4, were added to a fixed volume (1.00 mL) of fluorophore (1×10^{-5} M ANS or 2×10^{-6} M pyrene) directly in the quartz cell. In the ANS method, the cmc values were determined by linear least-squares fitting of the fluorescence at 480 nm, upon excitation at 350 nm versus the amphiphile concentration as previously reported [57, 58]. In the pyrene method, the cmc values were determined from the break point of the fitting of I_1/I_3 upon excitation at 335 nm versus the amphiphile concentration.

Circular dichroism experiments

Far-UV CD spectra were collected at room temperature using a JASCO J-810 spectropolarimeter equipped with a NesLab RTE111 thermal controller unit using a 1-mm quartz cell. Other experimental settings were as follows: scan speed 10 nm min^{-1} ; sensitivity 50 mdeg; time constant 16 s; bandwidth 3 nm. CD measurements were conducted on solutions containing peptide surfactant at concentrations of 1×10^{-4} M in 2.5 mM phosphate buffer at pH 7.4. The CD spectra were collected from 260 to 195 nm, corrected for the blank and adjusted for dilution. Thermal profiles (CD vs. temperature, in the 10–80 and 80–10 °C ranges) of the aggregates were recorded every 10 °C, with an equilibration time of 20 min for each measurement point. All samples were run in duplicate. The T_i was determined from the maximum of the first derivative of the heating and cooling curves.

Small angle neutron scattering measurements

SANS measurements were performed at various temperatures (in the 10–80 and 80–10 °C ranges) at the LOQ instrument sited at the ISIS facility of the Rutherford Appleton Laboratory (Chilton, UK). At the ISIS pulsed neutron source, the LOQ instrument uses neutrons of wavelengths ranging between 2.2 and 10 Å detected by a time-of-flight analysis on a 64-cm^2 two-dimensional detector placed 4.1 m from the sample [59], giving a q range of 0.006–0.24 Å⁻¹. Raw data were corrected for wavelength-dependent sample transmissions, incident spectrum, and detector efficiency and then put into absolute scattering cross sections $d\Sigma/d\Omega$ by comparison with scattering from a partially deuterated polystyrene standard. Samples were heated up from 10 to 80 °C at a rate of 1.0 °C min^{-1} , and cross sections were measured at 10, 40, 50, 60, and 80 °C. After that, they were cooled down at a rate of 1.0 °C min^{-1} , and cross sections were recorded at 50, 20, and 10 °C.

Water proton relaxation measurements

The longitudinal water proton relaxation rates were measured with a Stellar Spinmaster (Mede, Pavia, Italy)

spectrometer operating at 20 MHz, by means of the standard inversion-recovery technique (16 experiments, two scans). A typical 90° pulse width was 4 μs and the reproducibility of the T_1 data was $\pm 0.5\%$. The temperature was maintained at 25 °C with a Stellar VTC-91 air-flow heater equipped with a copper-constantan thermocouple (uncertainty $\pm 0.1 \text{ °C}$). The proton $1/T_1$ NMRD profiles were measured over a continuum of magnetic field strength from 0.00024 to 0.28 T (corresponding to 0.01–12 MHz proton Larmor frequency) using a Stellar fast field-cycling relaxometer. This relaxometer works under complete computer control with an absolute uncertainty in $1/T_1$ of $\pm 1\%$. Data points at 20 and 90 MHz were added to the experimental NMRD profiles and were recorded with the Stellar Spinmaster (20 MHz) and with a JEOL (Tokyo, Japan) EX-90 (90 MHz) spectrometer, respectively.

¹⁷O measurements

Variable-temperature ¹⁷O NMR measurements were recorded at 2.1 T using the JEOL EX-90 spectrometer, equipped with a 5-mm probe, by using a D₂O external lock. The experimental settings were as follows: spectral width 10,000 Hz; 90° pulse (7 μs); acquisition time 10 ms; 1,000 scans; no sample spinning. Aqueous solutions containing 2.6% of the ¹⁷O isotope (Yeda, Israel) were used. The observed transverse relaxation rates ($R_{2\text{obs}}^0$) were calculated from the signal width at half-height ($\Delta\nu_{12} = R_{2\text{obs}}\pi\Delta\nu_{12}$).

Acknowledgments We are indebted to EML, European Molecular Imaging Laboratoires, for financial support. The authors wish to thank the Rutherford Appleton Laboratory for provision of beam time. L.P., M.V., and G.Ma. wish to thank CSGI and MIUR (PRIN-2006) for funding the research.

References

- Caravan P, Ellison J, McMurry T, Lauffer R (1999) *Chem Rev* 99:2293–2352
- Meade TJ, Taylor AK, Bull SR (2003) *Curr Opin Neurobiol* 13:597–602
- Toth E, Helm L, Merbach AE (2001) *The chemistry of contrast agents in medical magnetic resonance imaging*, 1st edn. Wiley, London, pp 45–120
- Aime S, Botta M, Fasano M, Terreno E (1998) *Chem Soc Rev* 27:19–29
- Weinmann HJ, Mühler A, Radüchel B (2000) *Methods in biomedical magnetic resonance. Imaging and spectroscopy*. Wiley, Chichester
- Banci L, Bertini I, Luchinat C (1991) *Nuclear and electronic relaxation*. VCH, Weinheim
- Laus S, Sour A, Ruloff R, Toth E, Merbach AE (2005) *Chem Eur J* 11:3064–3076
- Nasongkla N, Bey E, Ren J, Ai H, Khemtong C, Guthi JS, Chin S-F, Sherry AD, Boothman DA, Gao J (2006) *Nano Lett* 6:2427–2430

9. Dirksen A, Langereis S, de Waal BFM, van Genderen MHP, Hackeng TM, Meijer EW (2005) *Chem Commun* 2811–2813
10. Toth E, Bolskar RD, Borel A, Gonzalez G, Helm L, Merbach AE, Sitharaman B, Wilson LJ (2005) *J Am Chem Soc* 127:799–805
11. Accardo A, Tesauro D, Roscigno P, Gianolio E, Paduano L, D'Errico G, Pedone C, Morelli G (2004) *J Am Chem Soc* 126:3097–3107
12. Gløgård C, Stensrud G, Hovland R, Fosshem SL, Klaveness J (2002) *Int J Pharm* 233:131–140
13. Nasongkla N, Shuai X, Ai H, Weinberg BD, Pink J, Boothman DA, Gao J (2004) *Angew Chem Int Ed* 43:6323–6327
14. King CP, Li, Bednarski MD (2002) *J Magn Reson Imaging* 16:388–393
15. Reubi JC (2003) *Endocr Rev* 24:389–427
16. Accardo A, Tesauro D, Morelli G, Gianolio E, Aime S, Vaccaro M, Mangiapia G, Paduano L, Schillen K (2007) *J Biol Inorg Chem* 12:267–276
17. Tesauro D, Accardo A, Gianolio E, Paduano L, Teixeira J, Schillen K, Aime S, Morelli G (2007) *Chembiochem* 8:950–955
18. Vaccaro M, Mangiapia G, Paduano L, Gianolio E, Accardo A, Tesauro D, Morelli G (2007) *Chemphyschem* 8:2526–2538
19. Wank SA (1995) *Am J Physiol Gastrointest Liver Physiol* 269:G628–G646
20. Menger FM, Littau CA (1991) *J Am Chem Soc* 113:1451–1452
21. Zana R (2002) *Adv Colloid Interface Sci* 97:205–253
22. Jennings K, Marshall I, Birrell H, Edwards A, Haskins N, Sodermann O, Kirby AJ, Camilleri P (1998) *Chem Commun* 18:1951–1952
23. Camilleri P, Kremer A, Edwards AJ, Jennings KH, Jenkins O, Marshall I, McGregor C, Neville W, Rice SQ, Smith RJ, Wilkinson MJ, Kirby AJ (2000) *Chem Commun* 14:1253–1254
24. Ronsin G, Kirby AJ, Rittenhouse S, Woodnutt G, Camilleri PJ (2002) *Chem Soc Perkin Trans* 2:1302–1306
25. Lowik DW, Garcia-Hartjes J, Meijer JT, van Hest JCM (2005) *Langmuir* 21:524–526
26. Hamley IW, Ansari IA, Castelletto V, Nuhn H, Rosler A, Klok HA (2005) *Biomacromolecules* 6:1310–1315
27. Gorski N, Kalus J (2001) *Langmuir* 17:4211–4215
28. Bott R, Wolff T, Zierold K (2002) *Langmuir* 18:2004–2012
29. Chang WC, White PD (2000) *Fmoc solid phase peptide synthesis*. Oxford University Press, New York
30. Ellmann GL (1959) *Arch Biochem Biophys* 82:70–77
31. Barge A, Cravotto G, Gianolio E, Fedeli F (2006) *Contrast Med Mol Imaging* 1:184–188
32. Diwu Z, Lu Y, Zhang C, Klaubert DH, Haugland RP (1997) *Photochem Photobiol* 66:424–431
33. Menger FM (1979) *Acc Chem Res* 12:111–117
34. Zana R (2002) *Langmuir* 18(20):7759–7760
35. Menger FM, Jerkunica JM, Jhonston JC (1978) *J Am Chem Soc* 100:4676–4678
36. Mangiapia G, Accardo A, Lo Celso F, Tesauro D, Morelli G, Radulescu A, Paduano L (2004) *J Phys Chem B* 108:17611–17617
37. Underfriend S, Meienhofer J (1985) In: Ihruby VJ (ed) *The peptides*, vol 7. Academic Press, New York
38. Pellegrini M, Mierke DF (1999) *Biochemistry* 38:14775–14783
39. Moroder L, D'Ursi A, Picone D, Amodio P, Temussi PA (1993) *Biochem Biophys Res Commun* 190(3):741–746
40. Accardo A, Tesauro D, Mangiapia G, Pedone C, Morelli G (2007) *Biopolymers* 88:115–121
41. Radulescu A, Mathers RT, Coates GW, Richter D, Fetters L (2004) *Macromolecules* 37:6962–6971
42. Kotlarchyk M, Chen SH (1983) *J Chem Phys* 79:2461–2469
43. Nicolle GM, Toth E, Eisenwiener KP, Macke HR, Merbach AE (2002) *J Biol Inorg Chem* 7:757–769
44. Laus S, Sour A, Ruloff R, Toth E, Merbach AE (2005) *Chem Eur J* 11:3064–3076
45. Delli Castelli D, Gianolio E, Geninatti Crich S, Terreno E, Aime S (2008) *Coord Chem Rev* 252:2424–2443
46. Powell DH, Ni Dhubhghaill OM, Pubanz D, Helm L, Lebedev YS, Schlaepfer V, Merbach AE (1996) *J Am Chem Soc* 118:9333–9346
47. Aime S, Botta M, Fasano M, Terreno E (1999) *Acc Chem Res* 32:941–949
48. Lipari G, Szabo A (1982) *J Am Chem Soc* 104:4546–4559
49. Lipari G, Szabo A (1982) *J Am Chem Soc* 104:4559–4570
50. Nicolle GM, Helm L, Merbach AE (2003) *Magn Reson Chem* 41:794–799
51. Torchilin VP (2005) *Nat Rev Drug Discov* 4:145–154
52. Brandwijk RJMGE, Mulder WJM, Nicolay K, Mayo KH, Thijssen VLJL, Griffioen AW (2007) *Bioconjug Chem* 18:785–792
53. Reubi JC, Schaer JC, Waser B (1997) *Cancer Res* 57:1377–1386
54. Anelli PL, Fedeli F, Gazzotti O, Lattuada L, Lux G, Rebasti F (1999) *Bioconjug Chem* 10:137–140
55. Edelhoch H (1967) *Biochemistry* 6:1948–1954
56. Pace CN, Vajdos F, Fee L, Grimsley G, Gray T (1995) *Protein Sci* 4:2411–2423
57. Birdi KS, Singh HN, Dalsager SU (1979) *J Phys Chem* 83:2733–2737
58. De Vendittis E, Palumbo G, Parlato G, Bocchini V (1981) *Anal Biochem* 115:278–286
59. Heenan RK, Penfold J, King SM (1997) *J Appl Crystallogr* 30:1140–1147

Micelles derivatized with octreotide as potential target-selective contrast agents in MRI^{‡§}

Anna Morisco,^a Antonella Accardo,^a Eliana Gianolio,^b Diego Tesauro,^a Ettore Benedetti^a and Giancarlo Morelli^{a*}

New amphiphilic monomers (OCA-DTPAGlu and OCA-DOTA) containing, in the same molecule, three different functions: (i) the chelating agent (DTPAGlu or DOTA) able to coordinate gadolinium ion, (ii) the octreotide bioactive peptide able to target somatostatin receptors, and (iii) a hydrophobic moiety with two 18-carbon atoms alkyl chains have been designed and synthesized by solid-phase methods. The novel amphiphilic monomers aggregate, in water solution, giving stable micelles at very low concentration (cmc values of 2.3×10^{-6} mol kg⁻¹ and 2.5×10^{-6} mol kg⁻¹ for OCA-DTPAGlu and OCA-DOTA, respectively) as confirmed by fluorescence spectroscopy. Fluorescence studies and circular dichroism experiments indicate, for the two compounds as well as for their gadolinium complexes (OCA-DOTA(Gd) and OCA-DTPAGlu(Gd)), the complete exposure of octreotide on the micelle surface, and the predominant presence of an antiparallel β -sheet peptide conformation characterized by a β -like turn. The high relaxivity value ($r_{1\rho} = 13.9$ mm⁻¹ s⁻¹ at 20 MHz and 25 °C), measured for micelles obtained by the gadolinium complex OCA-DTPAGlu(Gd), indicates these aggregates as promising target-selective magnetic resonance imaging (MRI) contrast agents. Copyright © 2008 European Peptide Society and John Wiley & Sons, Ltd.

Keywords: octreotide; micelles; fluorescence spectroscopy and circular dichroism; MRI contrast agent

Introduction

Somatostatin (SST) is a neuropeptide with a wide role in the physiological control and pharmacological action as inhibitor of growth hormone, insulin and glucagon secretion; its effect is mediated via five G protein coupled membrane receptors (SSTR1-5) [1]. The five SST receptors, especially SSTR2, are widely overexpressed in homogenous and heterogeneous manner in tumor tissues such as gastroenteropancreatic neuroendocrine tumors, gliomas, meningiomas and breast tumors [2–4]. This is a challenging issue in oncology allowing the use of regulatory SST peptide to recognize receptors overexpressed in tumor cells. Unfortunately, SST half-life in plasma is extremely short [5] and the availability of synthetic analogs became an absolute necessity for any progress in this field. Many efforts were dedicated to synthesize a large variety of analogs and to select low molecular weight peptides stable *in vivo* and able to recognize most of the SSTRs. This research led to a cyclic eight-amino acid peptide (octreotide) (Sandostatin) [6] (Figure 1) able to bind to the most frequently overexpressed SSTR2 and to a lesser extent to SSTR5 [7]. For the presence of unnatural D amino acid residues and the alcoholic C-terminus, this peptide is highly resistant to enzymatic degradation and is able to restore the β -turn conformation unavoidable to interact with the receptors [8]. In light of these properties and of nontoxic side effects, octreotide is clearly a useful tool in the cancer management and more than 10 years ago was introduced in clinical practice to limit tumor growth [9]. Several preclinical studies strongly support the concept that binding of octreotide to SSTR is followed by rapid internalization of the receptor–ligand complex [10]. The mechanism of endocy-

tos is exploited to transport in the cell octreotide-conjugates containing therapeutics and diagnostics, such as the spindle poison taxol [11], and PNA sequences as antisense therapeutics [12]. Moreover, for diagnostic use, several octreotide derivatives, modified on the N-terminal moiety with a bifunctional chelator suitable for labeling radiometals such as ^{99m}Tc, ¹¹¹In, ^{67/68}Ga, have been designed, synthesized, and used as *in vivo* contrast agents in nuclear medicine techniques positron (emission tomography (PET) and single photon emission computed tomography (SPECT)) [13–16].

These results suggest the application of octreotide as the vehicle of contrast agents in magnetic resonance imaging (MRI). MRI is one of the most efficient *in vivo* imaging techniques, giving very resolved images with anatomical information. In these diagnostic procedures, the images are obtained by accumulating contrast agents. In SPECT or PET, the request concentration of radionuclides in the cancer tissues is 10⁻¹⁰ M, while MRI technique, due to its lower sensitivity, needs high concentration (at least 10⁻⁴ M) of

* Correspondence to: Giancarlo Morelli, Department of Biological Sciences, CIRPeB University of Naples "Federico II" and IBB CNR, Via Mezzocannone 16, 80134 Naples, Italy. E-mail: gmorelli@unina.it

a Department of Biological Sciences, CIRPeB, University of Naples "Federico II" and IBB CNR, Via Mezzocannone 16, 80134 Naples, Italy

b Department of Chemistry I.F.M. and Molecular Imaging Centre, University of Turin Via Nizza, 52, 10125 Turin, Italy

‡ 11th Naples Workshop on Bioactive Peptides.

§ Dedicated to Prof. Carlo Pedone on the occasion of his 70th birthday.

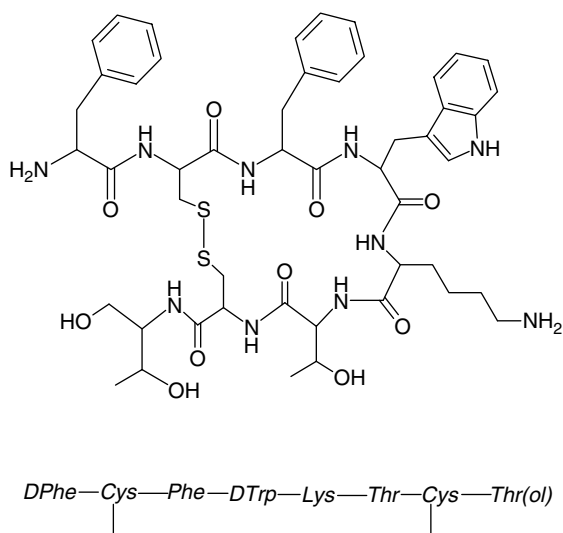


Figure 1. Amino acid sequence and structure of octreotide peptide (Sandostatin).

paramagnetic gadolinium complexes. This critical point can be overtaken by accumulating high concentration of contrast media in the site of interest. The use of a peptide probe based on only one unit of gadolinium complex for a peptide molecule could not overcome the problem of concentration of the contrast agent: most of tumor cells overexpress on their membrane approximately some million of SSTRs leading a number of contrast agents too low in the cells.

To increase the number of contrast agents on the target cells, the binding of a large number of gadolinium complexes to the peptide probe is required. During last years, supramolecular aggregates, such as micelles [17], vesicles and liposomes [18], all containing a high number of stable Gd(III) complexes were prepared. Moreover, supramolecular aggregates derivatized on their external surface with bioactive molecules (peptides or antibodies) have been proposed as target-selective contrast agents in MRI [19]. Following this strategy, we developed several supramolecular aggregates by assembling together two amphiphilic monomers, one containing a gadolinium complex and the other the CCK8 octapeptide able to recognize cholecystokinin receptors overexpressed in human tumor cells [20,21].

More recently we reported the synthesis, the aggregation behavior, the structural characterization and the relaxometric properties of a monomer with an 'upsilon' shape (*MonY*) [22]. The core of this molecule is a lysine residue in which the three reactive functions are derivatized with: the chelating agent *N,N*-bis[2-[bis(carboxy-ethyl)amino]ethyl]-L-glutamic acid (DTPAGlu), a DTPA derivative able to give very stable Gd(III) complex; the bioactive C-terminal octapeptide sequence of the cholecystokinin hormone (CCK8); and a hydrophobic moiety containing two alkyl chains with 18 carbon atoms each. In this paper we report, the synthesis in solid phase, the aggregation properties and the relaxometric behavior of two novel octreotide-conjugate amphiphiles (OCA: OCA-DOTA and OCA-DTPAGlu) in which the hydrophobic moiety is formed by two hydrocarbon tails at 18 carbon atoms each, while the hydrophilic head group still contains the DTPAGlu or tetraazacyclododecane-tetraacetic acid (DOTA) chelating agents or their gadolinium complexes, and the octreotide bioactive peptide (Figure 2).

Results and Discussion

Monomers Design and Synthesis

The monomers design has to fulfil two requirements: (i) chemical modifications on octreotide should preserve the peptide receptor binding capability; (ii) after the aggregation process, the peptide molecules and the gadolinium complexes have to lie in hydrophilic shell of the supramolecular aggregates to preserve the peptide bioactivity and to allow water exchange in the gadolinium coordination sphere. The first requirement was fulfilled by introducing modifications at *N*-terminal end of the peptide sequence. In fact, recent studies show that a hydrophilic or hydrophobic chain covalently bound on the *N*-terminus of DPhe residue results in low effect on binding constants of octreotide to the receptors [23]. The second need could be satisfied by introducing two units of 21-amino-4,7,10,13,16,19-hexaoxaheneicosanoic acid (AhOH) between the lysine residue and the octreotide *N*-terminal residue. The AhOH linker was chosen to increase the hydrophilicity of the head without change the charge of the monomers. Moreover, the oxoethylene moieties are not toxic, are able to reduce aggregate clearance through the reticulo-endothelial system (RES) [24] and they avoid adsorption of blood proteins into the supramolecular aggregates.

The length of linkers was selected, according to the biological results previously obtained on similar aggregates derivatized with CCK8 or 7-14-bombesin, in order to favor a good exposure of octreotide on the external aggregate surface. The branching of the monomers headgroup was achieved using a lysine residue. On its α amine function, another unit of the linker was bound to space the hydrophilic head from the lipophilic tails; while on lysine side chain, the selected DOTA or DTPAGlu chelating agents were condensed to distance them far away from the octreotide moiety.

DOTA belongs to the macrocycle class of chelating agents while DTPAGlu is a branched chelating agent. Both ligands are able to coordinate Gd(III) ions with high-stability constants saturating eight coordination positions, thus leaving the last position for water coordination and allowing water exchange in gadolinium coordination sphere. They were selected to study the influence of the steric hindrance and of the residual charge present in the hydrophilic shell on the aggregation behavior.

The chemical synthesis of the two monomers, OCA-DOTA and OCA-DTPAGlu, was fully performed on solid support according to standard SPPS protocols following the Fmoc/*t*Bu chemistry [25]. The synthetic scheme is reported in detail in Figure 3. The preloaded H-Thr(*t*Bu)-ol-(2-chloro-trityl) polymeric resin was used to obtain the alcoholic function on the C-terminus. The asymmetric compounds were obtained by the introduction of a lysine residue, orthogonally protected by Dde and Fmoc on the α and ϵ amine functions, respectively. The Dde protecting group was preferred to Mtt protecting group to avoid a partial cleavage from the resin in acid-labile removal conditions and because of its stability during the Fmoc removal by treatment with piperidine. After removal of Fmoc, DTPAGlu-pentaester or DOTA-triester, activated by HATU, were condensed on lysine side chain. The Dde removal was obtained by brief treatment with 2% hydrazine in *N,N*-dimethylformamide, giving the α free amine function, on which the AhOH linker and *N,N*-dioctadecylsuccinamic acid were condensed. At the end of the monomers assembly, acetamidomethyl (Acm) removal from the cysteine residues and disulfide bridge formation were achieved by $\text{Ti}(\text{CF}_3\text{CO}_2)_3$ treatment on a solid support. Cleavage was performed using standard trifluoroacetic acid (TFA)/tri-isopropylsilane (TIS)/ H_2O mixtures, to allow complete removal of protecting groups from all the amino acid side chains

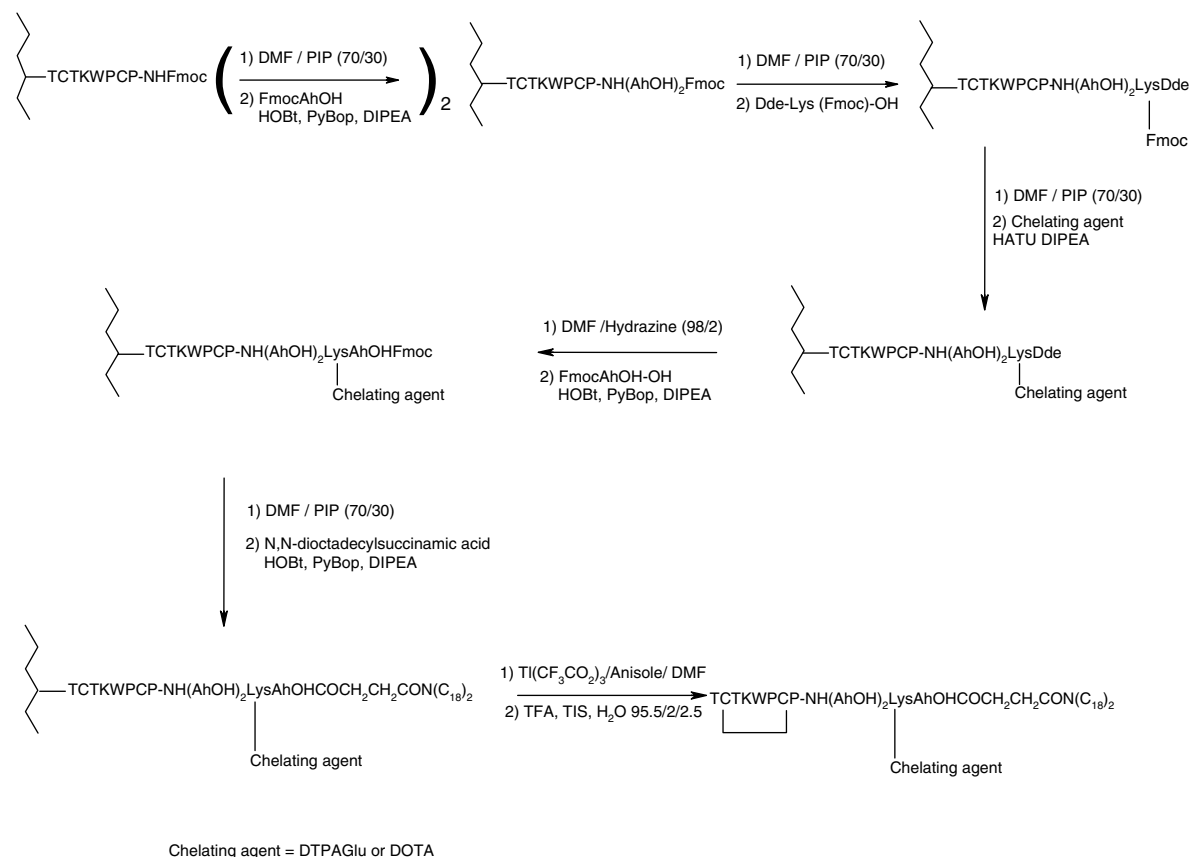


Figure 3. Scheme of the chemical procedures for the solid-phase synthesis of the two monomers OCA-DTPAGlu and OCA-DOTA. Resin is schematically represented as a broken curve.

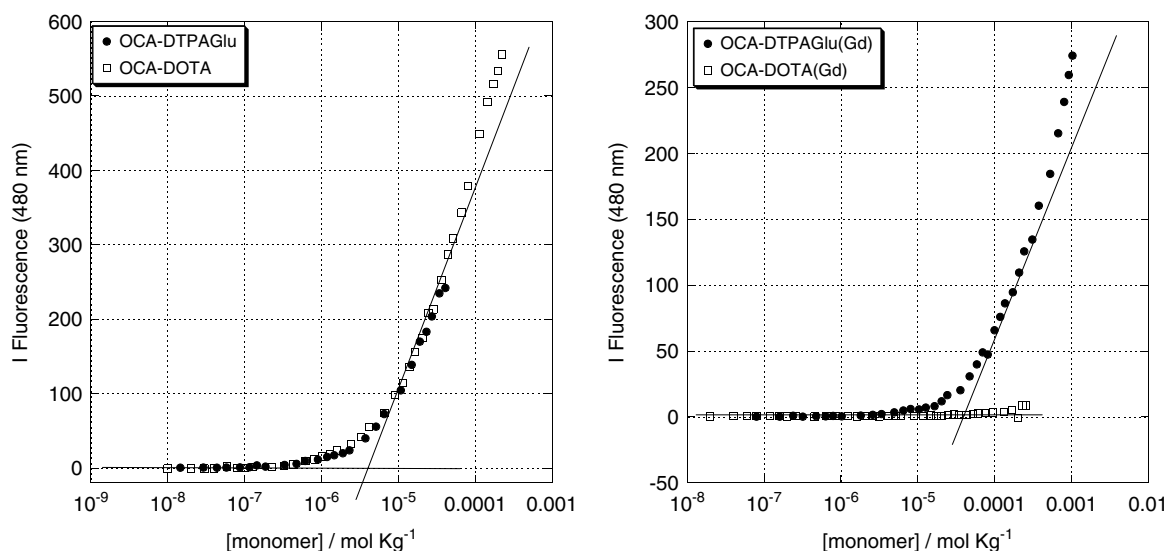


Figure 4. Fluorescence intensity of ANS fluorophore at 480 nm versus: (a) OCA-DTPAGlu and OCA-DOTA concentration; (b) OCA-DTPAGlu(Gd) and OCA-DOTA(Gd) concentration. The cmc values are established from graphical break points.

Physicochemical Studies on the Octreotide Moiety

Biological data concerning SST analogs obtained by introducing covalent conformational constraints, suggested that -Phe-D-Trp-Lys-Thr-amino acid sequence contains all the elements necessary for the expression of the SST biological activities versus SSTR2 [7]. Literature NMR studies indicated that octreotide adopts a

predominant antiparallel β -sheet conformation characterized by a type II' β -like turn across residues D-Trp⁴ and Lys⁵ [28], and these results were also confirmed by X ray structural studies [29]. Therefore, all octreotide conjugates should preserve this conformation and chemical alterations should not affect the D-Trp residue. Fluorescence experiments and CD studies were

carried out to prove that the peptide moiety in the amphiphilic molecules keeps the conformational requirements unaltered also after micelles formation and that it remains well exposed on the micelle surface. The exposure of the bioactive portion of the monomers on aggregates surface was assessed by monitoring the fluorescence emission due to the indole moiety of the tryptophan residue. Usually, this fluorophore shows an emission peak centered at 350 nm in polar solvents while in hydrophobic solvents the maximum shifts occurs at 330 nm [30]. The fluorescence emission spectra of the three aggregates (Figure 5) were recorded at 25 °C and at monomer concentration (1.0×10^{-5} M for OCA-DOTA and OCA-DTPAGlu; 1.0×10^{-4} for OCA-DTPAGlu(Gd)), higher than cmc to be sure of the presence of aggregates in solution. The fluorescence maximum at 350 nm suggests for OCA-DOTA, a complete exposure of D-Trp residue in the hydrophilic external space. In the case of OCA-DTPAGlu and OCA-DTPAGlu(Gd), the maximum is centered at 346 nm, this value, slightly shifted with respect to 350 nm, indicates that most of the indole groups on tryptophan side-chain lies in the hydrophilic environment. The slight difference between OCA-DOTA and OCA-DTPAGlu could be attributed to the different steric hindrance of the chelating agents which can drive the micelle structure. Instead, the octreotide disposition seems not to be affected by gadolinium coordination, reducing the negative charge on the hydrophilic surface. This result suggests the use of the octreotide peptide to drive the entire aggregate toward SST receptors present on cell membranes.

The effects on the conformational structure of the octreotide peptide in the two amphiphilic molecules were assayed by CD measurements. Figure 6(a) shows the CD spectra of OCA-DOTA and OCA-DTPAGlu at 1.0×10^{-4} M concentration, above their cmc values. The octreotide wild-type spectrum was also reported for comparison. All spectra indicate predominant presence of an antiparallel β -sheet conformation characterized by a β -like turn, clearly suggesting that the disulphide bridge is conserved on the aggregates surface. OCA-DTPAGlu and octreotide spectra are nearly superimposable in the 190–260 nm range. Instead, the OCA-DOTA spectrum in 190–210 nm range shows a blue shift of the minimum, which may indicate some conformational modifications, but widely confirms the β -sheet conformation.

Moreover, OCA-DTPAGlu spectra at three different concentrations are also reported in Figure 6(b). The presence of oxoethylenic linkers and lipophilic tails on peptide N-terminus could

induce some changes in peptide conformation. By decreasing concentration below the cmc, even if some spectral modifications are observed, the β -sheet rearrangement is preserved. This variation disappears when the monomer self-aggregates in solution above cmc. The steric hindrance on micelles surface might reduce the degree of freedom and restore the minimum octreotide conformation.

Relaxivity Measurements

The parameter for an evaluation of an MRI contrast agent is its relaxivity, i.e. the potency to shorten the relaxation times of the solvent water protons. The measured relaxivity value (r_{1p}) is defined as the paramagnetic contribution to the measured proton longitudinal relaxation rate (R_{1obs}) of a solution containing 1.0 mM concentration of gadolinium according to Eqn (1) [31]

$$R_{1obs} = [Gd] \cdot r_{1p} + R_{1w} \quad (1)$$

where R_{1w} is the diamagnetic contribution of pure water (0.38 s^{-1}).

The relaxivity of OCA-DTPAGlu(Gd), was measured at monomer concentration higher than the calculated cmc to be sure that the molecules are aggregated in the micellar form. A value of $13.9 \text{ mM}^{-1} \text{ s}^{-1}$ has been determined at 20 MHz and 25 °C (Figure 7). This value was then confirmed mineralizing, with HCl 37% at 120 °C overnight, a given quantity of sample solution to determine the exact concentration of Gd(III) present in the solution: from the measure of the observed relaxation rate (R_{1obs}) of the acidic solution, knowing the relaxivity (r_{1p}) of Gd(III) aquoion in acidic conditions ($13.5 \text{ mM}^{-1} \text{ s}^{-1}$), it was possible to calculate the exact Gd(III) concentration (Eqn (1)) (This method was calibrated using standard inductively coupled plasma (ICP) solutions, and the accuracy was determined to be 1%). At this point, knowing [GdL] and measuring R_{1obs} of the micellar mother solution, the same Eqn (1) was used to calculate the micellar relaxivity. Relaxivity value of OCA-DTPAGlu(Gd) micelles ($13.9 \text{ mM}^{-1} \text{ s}^{-1}$) is in the same range of the value previously reported ($15.0 \text{ mM}^{-1} \text{ s}^{-1}$) for aggregates obtained by self assembling of a similar monomer containing the CCK8 peptide (*MonY*-Gd) [22]. The slight difference could be probably ascribed to different aggregation number or size.

The analysis of nuclear magnetic relaxation dispersion (NMRD) profile of the lipophilic aggregated system has been made according to the Solomon–Bloembergen–Morgan model, modified

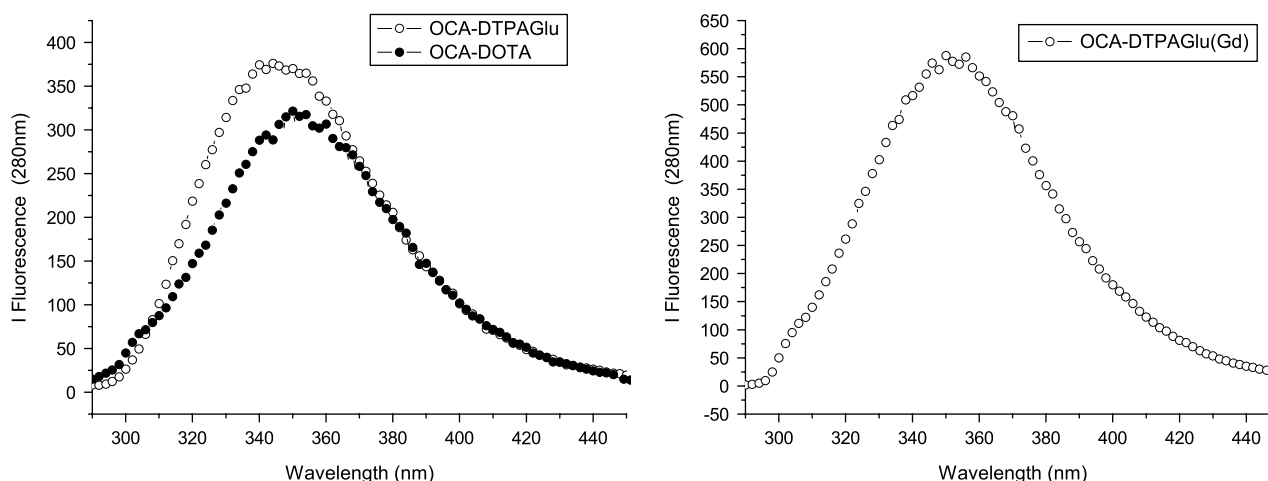


Figure 5. Fluorescence spectrum of tryptophan residue of: (a) OCA-DTPAGlu and OCA-DOTA aggregates; (b) OCA-DTPAGlu(Gd) aggregate. Fluorescence spectra were excited at 280 nm.

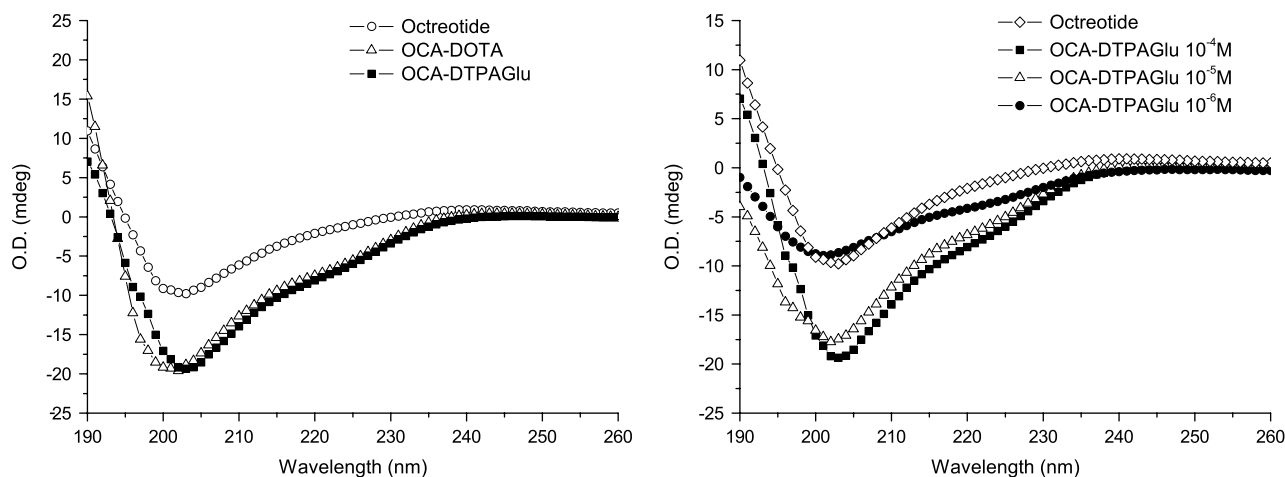


Figure 6. Circular dichroism profiles of: (a) octreotide, OCA-DTPAGlu and OCA-DOTA (b) of octreotide and OCA-DTPAGlu at 1.0×10^{-4} M, 1.0×10^{-5} M, 1.0×10^{-6} M concentrations.

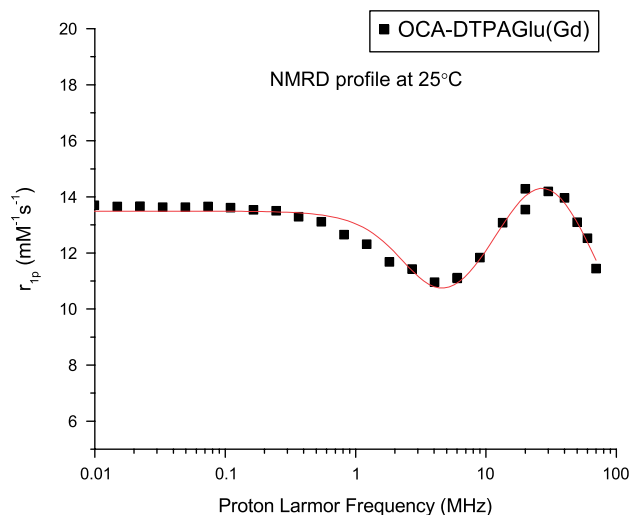


Figure 7. $1/T_1$ NMRD profile of OCA-DTPAGlu(Gd) at pH 7.4 and 25 °C, normalized to 1 mM Gd (III) ion. This figure is available in colour online at www.interscience.wiley.com/journal/jpepsci.

according to the Lipari-Szabo approach [32–34] to obtain an accurate determination of the reorientational correlation time (τ_R), that is strictly related to the molecular size of the investigated system. This model is generally applied to the systems with a faster local motion (governed by τ_1) and a slower global motion (governed by τ_g); the extent of local to global contribution to the overall motion is determined by an order parameter (S^2) that can vary from 0 to 1.

The experimental data $\tau_1 = 250$ ps, $\tau_g = 2900$ ps and $S = 0.3$ were fitted by considering one water molecule in the inner coordination sphere for each Gd(III) complex ($n_w = 1$) and fixing the exchange lifetime of the coordinated water molecule (τ_M) to the (60 ns) previously determined for the similar micellar system containing the CCK8-peptide functionalized monomer (*MonY*-Gd) [22] because of the low solubility of OCA-DTPAGlu(Gd) system, which prevents any direct ^{17}O -NMR R_{2p} versus T measurement.

In Vitro Biological Assays

Receptor binding ability of OCA-DTPAGlu in micellar form has been evaluated by standard nuclear medicine experiments.

Radiolabeling of the aggregates was performed at concentrations above critical micellar concentration to avoid the presence of free monomers in solution. Trace amounts of $^{111}\text{InCl}_3$ and up to 500 μCi were added to the aggregate formulation after addition of an equal volume of 0.5 N sodium citrate. Confirmation of incorporation of the radioactive label into the aggregates was obtained by gel filtration. ^{111}In -labeled aggregates showed preferential binding to A431 cells overexpressing the *sstr2* by transfection compared to control cells; in fact 3.8% of bound plus internalized radioactivity in receptor expressing cell against 1.6% for control cells was obtained in a preliminary experiment performed at 37 °C.

Conclusions

New amphiphilic monomers (OCA-DTPAGlu and OCA-DOTA) containing, in the same molecule, three different functions: (i) the chelating agent (DTPAGlu or DOTA) able to coordinate gadolinium ion, (ii) the octreotide bioactive peptide able to target SSTR2 and SSTR5 SST receptors and (iii) a hydrophobic moiety with two 18-carbon atoms alkyl chains, have been designed and synthesized by solid-phase methods. In water solution at pH 7.4, the peptide-conjugate amphiphiles self-assemble as micelles at low concentration as confirmed by fluorescence measurements, using the fluorescent ANS probe. The corresponding gadolinium complexes present a different aggregation behavior: While OCA-DTPAGlu(Gd) gives stable micelles, OCA-DOTA(Gd), which does not contain charges on the hydrophilic head, remains in the nonaggregated state in the explored concentration range. As consequence of this aggregation behavior, OCA-DTPAGlu(Gd) seems a very promising target-selective MRI contrast agent. It presents the high relaxivity value expected for amphiphilic gadolinium complexes in aggregated form; a high stability of the micelles, and above all the exposure of the bioactive octreotide peptide on the micelle external surface, in the correct conformation to bind the target receptors. The selective binding of OCA-DTPAGlu in micellar form was determined in a preliminary experiment, in which the octreotide derivative, at concentration higher than its cmc, is labeled with ^{111}In . ^{111}In -labeled aggregates show preferential binding to A431 cells overexpressing SSTR2 compared to control cells (3.8% against 1.6% of bound plus internalized radioactivity). As already reported in the case of

a similar compound containing the CCK8 peptide, *MonY-Gd*, micelles of OCA-DTPAGlu(Gd) belongs to novel class of MRI contrast agents. They could be able to target SSTR2 and SSTR5 receptors, well-assessed targets for several human tumors.

Experimental Methods

Materials and Methods

Protected *N*^α-Fmoc-amino acid derivatives, coupling reagents and H-Thr(*t*Bu)-ol-(2-chloro-trityl)-resin were obtained from Calbiochem-Novabiochem (Laufelfingen, Switzerland) and INBIO (Napoli, Italy). Fmoc-21-amino-4,7,10,13,16,19-hexaaxaheneicosanoic acid (Fmoc-AhOH-OH) was purchased from Neosystem (Strasbourg, France). The 1,4,7,10-tetraazacyclododecane-1,4,7,10-tetraacetate *tert*butyl ester [(DOTA(*t*Bu)₃] was purchased from Macrocycles (Richardson, Texas). DTPAGlu pentaester chelating agent (*N*₂,*N*₂-bis[2-[bis[2-(1,1-dimethylethoxy)-2-oxoethyl]-amino]ethyl]-L-glutamic 1,1-dimethylethyl ester) and the *N,N*-dioctadecylsuccinamic acid were synthesized according to the experimental procedure reported in literature [35,36]. All other chemicals were commercially available at Sigma-Aldrich (Milwaukee WI, USA) or Fluka (Buchs, Switzerland) and were used without further purification. All solutions were prepared by weight using doubly distilled water. The pH of all solutions was kept constant at 7.4 in phosphate buffer.

Synthesis of OCA-DOTA and OCA-DTPAGlu

Peptide synthesis was carried out in solid-phase under standard conditions using Fmoc strategy, [25] on H-Thr(*t*Bu)-ol-(2-chloro-trityl)-resin (0.70 mmol/g, 0.15 mmol scale, 0.214 g). The peptide chain was built by sequential coupling and Fmoc deprotection of the following seven Fmoc-amino acid derivatives: Fmoc-Cys(Acm)-OH, Fmoc-Thr(*Ot*Bu)-OH, Fmoc-Lys(Boc)-OH, Fmoc-DTrp(Boc)-OH, Fmoc-Phe-OH, Fmoc-Cys(Acm)-OH, Fmoc-DPhe-OH. All couplings were performed twice for 60 min, by using an excess of four equivalents for the single amino acid derivative. The carboxylic functions of α -amino acids were activated *in situ* by the standard 1-hydroxybenzotriazole/benzotriazol-1-yl-oxy-tris-pyrrolidino-phosphonium/*N,N*-diisopropylethylamine (HOBt/PyBop/DIPEA) procedures in DMF. Fmoc deprotections were obtained by 30% piperidine solution in DMF. The coupling steps were monitored by the qualitative Kaiser test. When the peptide synthesis was complete, the Fmoc *N*-terminal protecting group was removed and two residues of Fmoc-AhOH-OH were condensed by using, for each residue, an excess of two equivalents activating the carboxylic function similarly in a single coupling for 60 min under N₂ flow at room temperature. After Fmoc removal from the *N*-terminal end of the peptide derivative, 0.320 g (0.60 mmol) of Dde-Lys(Fmoc)-OH, activated by a stoichiometric amount of PyBop and HOBt and two equivalents of DIPEA in DMF, were coupled by stirring the slurry suspension of the resin for 60 min. The solution was filtered and the resin was washed with three portions of DMF. After removal of the Fmoc group on side chain of lysine residue, the chelating agent (DTPAGlu pentaester or DOTA trisester) was linked, through its free carboxyl function, to the ϵ -NH₂ of the lysine residue. This coupling step was performed using two equivalents of the chelating agent, HATU and four equivalents of DIPEA in DMF as a solvent. The coupling time, compared with the classical solid-phase peptide synthesis protocol, was increased up to 120 min. The resin was washed three times with DMF, then, the

1-(4,4-dimethyl-2,6-dioxo-cyclohexylidene)3-methylbutyl group (Dde) was removed by treatment with DMF/Hydrazine mixture (98:2). The peptide-resin was stirred with 3.0 ml of this solution for 10 min. The treatment was repeated twice, and the reaction was monitored by the qualitative Kaiser test. On *N*-terminal moiety, the Fmoc-AhOH-OH linker was coupled following the same procedure above described. After the removal of *N*-terminal Fmoc protecting group, *N,N*-dioctadecylsuccinamic acid (0.187 g, 0.3 mmol) in DMF/DCM (1/1) mixture were condensed. The coupling reaction was repeated twice under N₂ flow for 60 min. The lipophilic moiety was activated *in situ* by the standard HOBt/PyBop/DIPEA procedure. The deprotection (Acm removal) and the oxidation reaction of cysteine residues were carried out at same time adding 1.2 eq Ti(CF₃CO₂)₃ to a suspension of the peptidyl resin in DMF/anisole (19:1) stirring the mixture for 18 h at 0 °C monitoring at times by the colorimetric Ellmann test [37].

The peptide derivatives were cleaved from the solid support by suspending the resin in 10 ml of TFA/TIS/H₂O (95.5/2/2.5) mixture for 120 min. During this step all the amino acid side chains and the carboxylic groups of the chelating moiety were simultaneously freed from their protecting groups. Free peptide derivatives were precipitated in cold water and lyophilized from a 50% H₂O/CH₃CN solution. The crude compounds were purified by RP-HPLC. Preparative RP-HPLC was carried out on a Shimadzu 8A (Kyoto, Japan) apparatus equipped with an UV Shimadzu detector using a Phenomenex (Torrance, CA) C4 column, 22 mm × 250 mm with a flow rate of 20 ml min⁻¹. The single peaks were analyzed by HPLC and mass spectrometry. Analytical RP-HPLC runs were carried out on a HP Agilent Series 1100 apparatus (Santa Clara, CA, USA) using a Phenomenex (Torrance, CA) C18 column, 4.6 mm × 250 mm with a flow rate of 1.0 ml min⁻¹. For all the RP-HPLC procedures, the system solvent used was H₂O 0.1% TFA (A) and CH₃CN 0.1% TFA (B), with a linear gradient from 5 to 70% B in 30 min followed by 70 to 95% B in 10 min. Mass spectral analysis were carried out on MALDI-TOF Voyager-DE mass spectrometer Perseptive Biosystems (Framingham, MA, USA). The desired compounds (~180 mg) were obtained at HPLC purity higher than 95% with a final yield of around 10%.

(C18)₂-(AhOH)-Lys(DTPAGlu)-(AhOH)₂-octreotide,
OCA-DTPAGlu, *R*_t = 41.0 min; *MW* = 3204 amu.
(C18)₂-(AhOH)-Lys(DOTA)-(AhOH)₂-octreotide,
OCA-DOTA, *R*_t = 41.3 min; *MW* = 3144 amu.

Preparation of Gadolinium Complexes

Gadolinium complexes have been obtained by adding light excess of the GdCl₃ to aqueous solution of OCA-DTPAGlu and OCA-DOTA ligands at neutral pH and room temperature. The formation of the gadolinium complexes was followed by measuring the solvent proton relaxation rate (1/*T*₁). The excess of uncomplexed Gd(III) ions, which yields a variation of the observed relaxation rate, was removed by centrifugation of the solution brought to pH 10; further relaxation rate measurements were made to check the complete Gd(III) ions removal.

Preparation of Micelle Containing Solutions

Stock solutions of OCA-DTPAGlu and OCA-DOTA monomers and of their gadolinium complexes were prepared by stirring the monomers until complete dissolution in 0.1 M phosphate buffer at pH 7.4 and filtering through a 0.45 μ m filter. Concentrations of all solutions (1.0 × 10⁻³ M for OCA-DTPAGlu, OCA-DOTA

and OCA-DTPAGlu(Gd); and 1.0×10^{-4} M for OCA-DOTA(Gd) were determined by absorbance on a UV-vis Jasco V-5505 spectrophotometer (Easton, MD, USA) equipped with a Jasco ETC-505T Peltier temperature controller with a 1-cm quartz cuvette using a molar absorptivity (ϵ_{280}) of $5630 \text{ M}^{-1} \text{ cm}^{-1}$ for octreotide, due to the contribution of tryptophan residue present in the primary octreotide structure [38,39].

Fluorescence Measurements

Emission spectra were recorded using a Jasco Model FP-750 spectrofluorimeter equipped with a Peltier temperature controller in 1.0-cm path length quartz cell at 25 °C. Equal excitation and emission bandwidths were used throughout experiments, with a recording speed of 125 nm min^{-1} and automatic selection of the time constant. The cmc values were obtained by using 8-anilino-naphthalene-1-sulfonate (ANS) as a fluorescent probe. Small aliquots of 1×10^{-4} M aggregates solution, were added to a fixed volume of fluorophore in the cell (1×10^{-5} M ANS) dissolved in the same buffer. The cmc values were determined by linear least-squares fitting of the fluorescence emission at 480 nm, upon excitation at 350 nm versus the amphiphile concentration as previously reported [26,40].

Tryptophan emission spectra in 290–450 nm range were obtained exciting at 280 nm micelle solutions at monomer concentration of 1.0×10^{-5} M for OCA-DTPAGlu and OCA-DOTA; and 1.0×10^{-4} M for OCA-DTPAGlu(Gd) and OCA-DOTA(Gd).

Circular Dichroism (CD) Experiments

Far-UV CD spectra were collected at room temperature on a Jasco J-810 spectropolarimeter equipped with a NesLab RTE111 thermal controller unity using a 1-mm quartz cell. Other experimental settings were: scan speed, 10 nm/min; sensitivity, 50 mdeg; time constant, 16 s; bandwidth, 3 nm. CD measurements were conducted on solutions containing peptide amphiphilic surfactant at concentrations of 1×10^{-4} M, 1×10^{-5} M and 1×10^{-6} M in 2.5 mM phosphate buffer at pH 7.4. The CD spectra were collected from 260 to 190 nm, corrected for blank and adjusted for dilution.

Water Proton Relaxation Measurements

The longitudinal water proton relaxation rates were measured on a Stellar Spinmaster (Mede, Pavia, Italy) spectrometer operating at 20 MHz, by means of the standard inversion-recovery technique (16 experiments, 2 scans). A typical 90° pulse width was 4 μs and the reproducibility of the T_1 data was $\pm 0.5\%$. The temperature was maintained at 298 K with a Stellar VTC-91 air-flow heater equipped with a copper-constantan thermocouple (uncertainty $\pm 0.1^\circ\text{C}$). The proton $1/T_1$ NMRD profiles were measured over a continuum of magnetic field strength from 0.00024 to 0.28 T (corresponding to 0.01–20 MHz proton Larmor Frequency) on a Stellar fast field-cycling relaxometer. This relaxometer works under complete computer control with an absolute uncertainty in $1/T_1$ of $\pm 1\%$. Data points from 0.47 T (20 MHz) to 1.7 T (70 MHz) were collected on a Stellar Spinmaster spectrometer working at variable field.

Biological Assays

Radiolabeling of OCA-DTPAGlu aggregates was performed at monomer concentration of 1.0×10^{-3} M. Trace amounts of $^{111}\text{InCl}_3$

and up to 500 μCi were added to the aggregate formulation after addition of an equal volume of 0.5 N sodium citrate. Confirmation of incorporation of the label into the aggregates was obtained by gel filtration on Sephadex G-50 prepacked columns (Pharmacia Biotech). Binding activity was tested on A431 cells overexpressing the SSTR2 by stable transfection and compared to control cells. Assays were performed at 37 °C on cell suspensions that were incubated with the radiolabel aggregates for 1 h. Concentration of the monomers in the cell binding assays were always kept above 10^{-4} M. Radioactivity bound to cells was separated from unbound activity by centrifugation through dibutyl phthalate in 1.5 ml tubes which were subsequently frozen on dry ice, the cell pellet containing portion of the tube excised and counted in a Wallac gamma counter. Unbound radioactivity was placed in a separate vial and counted as well.

Acknowledgements

The authors thank the European Molecular Imaging Laboratories Network (EMIL) and the Italian Consortium CIRCMSB for financial support. The authors thank Dr Francesca Arena for support in relaxivity measurements.

References

1. Brazeau P, Vale W, Burgus R, Ling N, Butcher M, Rivier J, Guillemin R. Hypothalamic polypeptide that inhibits the secretion of immunoreactive pituitary growth hormone. *Science* 1973; **179**: 77–79.
2. Bell G, Reisine T. Molecular biology of somatostatin receptors. *Trends Neurosci.* 1993; **16**: 34–38.
3. Reubi JC, Horisberger U, Laissus J. High density of somatostatin receptors in veins surrounding human cancer tissue: role in tumour host interaction? *Int. J. Cancer* 1994; **56**: 681–688.
4. Reubi JC, Schaer JC, Waser B, Mengod G. Expression and localization of somatostatin receptor SSTR1, SSTR2, and SSTR3 messenger RNAs in primary human tumors using in situ hybridization. *Cancer Res.* 1994; **54**: 3455–3459.
5. Patel YC, Wheatley T. *In vivo* and *in vitro* plasma disappearance of somatostatin-14 and somatostatin-28 in the rat. *Endocrinology* 1983; **112**: 220–225.
6. Lamberts SWJ. *Octreotide: The Next Decade*. BioScientifica: Bristol, 1999.
7. Bauer W, Briner U, Doepfner W. SMS 201–995: A very potent and selective octapeptide analogue of somatostatin with prolonged action. *Life Sci.* 1982; **31**: 1133–1140.
8. Veber DF, Freidinger RM, Schwenk-Perlow D, Paleveda WJ Jr, Holly FW, Strachan RG, Nurr RF, Arison BH, Homnick C, Randall WC, Glitzer MS, Saperstein R, Hirschmann R. A potent cyclic hexapeptide analogue of somatostatin. *Nature* 1981; **292**: 55–58.
9. Patel CY. Somatostatin and its receptor family. *Front. Neuroendocrinol. Rev.* 1999; **20**: 157–198.
10. Hofland LJ. Internalization of [DOTA, ^{125}I -Tyr 3]octreotide by somatostatin receptor-positive cells *in vitro* and *in vivo*: implications for somatostatin receptor-targeted radio-guided surgery. *Proc. Assoc. Am. Phys.* 1999; **111**: 63–69.
11. Huang CM, Wu YT, Chen ST. Targeting delivery of paclitaxel into tumor cells via somatostatin receptor endocytosis. *Chem. Biol.* 2000; **7**: 453–461.
12. Mier W, Eritja R, Ashour M, Haberkorn U, Eisenhut M. Peptide-PNA conjugates targeted transport of antisense therapeutics into tumors. *Angew. Chem., Int. Ed. Engl.* 2003; **42**: 1968–1971.
13. Lamberts SWJ, Krenning EP, Reubi JC. The role of somatostatin and its analogs in the diagnosis and treatment of tumors. *Endocrinol. Rev.* 1991; **12**: 450–482.
14. Krenning EP, Kwekkeboom DJ, Pauwels S, Kvols LK, Reubi JC. Somatostatin receptor scintigraphy. *Nucl. Med. Annu.* 1995; 1–50.

15. Reubi JC, Waser B, Schaer JC, Laissue JA. Somatostatin receptor sst1-sst5 expression in normal and neoplastic human tissues using receptor autoradiography with subtype-selective ligands. *Eur. J. Nucl. Med.* 2001; **28**: 836–846, Erratum in *Eur. J. Nucl. Med.* 2001; **28**: 1433.
16. Froidevaux S, Eberle AN. Somatostatin analogues and radiopeptides in cancer therapy. *Biopolymers (Pept. Sci.)* 2002; **66**: 161–183.
17. Andre JP, Toth E, Fischer H, Seelig A, Maecke HR, Merbach AE. High relaxivity for monomeric Gd(DOTA)-Based MRI contrast agents, thanks to micellar self-organization. *Chem.–Eur. J.* 1999; **5**: 2977–2983.
18. Glogård C, Stensrud G, Hovland R, Fossheim SL, Klaveness J. Liposomes as carriers of amphiphilic gadolinium chelates: The effect of membrane composition on incorporation efficacy and in vitro relaxivity. *Int. J. Pharm.* 2002; **233**: 131–140.
19. Mulder WJM, Strijkers GJ, Griffioen AW, Van Bloois L, Molema G, Storm G, Koning A, Nicolay K. A liposomal system for contrast-enhanced magnetic resonance imaging of molecular targets. *Bioconjugate Chem.* 2004; **15**: 799–806.
20. Accardo A, Tesaro D, Roscigno P, Gianolio E, Paduano L, D'Errico G, Pedone C, Morelli G. Physicochemical properties of mixed micellar aggregates containing CCK peptides and Gd complexes designed as tumor specific contrast agents in MRI. *J. Am. Chem. Soc.* 2004; **126**: 3097–3107.
21. Accardo A, Tesaro D, Morelli G, Gianolio E, Aime S, Vaccaro M, Mangiapia G, Paduano L, Schillén K. High-relaxivity supramolecular aggregates containing peptides and Gd complexes as contrast agents. *J. Biol. Inorg. Chem.* 2007; **12**: 267–276.
22. Vaccaro M, Mangiapia G, Paduano L, Gianolio E, Accardo A, Tesaro D, Morelli G. Structural and relaxometric Characterization peptide aggregates containing gadolinium complexes as potential selective contrast agents in MRI. *ChemPhysChem* 2007; **8**: 2526–2538.
23. Wang Q, Graham K, Schauer T, Fietz T, Mohammed A, Liu X, Hoffend J, Haberkorn U, Eisenhut M, Mier W. Pharmacological properties of hydrophilic and lipophilic derivatives of octreotate. *Nucl. Med. Biol.* 2004; **31**: 21–30.
24. Torchilin VP, Omelyanenko VG, Papisov MI, Bogdanov AJ, Trubetskoy VS, Herron JN, Gentry CA. Poly(ethylene glycol) on the liposome surface: on the mechanism of polymer-coated liposome longevity. *Biochim. Biophys. Acta* 1994; **119**: 11–20.
25. Chang WC, White PD. *Fmoc Solid Phase Peptide Synthesis*. Oxford University Press: New York, USA; 2000.
26. Birdi KS, Singh HN, Dalsager SU. Interaction of ionic micelles with the hydrophobic fluorescent probe 1-anilino-8-naphthalenesulfonate. *J. Phys. Chem.* 1979; **83**: 2733–2737.
27. Morag O, Ahmad A, Kamaly N, Perouzel E, Caussin A, Keller M, Herlihy A, Bell J, Miller AD, Jorgensen MR. MAGfect: a novel liposome formulation for MRI labelling and visualization of cells. *Org. Biomol. Chem.* 2006; **4**: 3489–3497.
28. Wynants C, Van Binst G, Loosli HR. SMS 201–995, a very potent analogue of somatostatin. Assignment of the ¹H 500 MHz NMR spectra and conformational analysis in aqueous solution. *Int. J. Pept. Protein Res.* 1985; **25**: 608–614.
29. Pohl E, Heine A, Sheldrick GM, Dauter Z, Wilson KS, Kallen J, Huber W, Pfaefli PJ. Structure of octreotide, a somatostatin analogue. *Acta Crystallogr.* 1995; **D51**: 48–59.
30. Lackowicz JR. *Principles of Fluorescence Spectroscopy*. Plenum Press: New York, 1983.
31. Caravan P, Ellison JJ, McMurry TJ, Lauffer RB. Gadolinium(III) chelates as MRI contrast agents: Structure, dynamics and applications. *Chem. Rev. (Washington, DC)* 1999; **99**: 2293–2352.
32. Bloembergen N, Morgan LO. Proton relaxation times in paramagnetic solutions. Effects of electron spin relaxation. *J. Chem. Phys.* 1961; **34**: 842–850.
33. Lipari G, Szabo A. Model-free approach to the interpretation of nuclear magnetic resonance relaxation in macromolecules. 1. Theory and range of validity. *J. Am. Chem. Soc.* 1982; **104**: 4546–4559.
34. Lipari G, Szabo A. Model-free approach to the interpretation of nuclear magnetic resonance relaxation in macromolecules. 2. Analysis of experimental results. *J. Am. Chem. Soc.* 1982; **104**: 4559–4570.
35. Anelli PL, Fedeli F, Gazzotti O, Lattuada L, Lux G, Rebasti F. L-glutamic acid and L-Lysine as Useful Building Blocks for the Preparation of Bifunctional DTPA-like Ligands. *Bioconjugate Chem.* 1999; **10**: 137–140.
36. Schmitt L, Dietrich C. Synthesis and characterization of chelator-lipids for reversible immobilization of engineered proteins at self-assembled lipid interfaces. *J. Am. Chem. Soc.* 1994; **116**: 8485–8491.
37. Ellmann GL. Tissue sulfhydryl groups. *Arch. Biochem. Biophys.* 1959; **82**: 70–77.
38. Edelhoch H. Spectroscopic determination of tryptophan and tyrosine in proteins. *Biochemistry* 1967; **6**: 1948–1954.
39. Pace CN, Vajdos F, Fee L, Grimsley G, Gray T. How to measure and predict the molar absorption coefficient of a protein. *Protein Sci.* 1995; **4**: 2411–2423.
40. De Vendittis E, Palumbo G, Parlato G, Bocchini V. A fluorimetric method for the estimation of the critical micelle concentration of surfactants. *Anal. Biochem.* 1981; **115**: 278–286.